Coupled Neutronics/ Thermal-hydraulics Analysis of a High-Performance Light-Water Reactor Fuel Assembly

C. L. Waata

Institut für Kern- und Energietechnik
Programm Nukleare Sicherheitsforschung

Coupled Neutronics/Thermal-hydraulics Analysis of a High-Performance Light-Water Reactor Fuel Assembly

Christine Lylin Waata

Institut für Kern- und Energietechnik
Programm Nukleare Sicherheitsforschung

Von der Fakultät für Maschinenbau der Universität Stuttgart
genehmigte Dissertation

Coupled Neutronics/Thermal-hydraulics Analysis of a High-Performance Light-Water Reactor Fuel Assembly

Von der Fakultät Maschinenbau der Universität Stuttgart
zur Erlangung der Würde eines Doktors der Ingenierwissenschaften (Dr.-Ing.)
genehmigte Abhandlung

Vorgelegt von

Christine Lilyn Waata

aus Kampala (Uganda)

Hauptberichter: Prof. Dr.-Ing. habil. E. Laurien

Mitberichter: Prof. Dr. -Ing. T. Schulenberg

Tag der mündlichen Prüfung: 24. Oktober 2005

Acknowledgment

Abstract

The use of water at supercritical pressure as coolant and moderator introduces a challenge in the design of a High-Performance Light-Water Reactor (HPLWR) fuel assembly. At supercritical pressure condition (P=25 MPa), the thermal-hydraulics behaviour of water differs strongly from that at sub-critical pressure due to a rapid variation of the thermal-physical properties across the pseudo-critical line. Due of the strong link between the water (moderation) and the neutron spectrum and subsequently the power distribution, a coupling of neutronics and thermal-hydraulics has become a necessity for reactor concepts operating at supercritical pressure condition. The effect of neutron moderation on the local parameters of thermal-hydraulics and vice-verse in a fuel assembly has to be considered for an accurate design analysis. In this study, the Monte Carlo N-Particle code (MCNP) and the sub-channel code STAFAS (Sub-channel Thermal-hydraulics Analysis of a Fuel Assembly under Supercritical conditions) have been coupled for the design analysis of a fuel assembly with supercritical water as coolant and moderator. Both codes are well known for complex geometry modelling. The MCNP code is used for neutronics analyses and for the prediction of power profiles of individual fuel rods. The sub-channel code STAFAS for the thermal-hydraulics analyses takes into account the coolant properties beyond the critical point as well as separate moderator channels. The coupling procedure is realized automatically. MCNP calculates the power distribution in each fuel rod, which is then transferred into STAFAS to obtain the corresponding thermal-hydraulic conditions in each sub-channel. The new thermal-hydraulic conditions are used to generate a new input deck for the next MCNP calculation. This procedure is repeated until a converged state is achieved.

The coupled code system was tested on a proposed fuel assembly design of a HPLWR. An under-relaxation was introduced to achieve convergence. The test results showed a satisfactory convergence with a small under-relaxation factor of 0.2. Results from the test analysis of a HPLWR fuel assembly showed an axial power profile with two peaks. A stronger peak in the lower part is caused by the strong moderation from the coolant and a weaker one in the upper part caused by moderator water. A 5% enrichment in the most inner fuel rods and lower enrichment of 4% in the corner rod was used to eliminate the hot spot at the corner of the fuel assembly and to obtain a well uniform power distribution in the fuel bundle. A well uniform temperature distribution was achieved in any cross section. A maximum temperature difference of 50°C in the upper part was obtained between the hottest and the coldest sub-channel. The local maximum cladding temperature of the bundle is within the allowable limit of 620°C.

Zusammenfassung

Gekoppelte neutronische und thermo-hydraulische Berechnung eines Brennelements für einen Leichtwasserreaktor mit überkritischen Dampfzuständen

Die Verwendung von Wasser bei überkritischem Druck als Kühlmittel und Moderator stellt eine große Herausforderung beim Design des High-Performance Light-Water Reactor (HPLWR) Brennelements dar. Bei überkritischem Druck (P=25 MPa) unterscheidet sich das thermodynamische Verhalten des Wassers infolge der starken Stoffwertschwankungen an der Pseudokritischen Linie vom Verhalten bei unterkritischen Druck. Aufgrund der gegenseitigen Abhängigkeit der Dichte des Moderatorwassers mit dem Neutronenspektrum besteht die Notwendigkeit der Kopplung zwischen der Neutronik und Thermohydraulik, was insbesondere zur Untersuchung lokaler Größen bei Designstudien notwendig ist. Gekoppelte Codes für Leichtwasserreaktoren können eine solch detaillierte Analyse des HPLWR-Brennelementdesigns nicht leisten, außerdem sind in ihnen keine Stoffwerte für überkritisches Wasser implementiert. Zu diesem Zweck sind der Monte Carlo N-Particle Code (MCNP) und der Unterkanalanalysecode STAFAS (Sub-channel Thermal-hydraulics Analysis of a Fuel Assembly under Supercritical conditions) gekoppelt worden. Beide Codes sind für die Modellierung komplexer Geometrien geeignet. Der MCNP Code wird für neutronische Analysen und die Vorhersage der Leistungsprofile einzelner Brennstäbe verwendet. Bei der thermohydraulischen Analyse berücksichtigt der Unterkanalcode STAFAS die Kühlmittelstoffwerte jenseits des kritischen Punktes sowie separate Moderatorkanäle. Wärmeübergangsmodelle vom Brennstab zum Kühlmittel, sowie vom Moderatorkasten zum Kühlmittel sind im Code implementiert. Mit diesem Codesystem werden Leistungs-, Druck- und Temperaturverteilungen in jedem beliebigen Brennelement berechnet.

Das gekoppelte Codesystem wurde anhand eines Designvorschlags für ein HPLWR-Brennelement getestet. Mit Hilfe eines Unterrelaxationsfaktors von 0,2 wurde eine schnelle Konvergenz der Rechnungen erreicht.

Das axiale Leistungsprofil eines HPLWR Brennelements besitzt zwei Maxima: Das größere Maximum tritt im unteren Bereich und ein kleineres im oberen Teil des Brennelements auf, was auf die Dichteverteilung von Kühlmittel und Moderator zurückgeführt werden kann. Die Analyse der Ergebnisse des HPLWR-Brennelements (konstante Anreicherung von 5%, 4% in den vier Eckstäben) ergab eine gleichmäßige axiale Leistungsverteilung im gesamten Brennelement. Auch die Temperaturverteilung des Kühlmittels in jedem Querschnitt ist sehr gleichmäßig. Eine Temperaturdifferenz von 50 °C liegt zwischen dem wärmsten und kältesten Unterkanal am oberen Ende des Brennelements. Die maximale Hüllrohraußentemperatur liegt immer unter der erlaubten Grenze von 620 °C.

Contents

List of Tables

List of Figures

1   INTRODUCTION

1.1   Supercritical water reactor concept

Innovation of nuclear power plants is needed to compete with other energy sources, such as advanced fossil fuel power (FFP). Since 2002 a Generation IV Nuclear Energy system development project has been initiated to enhance the future role of nuclear energy systems. Challenging technology goals for the generation IV (GEN-IV) nuclear reactor systems were defined in four areas: sustainability, economics, safety and reliability, proliferation resistance and physical protection.   Six nuclear systems were identified as GEN-IV reactors in the roadmap report, released in 2002 by the Department of Energy (DOE) in the United States [1], amongst which is the supercritical water reactor (SCWR). The background of the present research study is based on such GEN-IV supercritical water reactor, which is aimed at improving primarily the economy of current light water reactors by increasing the thermal efficiency substantially, simplifying systems involved and making equipments more compact.

The innovative concept of a supercritical water reactor (SCWR) has been studied over the past decade in Japan. A once-through cycle SCWR was developed by Oka and Koshizuka [2], [3] where the water enters into the core as liquid and exits at a high temperature and pressure. As supercritical water does not exhibit a change in phase, steam separation and coolant recirculation like in BWR are not necessary [2]. The outlet coolant is sent directly to the turbines without any intermediate heat exchanger. The significance of a once-through cycle is a one-loop system, which leads to a simplified plant system instead of a two-loop system in a typical PWR. The simplified plant system of a once-through cycle is compared to conventional LWR; coolant re-circulation system, steam separators and dryers of a BWR and steam generator, pressurizer and primary pumps of PWR are not necessary. The reactor pressure vessel (RPV) and control rods are similar to PWRs, containment and safety systems are compared to BWR and the balance of plant (BOP) is compared to supercritical fossil plants [2]. As a consequence, a comparison of the main characteristics of the once-through supercritical water reactor with other conventional light water reactors have shown an advantage, resulting also in a smaller containment as reported by Oka and Koshizuka [3]. The advantages of the SCWR over conventional light water reactor are summarised by Oka et al. [4]. A design of a direct supercritical water coolant breeder reactor is also investigated by Oka and Koshizuka [5]. Extensive research of the SCWR reactor concept has been reported from Japan since the launch of the concept. The elements of design of a high temperature LWR operating at supercritical conditions are described by Oka et al. [6], which

include: design of fuel rod, core, safety control and start-up system. Fuel rod design consisting of enriched uranium dioxide fuel pellets with Ni-alloy cladding for the SCWR is reported by Yamaji et al. [7]. Three dimensional core calculations with square fuel assembly for burn-up study have been presented by Yamaji et al. [8]. Details of the control system of the SCWR plant system are presented by Ishiwatari et al. [9]. Sub-channel analyses without any neutronics feedback is reported by Mukohara et al. [10] and Tanabe et al. [11]. The first 3D coupled thermal-hydraulics/neutronics for the SCWR was performed for a core by Yamaji et al. [12]. An improved core calculation with part of the coolant flowing downwards from the top of the core has been reported by Yamaji et al. [13], where the exit temperature increased to 530°C.

Due to the potential economic improvement reported by Oka et al. [14] the concept of a supercritical water reactor attracted international industries and research institutes to participate in the innovative concept. The concept studied in Japan Dobashi et al. [15], [16] introduced a core design with moderator rods to provide better moderation at the top part of the core because of the high heat-up. The first design of water rod core of a direct cycle supercritical water reactor was reported by Okano et al. [17]. In USA Buongiorno [18] proposed to study a SCWR with solid moderator instead of the water rod moderator adopted in Japan. In a separate study by Buongiorno et al. [19] zirconium hydrides were investigated as moderator material for a thermal spectrum SCWR. In Korea a feasibility study was started in 2002 by Joo et al. [20] on the thermal SCWR with cross-type solid moderators and single-pin. The research status of a supercritical pressure water cooled reactor in Korea was summarised by Bae et al. [21], where a rectangular fuel assembly was investigated. A thermo-hydraulic study without cross flow and neutronics feedback was reported by Bae et al. [22] for a hexagonal tight lattice core. In Russia channel type reactors with supercritical water coolant were considered as reported by Kuznetsov et al. [23]. In Europe a concept with water rods was adopted to enhance neutron moderation and a feasibility study of a SCWR was conducted in the between the years 2000 – 2002 under the 5th Framework European Programme. Due to the high pressure, high temperature and expected high efficiency, the European project was known as the High-Performance Light-Water Reactor (HPLWR). The HPLWR project was first announced in 2000 by Heusener et al. [24]. The main objective of the HPLWR was to determine the technical merit and economical feasibility of a supercritical water reactor. Selecting the fuel assembly design by Dobashi et al. [16] as a "reference point", partners in the HPLWR project investigated a wide range of technical issues, which were summarized by Squarer et al. [25]. The main study of the HPLWR concentrated on: The 'state-of-the-art status of supercritical water reactor', as reported by Oka and Koshizuka [3]. Basic design requirements of the HPLWR plant architecture was presented by

Bittermann et al. [26]. A square and hexagonal fuel assembly arrangement were proposed for the HPLWR core. The core design analysis for neutronics for the HPLWR was performed by Rimpault et al. [27] with the "reference design" by Dobashi et al. [16]. A first validation of the coupled neutron physics and thermal-hydraulics analysis was carried out by Broeders et al. [28] for the "reference design". Under the HPLWR project, Cheng et al. [29] - [31] performed a first sub-channel analysis on both the hexagonal and square fuel assemblies proposed by Bittermann et al. [26] without any coupling of neutron physics with thermal-hydraulics. Large uncertainties have been identified in heat transfer correlations as summarized in an intensive literature review on heat transfer at supercritical water pressure condition by Cheng and Schulenberg [31] in 2001. A preliminary study of material requirement for the HPLWR application was performed by Ehrlich et al. [32], showing that a maximum cladding temperature up to 620°C may be tolerated. The potential safety features of the HPLWR were reported by Aksan et al. [33]. The economical advantages for the HPLWR were presented by Bittermann et al. [34] defining a realistic target of 1000 €/kWe and 3-4 cent/kWh levelized generation cost. As a result a general plant concept of a 1000 MWe once-through supercritical water reactor was defined for the HPLWR in 2002 by Bittermann et al. [26]. The Reactor Pressure Vessel (RPV) of the HPLWR with 1000 MWe is outlined as shown in Figure 1.1.

The reactor consists of the core with an active height of 4.2 m and the reactor pressure vessel of about 4 m outer diameter and 13 m total height. The wall thickness of the lower cylindrical part of the RPV is 0.3 m, which reflects the high operating pressure. The RPV internal structure is designed such that the outlet steam is completely separate from the vessel. A hot box above the core collects the steam and supplies it to a co-axial pipe of the inlet and outlet lines in order to minimize thermal deformations and stresses. Guide rods are run through the hot box to each fuel assembly, carrying the moderator water, control rods and instrumentation tubes. The moderator water from the inlet of the RPV flows to the upper plenum and then downwards through moderator tube in the core as shown in Figure 1.1. The coolant water, which is a mixture of the down-comer flow and moderator water in the lower plenum, flows upwards through the sub-channels of each fuel assembly, see chapter.2 (Figure 2.3). The proposed characteristics of the HPLWR power plant outlined by Bittermann et al. [26] are summarized in Table 1.1.
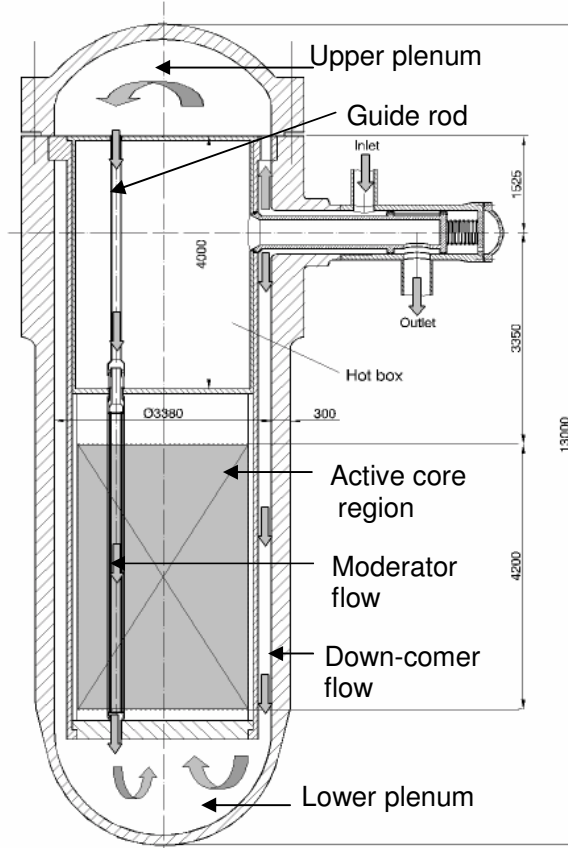
Figure 1.1: Reactor Pressure Vessel of HPLWR taken from Bittermann et al. [26]

Characteristics	Units	Approximate values
Gross plant electric output	MWe	1000
Efficiency	%	44
Thermal power	MW	2273
Nuclear steam supply system		
System pressure at the RPV	MPa	25
Fluid temperature at the RPV outlet	°C	500
Coolant mass flow rate	kg/s	1160
Core coolant inlet temperature	°C	280
Reactor core		
Active core height	mm	4200
Number of fuel assemblies		121
Fuel rod outer diameter	mm	8
Reactor pressure vessel		
Inner diameter	mm	3380
Design pressure	MPa	27.5
Design temperature	°C	350
Wall thickness of lower cylindrical section	mm	300

Table 1.1: Proposed characteristics of the HPLWR power plant by Bittermann et al. [26]

Despite substantial technical progress made by the HPLWR project open questions were identified, that required further investigation, if this type of reactor operating at supercritical water conditions shall be introduced in the market by vendors. Key technologies highlighted by the HPLWR project that required further investigation included:

- Cladding materials for temperature up to 620 ºC
- Improved coupled neutronics/thermal-hydraulics codes for design analysis
- Core and plant analysis
- Development of simplified sub-assembly design
- Optimisation of plant safety systems, including passive safety features

The main aim of the present work is focused on developing an improved method for the coupled neutronics/thermal-hydraulics design analysis of a HPLWR fuel assembly.

The motivation to perform a coupling of neutronics/thermal-hydraulics for design analysis of a HPLWR fuel assembly is due to the utilization of supercritical water in the core. At supercritical conditions, the thermal-physical properties of water shown by Wagner [35] vary strongly across the pseudo-critical line. The pseudo-critical line connects the maximum values of specific heat at different pressures above the critical point. The variation of specific heat with temperature is shown in Figure 1.2 at constant pressure. A maximum peak of 56 kW/kg.K at pressure of 25 MPa is obtained at the pseudo-critical temperature (384°C). The peak becomes higher the closer the pressure approaches the critical pressure. Exactly at critical pressure (22.1 MPa) the peak goes to infinity.
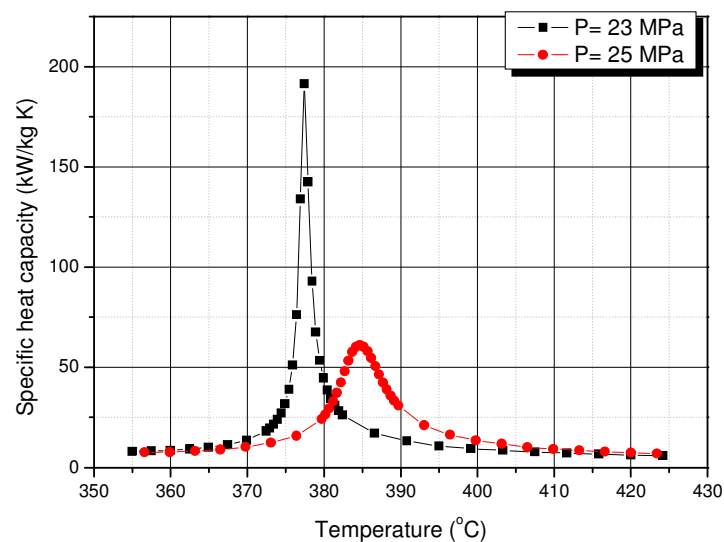
Figure 1.2: Specific heat of supercritical water obtained from Wagner [35]

Figure 1.3 shows the water density variation with temperature at different pressures. The water density decreases as the temperature increases in the core and in the vicinity of the pseudo-critical line where the specific heat has a maximum, a maximum density gradient is obtained. The coolant density drops by more than a factor of 7 from inlet to outlet of the core. Consequently, for a conventional LWR fuel assembly, this would lead to low moderation of the upper part of the core. At low moderation, less thermal neutrons are available for fission, which leads to lower power. For this reason, moderator water rods were introduced already in the first fuel assembly design by Dobashi et al. [15] in order to provide good moderation in the upper part of the core.
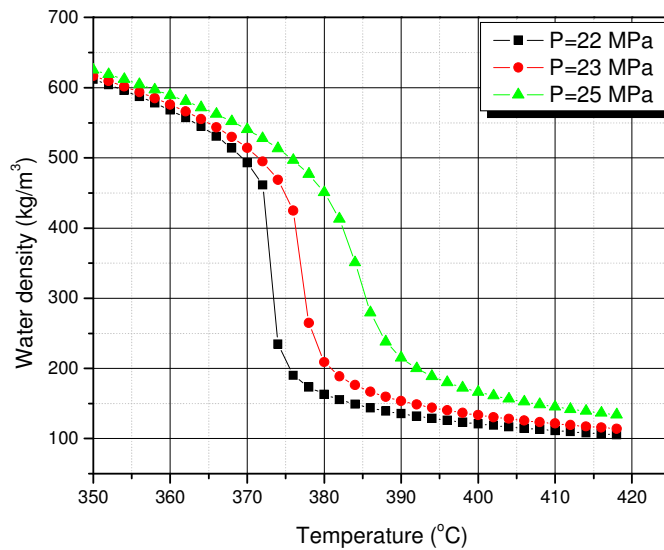
Figure 1.3: Density of supercritical water obtained from Wagner [35]

The water density distribution in the core is directly related to the moderation and subsequently to the neutron spectrum responsible for the fission power distribution. The power distribution, in turn, changes the coolant and moderator density. Due to the strong interaction between the power distribution and the water density distribution and the strong density variation of supercritical water in the core, a coupling of neutronics and thermal-hydraulics analysis is necessary for design analysis of a HPLWR fuel assembly.

The first thermal-hydraulic analysis by Cheng et al. [30] for the HPLWR fuel assemblies did not consider the effect of the water density variation on the power distribution. Instead a cosine power profile shape was assumed as in PWR. Also in the sub-channel analyses of a SCWR by Mukohara et al. [10] and Tanabe et al. [11] a cosine profile without any neutronics feedback was considered. The need to perform a coupled analysis of a HPLWR fuel assembly for accurate design analysis was argued. The first coupled approach carried out by

Broeders et al. [28] showed a strong effect of the water density on the power distribution. However, due to the limitations of computer codes for modelling complicated geometries, details of the fuel assembly, such as temperature distribution in the sub-channels and individual fuel rod power profiles could not be obtained Yamaji [12].

A more detailed coupled analysis of neutronics/thermal-hydraulics is presented in this study for design analysis of fuel assemblies at supercritical water conditions such as the HPLWR. The coupling procedure presented will also be applicable to other types of reactors with a density variation in the core such as in BWR.

1.2   Tools for Light-Water Reactor fuel assembly design

1.2.1   Requirements imposed by the reactor design

The design requirements of the computer codes necessary to perform a detailed coupled neutronics/thermal-hydraulics analysis of a HPLWR fuel assembly include:

i) Complex design modeling
The use of the moderator tubes with downward flow in the HPLWR fuel assembly introduces a challenge to the fuel assembly design. For accurate modeling, the computer codes must have the capability for downward flow phenomena in the moderator tube, to analyze the moderator effect on the design.

ii) Supercritical properties for water
One of the special features of the HPLWR is the utilization of supercritical water in the core. The computer codes must have the capabilities of water properties at supercritical pressure conditions.

iii) Heat transfer coefficient
The modeling of heat transfer between the solid surfaces and the coolant is needed in the thermal-hydraulics code for calculating the required cladding temperature. Flexibility of the thermal-hydraulic code is required to implement different heat transfer coefficients, in order to investigate the influence of the different heat transfer correlations, as there are still large uncertainties in heat transfer prediction at these supercritical conditions.

iv) Power distribution

Due to the strong density variation of supercritical water, the analysis of the power distribution in each fuel rod is mandatory for detailed design analysis of a HPLWR fuel assembly. The coupled computer codes must be capable of modelling the power distribution in individual rods of the fuel assembly without averaging in order to study the effect of the local power distribution on the thermal-hydraulics property variation.

1.2.2 Neutronics codes available for coupling

A literature review of available coupled codes for application to LWR's analysis has been conducted to investigate their capabilities for HPLWR applications. In order to identify the types of codes coupled, different types of methods implemented into neutronics codes and thermal-hydraulics codes need to be discussed. The neutron flux can be predicted with diffusion codes, deterministic codes and Monte Carlo methods.

i) Diffusion codes

Diffusion codes solve the neutron diffusion equation to obtain the neutron flux, from which the power distribution is computed. They use macroscopic cross section data for neutron particles, processed usually from two or more energy groups. The modelling of a reactor core or fuel assembly is homogenized for the diffusion approximations to be valid. Diffusion codes have been well suited to analyse reactors, which are designed with relatively homogeneous distributions of fuel, moderator and absorber materials. However, with higher heterogeneity such as in the HPLWR fuel assembly, the simplified model will produce inaccurate results. Details of the HPLWR fuel assembly such as coolant density in different sub-channels and power distribution of different fuel rods, which are needed in the coupling, cannot be obtained.

Until now, coupling experience for PWR and BWR reactor have been with diffusion codes coupled with system codes, which have been applied for various transient analyse. For transient analysis diffusion codes and system codes are restricted to simplified geometries and their application cannot be extended to complex geometries such as for fuel assembly design of a HPLWR. The CRISSUE-S partners under the work-package WP 2 and WP 3 published a list of available coupled diffusion codes for LWR application [36], [37], [38]. The neutron flux codes, based on such diffusion methods have been coupled with system codes and are discussed to give an insight into the different types of coupled application available in PWR and BWR reactors.

The neutronic code PARCS (Purdue Advanced Reactor Core Simulator) developed at the Purdue University is used to predict the dynamic response of the reactor to reactivity perturbations such as control rod movement or change in temperature/fluid conditions in the reactor core. A coupling interface of PARCS with TRAC-M, a system code, was completed by Miller et al. [39]. The coupled code was tested using the OECD PWR main steam line break (MSLB). The coupled TRAC-M/PARCS was also applied for turbine trip (TT) transient analysis of the OECD/NRC BWR by Lee et al. [40]. The PARCS code has also been coupled with the system code RELAP5 for analysis of the peach bottom turbine trip (TT), Salah et al. [41].

DYN3D is a neutron kinetic code developed to investigate reactivity transients in the reactor core with hexagonal or quadratic fuel assembly. The neutron diffusion equations are solved for two groups. An internal coupling approach of DYN3D with ATHLET, is a system code that has been developed by Grundmann et al. [42]. The coupled code DYN3D/ATHLET has been applied for analysis of BWR TT transient [43].

The SKETCH-N code solves neutron diffusion equation in x-y-z geometry for steady state and neutron kinetic problems. The code treats an arbitrary number of neutron energy group and delayed neutron precursors. The SKETCH code has been implemented in to thermal-hydraulic code TRAC for analysis of rod injection transients Asaka et al. [44].

NEM (Nodal Expansion Method) is a 3-D multi-group nodal code developed and used at the Pennsylvania State University for modelling both steady state and transient core conditions. The code has options for modelling 3-D Cartesian, cylindrical and hexagonal geometry [45]. NEM has been coupled to the system code TRAC-PF for MSLB transient analysis of a PWR Ivanov et al. [46], [47], Ziabletsev et al. [48] and for BWR core transient, NEM has been coupled with TRAC-BFI by Fu et al. [49].

NESTLE is a multi-dimensional neutron kinetic code developed at the North Carolina State University. It solves the two group or four group neutron diffusion equations in Cartesian or hexagonal geometry [50].

QUABOX is a neutron kinetic code developed in the 70s at GRS in Germany for 3-D core neutron flux and power calculations in steady state and transient conditions. It solves the two-group neutron energy diffusion equation through local polynomial approximation of the neutron flux. The QUABOX code has been coupled with ATHLET internally for analysis of the OECD/NRC BWR turbine trip benchmark by Langenbuch et al. [51]. A serial coupling is

applied. The T-H code ATHLET makes the first calculation step and when it is finished the core model QUABOX/CUBBOX calculates the same step for the neutronics on the same computer.

PANBOX is a three dimensional neutron kinetics code coupled with a multidimensional core thermal-hydraulics module, developed to perform PWR safety analysis and transients in which power distribution is significantly affected. The time-dependent few-group diffusion equation is solved in Cartesian geometry using a semi-analytical nodal expansion method (NEM). The PANBOX code system has been coupled with the thermal-hydraulic system code RELAP for analysis of the OECD/NEA PWR MSLB, Sanchez-Espinoza et al. [52]. Verification of the coupled PANBOX /RELAP was preformed by Jackson et al. [53] for core transient analysis.

ii) Deterministic codes

Deterministic codes are most commonly based on the discrete ordinates method. They solve the Boltzmann transport equation for the average particle behaviour to calculate the neutron flux. With discrete ordinate methods, the phase space is divided into many small boxes and particles are moved from one box to another. If this approach is to be used for modelling a HPLWR fuel assembly, the moderator rods, the coolant sub-channels, and fuel rodsl will be homogenized and the medium is discretised to solve the transport equation. This type of geometry modelling will not accurately represent the important design details essential for the HPLWR fuel assembly. Deterministic codes use macroscopic cross section data, which are processed from multi-group energies. Processed macroscopic cross section data from microscopic scale are required for different parts in the geometry. For complicated geometries with varying parameters such as coolant and moderator density, preparation of the macroscopic cross section data would also require a lot effort. Therefore deterministic codes need to be homogenized for complex geometries. The global solutions are obtained with truncated errors. Computer codes based on deterministic methods include DORT, two-dimensitional (X-Y, and R-Z) geometries, TORT, a three-dimensional discrete transport code [54], [55], DORT-TD, a transient neutron transport code [56], KARPOS, a modular system code developed by Broeders et al. [57].

iii) Monte Carlo Method

A Monte Carlo method does not solve an explicit equation like the deterministic code, but rather obtains the answers by simulating individual particles and recording some aspects (tallies) of their average behaviour. Monte Carlo codes use a continuous energy scale to represent the variation of cross section data. They are widely used because of the capability of complex geometries modelling and accurate solution produced with the continuous energy

scale used to represent the cross section data. Computer codes based on the Monte-Carlo methods include: MCNP (Monte Carlo N-Particle) is a general-purpose, continuous-energy, generalized-geometry, coupled neutron/photon/electron transport code. The MCNP code for neutronics analysis is described by Briesmesiter [58] from the Los Alamos National laboratory. Different versions of MCNP have been developed, for example MCNP4C for low energy calculation and MCNPX for higher energies. The application of the Monte Carlo codes in nuclear energy is increasing for fuel assembly and core design analysis typically in BWR [59] where the density varies in the core. Mori et al. [60], [61] has already coupled the Monte-Carlo MCNP has been successfully coupled with a thermal-hydraulics system code for power and reactivity analysis of a supercritical fast reactor (SCFR) core that does not include moderator tubes, hence a simplified design.

1.2.3 Thermal-hydraulics codes

i) System codes
System codes are based on a lumped parameter approach. This means, for nuclear power plant (NPP) application the components in the primary and secondary system are represented by a one-dimensional model. Details of a fuel assembly such as moderator rod, individual sub-channels for density variation study cannot be revealed through such means. The basic equations for continuity, momentum and energy are applied and averaged and the thermal-hydraulic properties for each component are obtained. The smallest volume is typically a total core or major parts of it. System codes are commonly used in LWR application for different types of transient and safety analysis. Widely used system codes include:

ATHLET, (Analysis of Thermal-hydraulics of LEaks Transient) has been developed by the Gesellschaft für Reaktorsicherheit (GRS) for analysis of anticipated and abnormal plant transients, small and intermediate leaks and large breaks in light water reactors. The concept of ATHLET for analysis of PWR and BWR system has been described by Burwell et al. [62]. The ATHLET code has been coupled with the 3-D core model neutronic code DYN3D for analysis of BWR turbine trip benchmark, Grundmann et al. [43]. Validation of the ATHLET thermal-hydraulics code for PWR and BWR was presented by Glaeser [63]. The coupling interface of ATHLET with the neutronic core model DYN3D has been reported by Langenbuch et al. [64]. The coupled code ATHLET – QUABOX/CUBBOX has been used by Langenbuch et al. [51] for analysis of the OECD/NRC BWR turbine trip benchmark.

RELAP (Reactor Excursion and Leak Analysis Program) is used for transient simulation of LWRs. It is widely used for LWR transient analysis in PWR and BWR. The RELAP5 code has been coupled with point kinetic code for analysis of OCED/NEA PWR MSLB by Sanchez-Espanioza [65], [66] and Nigro et al. [67]. Bovalini et al. [68] reported coupled application of RELAP and comprison with different codes for TMI-MSLB.

The CATHARE code is used for transient analysis of PWR plants, VVER and BWR. The CATHARE code has been coupled with CRONOS2-FLICA4 for BWR turbine trip analysis Mignot et al. [69].

ii) Sub-channel codes

Sub-channel codes are used for multi-component modelling in the core. A core is represented by the sub-assemblies and the sub-assembly by different sub-channels and other water channels and fuel rods. The basic equations are solved for control volumes in the scale of sub-channels. The sub-channel codes are capable of three-dimensional geometry modelling. Codes that are based on this approach include:

COBRA (Coolant Boiling in Rod Arrays) is a public computer code used for thermal-hydraulics analysis with implicit cross-flow between adjacent sub-channels, single flow and homogeneous two-phase fluids. It is used world-wide for DNBR (departure from nucleate boiling ratio) analysis in LWR sub-channels as well as for 3-D whole PWR core simulation with one or more channels per fuel assembly, Wheeler et al. [70].

MATRA (Multi-channel Analyser for steady states and Transient in Rod Arrays) is a sub-channel analysis code developed at KAERI (Korea Atomic Energy Research Institute), Yoo et al. [71]. The main concept of the MATRA code is based on COBRA.

The STAFAS (Sub-channel Thermal-hydraulics Analysis of Fuel Assembly under Supercritical Conditions) code was developed by Cheng et al. [29]. It is based on the concept of the COBRA code but includes special features of the HPLWR such as: downward flow of the moderator water and incorporates steam table, that allows the prediction of supercritical water properties. The code is flexible and allows for complex geometry modelling. Heat transfer from solid surfaces can be easily implemented. The present version of the STAFAS code is for steady state conditions and single-phase flow only.

FLICA-4 is a thermo-hydraulic code developed at the French Atomic Energy Commission (CEA) for computing three-dimensional, transient or steady, two-phase flows in nuclear

reactors. The code is described in the paper by Allaire [72] for 3-D transient computation. The FLICA code has been coupled with the system code CATHARE and CRONOS2, a 3D neutronics code for computation of a BWR turbine trip, Mignot et al. [69].

iii) Computational Fluid Dynamics (CFD) codes

The strategy of CFD is to replace the continuous domain with a discrete domain using a grid. The geometry is discretized with a typical mesh size of less than a volume and the thermal-hydraulics properties are computed for every grid point defined. The conservation equations for mass momentum and energy are solved in a discrete form. Any complex geometry is possible, the extremely fine resolution costs computation time. The CFD approach is mostly preferred for small geometries. Existing CFD codes include: FLUENT [73], CFX [74].

1.2.4 Coupled computer codes for LWR application

An overview of available coupled neutronics/thermal-hydraulics code published up to now has been reported by CRISSUE-S partners, in the work package 2 (WP2) for PWR and BWR [37]. Table 3 summarises a list of coupled codes for PWR, BWR and HPLWR to date, from the CRISSUE-S WP 2 report, with the computer codes described in the previous chapters.

Coupled code	Nuclear power plant	Transient type
J-TRAC TRACE-BFI SKETCH-N	PWR	Reactivity Initiated Accidents (RIA)
RELAP5/MOD3.2 COBRA IIIC QUABOX/CUBBOX	PWR	Main Steam Line Brake (MSLB)
RELAP5/MOD3.2.2 NESTLE	PWR and AP 1000	MSLB
RELAP5/MOD3.2.2 PARCS	PWR(B&W TM1-1)	MSLB
RELAP5/MOD3.2.2 QUABBOX		
RELAP5/MOD3.2.		
RELAP5/3-D NESTLE		
TRAC-PF1 NEM	PWR(B & W)TM-1	Rapid Environmental Assessment
	BWR Peach bottom unit 2	Turbine trip (TT)
PANBOX	PWR	Maximum local heat flux investigation
RELAP5 KAPROS	HPLWR	Fuel Assembly test (FA)
TRAC-PF NEM	PWR (B & W)TM-1	MSLB
RELAP PARCS	Three loop PWR	Peripheral rod ejection

Table 1.2: Summary of coupled computer codes for PWR, BWR and HPLWR

From the literature review, most of the available coupled codes for neutronics/thermal-hydraulics are based on diffusion and system codes resulting in a rather coarse resolution of the core. For a detailed analysis of a HPLWR fuel assembly analysis, diffusion codes and system codes are not giving enough local information. All prior application had been to PWR and BWR transient analysis. The first coupled code for the HPLWR fuel assembly study was a deterministic code KAPROS (KArlsruhe PROgram System) and the system code RELAP5 [28]. With this coupled analysis the fuel assembly of the HPLWR was modelled using a

supercell model. A supercell model defines a finite fuel assembly model by a single cell. The details of individual sub-channels and fuel rods are averaged. Therefore exact parameters within the fuel assembly were not obtained. However the strong interaction of the power distribution and water density was already observed. To accurately analyse a HPLWR fuel assembly a more detailed analysis fuel rod wise and sub-channel wise is required to predict a hot spot and the temperature distribution around the circumference of a fuel rod. In order to perform such detailed analysis of the HPLWR fuel assembly, a new coupled code system is required.

From the reviewed neutronics and thermal-hydraulic computer codes, the Monte Carlo code and sub-channel codes show to be the best choice of codes to be coupled for detailed fuel assembly analysis. Both have similar spatial resolution. The smallest control volume is in the order of a few cm in both cases. System codes on the other hand would be too coarse for MCNP and CFD codes too fine in resolution.

1.2.5 Requirements to the coupling algorithm

Certain requirements with regards to the coupling of thermal-hydraulics codes and neutronics codes have been discussed in the CRISSUES-S work package-2 report, [37]. Detailed description of the interface requirement to couple thermal-hydraulic code to 3-D neutronic code has been reported by Langenbuch et al. [64]. The objective to couple neutronics code with a thermal-hydraulics code is to provide an accurate solution in a reasonable amount of CPU time. For the present study, the basic components that are considered for the coupling methodology include:

i) Coupling design
Two different approaches are generally utilized to couple neutronics codes with thermal-hydraulics. There is the serial integration coupling and parallel processing coupling. Serial integration requires modifications of the codes usually performed by implementing a neutronics sub-routine into the thermal-hydraulic code. Parallel processing allows the code to run separately and exchange data during the calculation. In this study the serial integration approach is required to allow for modification of the codes for application of HPLWR fuel assembly.

ii) Coupling method
There are two different ways of coupling, internal and external coupling. With internal coupling the neutronics code is integrated within the thermal-hydraulic code. While with

external coupling, the two codes run externally and exchange information between each other. An external coupling is considered in the present study.

iii) Spatial mesh overlay

Accurate mapping of mesh or volumes between the two codes is important to exchange information between each other.

iv) Coupled convergence schemes

A convergence scheme of the two codes needs to be defined. For a final convergence of the coupled codes, independent convergence in the individual codes is required.

1.3   Aim of the study

The aim of this study is to develop a coupled algorithm with a neutronics and thermal-hydraulics code. The coupled algorithm is to be used for a detailed design analysis of a fuel assembly where density variation in the sub-channels and power distribution in the fuel rods varies strongly. Typical application is the HPLWR concept operating at supercritical pressure condition. To satisfy the design requirements described in Section 1.2.1, the Monte Carlo code MCNP and sub-channel code STAFAS have been selected for the coupling. The Monte Carlo code MCNP is an internationally recognised code for nuclear reactor application and the STAFAS code is capable of modelling downward flow in the moderator tube and includes supercritical water properties. The STAFAS code is based on the well-known thermal-hydraulics code COBRA. Both codes are capable of similarly complex geometry modelling. The parameters that are exchanged between the two codes for the coupling are: power distribution from MCNP code, water density distribution, water temperature distribution and fuel temperature distribution from STAFAS code, as shown in Figure 1.4. A serial integration coupling approach is used. The STAFAS code, which is written in FORTRAN 90 language, is modified to include the power distribution obtained from neutronics analysis. An external approach of data exchange is used, where both codes run separately and exchange data after each run via a batch file.

- Power distribution in the fuel rods

| **MCNP code**
Neutronics analysis | **STAFAS code**
Thermal-hydraulics analysis |

- Water density, water temperature distribution in
  the sub-channels
- Fuel temperature distribution in the fuel rods
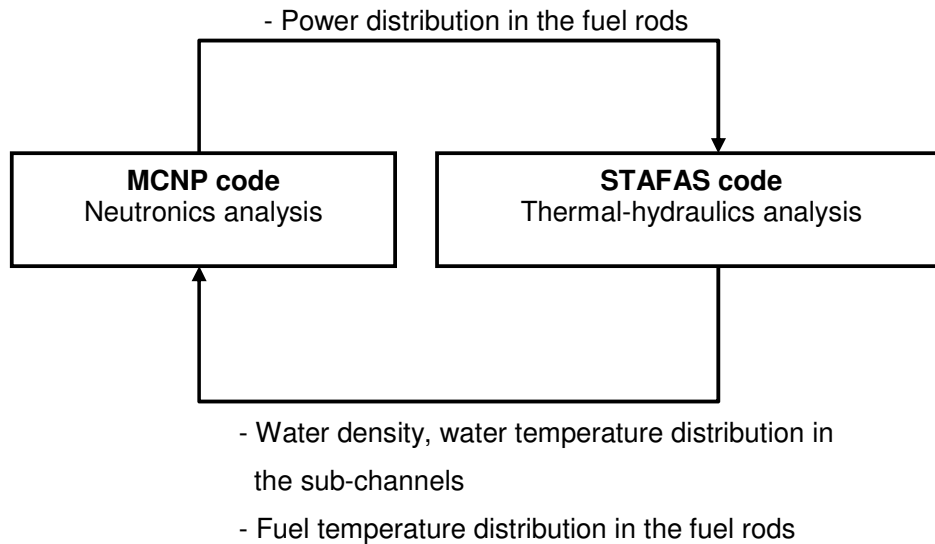
Figure 1.4: Coupled MCNP/STAFAS method

Chapter 2 describes the mathematical models for the MCNP power distribution and STAFAS for thermal-hydraulics conditions. The numeral models of the individual code and coupled code system are described in chapter 3. The coupled code system of MCNP/STAFAS was tested on a one-eighth fuel assembly design and results from the analyses on the coupling procedure are described. The results from the test analysis on the fuel assembly design are reported in chapter 4. A conclusion on the coupling method tested for analysis of a HPLWR fuel assembly design analysis is given in chapter 5.

2 DESCRIPTION OF THE COUPLED METHOD APPLICATION

2.1 Fuel assembly configuration

To test the coupled code system of MCNP/STAFAS a recent HPLWR fuel assembly design proposed by Hofmeister et al. [75] has been analyzed. The fuel assembly configuration shown in Figure 2.1 consists of a 7 by 7 fuel rod array arranged in a square lattice and a single moderator tube at the centre displacing 9 fuel rods. The fuel rods have an outer diameter of 8 mm with a gap of 0.15 mm between the cladding and fuel pellet and a cladding thickness of 0.5 mm. The ratio of pitch to diameter (P/D) is 1.15. An active height of 4.2 m and the inactive part of 0.255 m of the fuel assembly is modelled. There is a gap of 10 mm filled with moderator water between the assemblies when arranged in the core, which is known here as assembly gap. The design parameters of the fuel assembly are shown in Table 2.1. Due to symmetry, only one-eighth of the square fuel assembly was modelled for the test analysis.
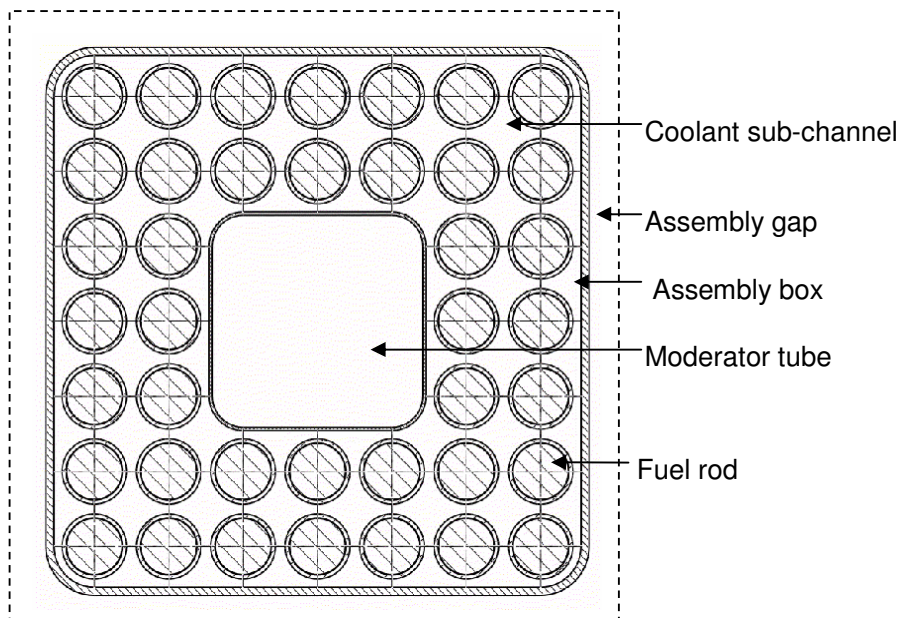
Figure 2.1: Fuel assembly design of the HPLWR obtained from Hofmeister et al. [75]

Parameters	Units	Values
Fuel rod diameter	mm	8.0
Cladding thickness	mm	0.5
Active height	mm	4200
Inactive part below and above the active part	mm	255
Pitch/Diameter ratio (P/D)	-	1.15
Moderator box length	mm	26
½ gap around one fuel assembly	mm	5.0
Gap between fuel rod and box wall	mm	1.0

Table 2.1: Fuel assembly geometry data

Details of the one-eighth fuel assembly are shown in Figure 2.2. The assumption of symmetry reduces the fuel assembly to 9 sub-channels and 7 fuel rods as labelled in Figure 2.2.
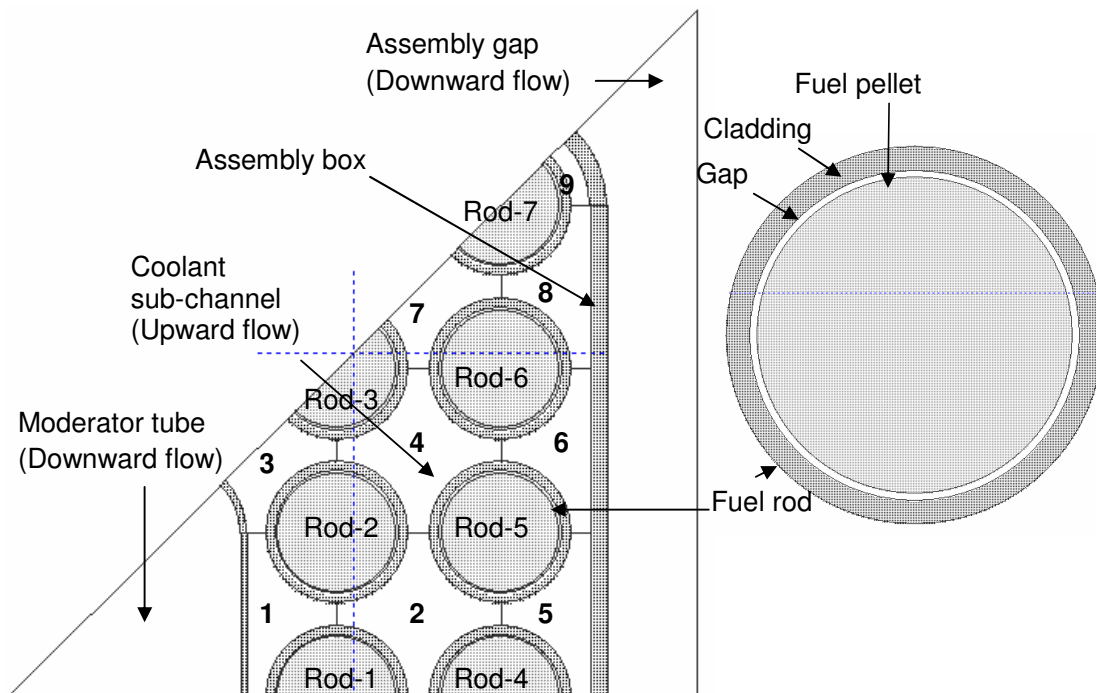
Figure 2.2: One-eighth of the square fuel assembly with sub-channel and fuel rod labels

The downward flow of the moderator water is considered same as that proposed in the design by Bittermann et al. [26]. Figure 2.3 shows a sketch of the flow path in the axial direction in the reactor pressure vessel (RPV) of a HPLWR.

19
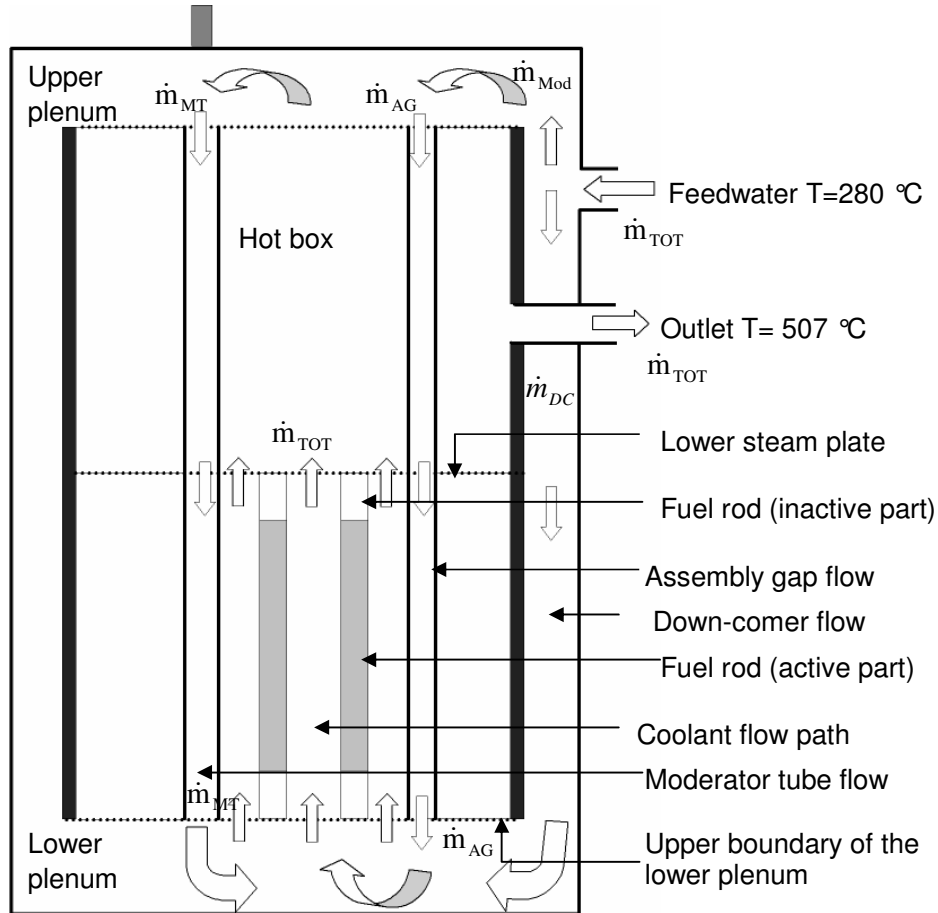
Figure 2.3: Sketch representing the main the flow path in the HPLWR RPV

The feedwater enters the reactor pressure vessel at 280°C, where it is divided into two parts. One part flows as the moderator water $\dot{m}_{Mod}$ to the upper plenum where it is sub-divided to flow through the moderator tubes $\dot{m}_{MT}$ and through the assembly gaps $\dot{m}_{AG}$ downwards. The other part goes through the down-comer $\dot{m}_{DC}$ to the lower plenum where it merges with the moderator flow. The total feedwater flows upwards as coolant through the sub-channels, where it is heated by the fuel rods and is assumed to exit the RPV at 507 °C.

A total power of 327.5 kW for the one-eighth fuel assembly and the total coolant mass flow rate of 0.167 kg/s were assumedf for the test analysis, from which an average coolant exit temperature of 507 °C was evaluated. With these assumptions, a total thermal power of 2620 kW was calculated. With the square fuel assembly design Hofmeister et al. [75] proposed a core arrangement with 88 clusters and 9 fuel assemblies per cluster. Therefore a total thermal power of 2075 MW can be obtained which is about 9% lower than that proposed by

Bittermann et al [26]. The average rod power and power density calculated for this fuel assembly configuration is 15.6 kW/m and 104 MW/m^3 respectively. The average power density computed is similar to that of a typical PWR. The average coolant mass flux of 890 kg/m^{2}s is slightly lower than that defined by Bittermann et al. [26].

Parameters	Units	Values
Coolant exit temperature	°C	507
Total power of the 1/8th fuel assembly	kW	327.5
Average rod power	kW/m	15.6
Power density	MW/m^3	104
Average coolant mass flux	kg/m^{2}s	890.3

Table 2.2: Parameters for the 1/8th square fuel assembly

The geometric parameters of the 9 sub-channels modelled in STAFAS are given in Table 2.3. The sub-channel parameters calculated in STAFAS are: - the cross-sectional flow area A, the heated perimeter (P_{ht}), which is the perimeter of the fuel rod connected to the sub-channel, wetted perimeter (P_{wt}), defined as the perimeter of the sub-channel covered by coolant, hydraulic diameter (D_h) (see Equation 2.1) and the inlet coolant mass flux (G_o). The mass flux at the inlet is adjusted using Equation (2.2) to obtain the same axial pressure drop over the first axial mesh for all sub-channels (see chapter 2.2.8 for inlet conditions). A large hydraulic diameter and area are calculated in sub-channels 2 and 4. Sub-channel 9 at the corner has the smallest hydraulic diameter. With this difference in hydraulic diameter a strong non-uniformity of the mass flux distribution in the fuel assembly can be expected.

Sub-channel label	Area (mm^2)	P_{ht} (mm)	P_{wt} (mm)	D_h (mm)	G_0 (kg/m^{2}s)
1	20.9	12.6	21.8	3.8	790.5
2	34.4	25.1	25.1	5.5	1003.2
3	14.7	9.4	12.7	4.6	894.3
4	34.4	25.1	25.1	5.5	1003.2
5	20.9	12.6	21.8	3.8	790.5
6	20.9	12.6	21.8	3.8	790.5
7	17.1	12.6	12.6	5.4	997.5
8	20.9	12.6	21.8	3.8	790.5
9	3.5	3.1	7.1	2.0	510.7

Table 2.3: Sub-channel data

The hydraulic diameter D_h of the sub-channel is defined as:

$$D_h = \frac{4A}{P_{wt}} \qquad (2.1)$$

where A is the sub-channel cross section area and P_{wt} is the wetted perimeter

The pressure drop in the sub-channels is calculated by (Equation 2.2), where G is the mass flux, D_h is the hydraulic diameter of the sub-channel, l the length between the sub-channels and the friction factor is represented by f. The friction factor is a function of the Reynolds number defined by the Blasius equation in Equation (2.3)

$$\Delta P = \frac{1}{2}\frac{G^2}{\rho}\frac{l}{D_h}f \qquad (2.2)$$

where G is the mass flux, ρ is the density.

The friction factor is defined as:

$$f = \frac{0.3164}{\sqrt[4]{\mathrm{Re}}} \quad 2320 < \mathrm{Re} < 10^5 \qquad (2.3)$$

where the Reynolds number is defined as:

$$\mathbf{Re} = \frac{\mathrm{GD_h}}{\mu} \qquad (2.4)$$

and μ is the dynamic viscosity.

2.1.1 Boundary conditions in MCNP

Table 2.4 shows the physical constraints in MCNP. A UO_2 fuel with 5% ^{235}U enrichment in the fuel rods 1 to 6 and 4% enrichment in the corner rod 7 is used. For the test case the coolant and moderator density and temperature and fuel temperature is constant as shown in Table 2.4 for the initial calculation in MCNP. The temperature variation of cross-section data of the fuel isotopes is included. The cross section data for the fuel are obtained from the JEFF-2.2 library. A stainless steel alloy 316 has been selected as the cladding material. This

is a high level corrosion resistant material with Iron (Fe) content of about 65%, nickel content of about 14% and chromium of about 17%. The composition of the alloy- 316 specified in MCNP is shown in Table 2.5.

Parameters MCNP input	Density (kg/m³)	Temperature of the cross section library (°C)
Fuel - UO_2 (5% enrichment and 4% in the corner rod)	10600	1227
Cladding - Alloy 316	7450	527
Moderator	769	287
Coolant	769	287

Table 2.4: Boundary conditions in MCNP

Alloy 316 composition			
Iron (Fe)	63.55 %	Molybdenum (Mo)	2.75%
Chromium (Cr)	17%	Manganese (Mn)	1.5 %
Nickel (Ni)	14%	Titanium (Ti)	0.4%
Silicon (Si)	0.7%	Copper (Cu)	0.1%

Table 2.5: Material composition for Alloy 316

The cross section data for the cladding material isotopes are obtained from JEFF-2.2 library at constant temperature of 527 °C. The region above and below the active fuel rod is filled with water, and is assumed to be at a constant temperature of 287 °C. The water density and water temperature of the coolant in the sub-channels and of the moderator water in the moderator tube and assembly gap are assumed constant for iteration 1 in MCNP calculation.

2.1.2 Boundary conditions in STAFAS

The constraints defined in the STAFAS code for the analysis of the one-eighth fuel assembly are given in Table 2.6. The system pressure of 25 MPa at the RPV is maintained at the inlet of the moderator tube and assembly gap. The mixed water of the down-comer flow and moderator water in the lower plenum is modelled as the inlet conditions of the coolant in the sub-channels. The heat-up of the moderator flow from the upper plenum via the hot box is not considered. Instead, the inlet temperature of the feedwater at 280°C in the RPV is

maintained as the inlet condition of the moderator water. For the test case, a total coolant mass flow rate of 0.167 kg/s is assumed to flow through the sub-channels in order to achieve the design criteria defined by Bittermann et al. [26] for the HPLWR. Out of the total mass flow 8.32% is assumed to flow through the assembly gap, 16.65% to flow through the moderator tube and the remaining 75% is assumed as down-comer flow.

Parameters	Unit	Value
Inlet pressure of the moderator channels	MPa	25
Inlet temperature of the moderator channels	°C	280
Total coolant mass flow rate	kg/s	0.167
Mass flow rate in the moderator tube	kg/s	0.0139 (8.32%)
Mass flow rate in the assembly gap	kg/s	0.0278 (16.65%)

Table 2.6: Boundary conditions in the STAFAS code for the 1/8th fuel assembly

2.2 Mathematical model

2.2.1 Total mass flow rate

The total mass flow rate of the feedwater entering into the RPV is denoted here by $\dot{m}_{TOT}$. The mass flow balance in the lower plenum is defined by the moderator mass flow $\dot{m}_{Mod}$ and down-comer mass flow $\dot{m}_{DC}$ as:

$$\dot{m}_{TOT} = \dot{m}_{Mod} + \dot{m}_{DC} \tag{2.5}$$

The total mass flow rate in the lower plenum goes upwards through the coolant sub-channels. To determine the mass flow in each sub-channel the different types of sub-channel geometry and the mass exchange at the interface of two sub-channels (i.e. transversal mass flow) have to be taken into consideration. For the square fuel assembly considered (see Figure 2.1) four different types of sub-channels are identified as shown in Figure 2.4.
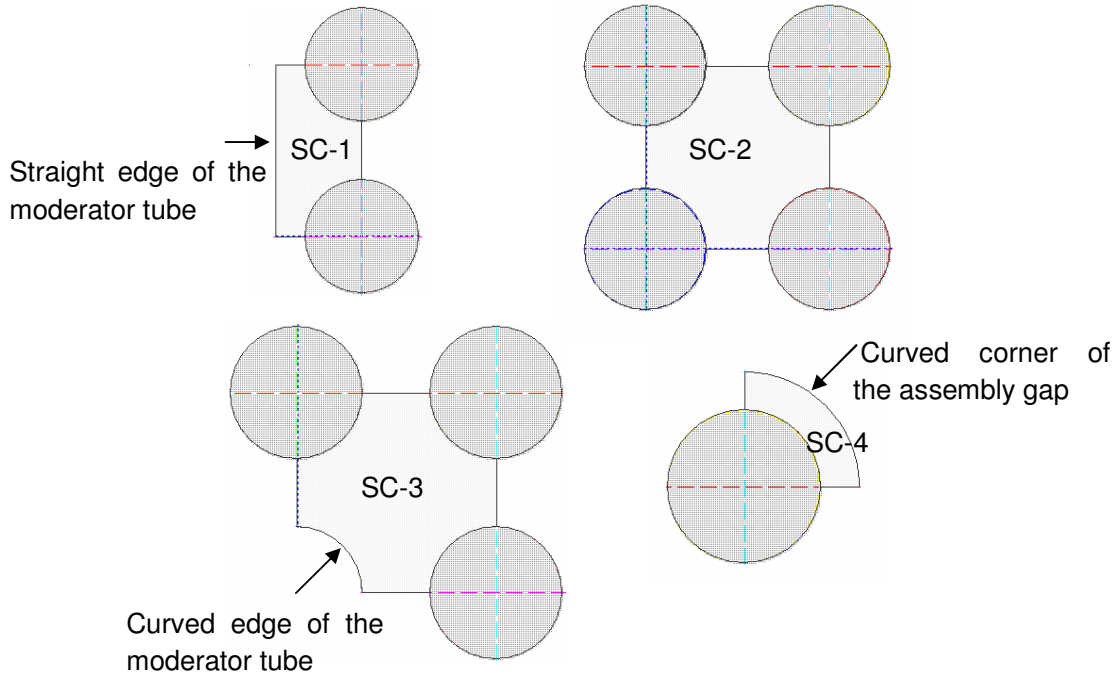
Figure 2.4: Sub-channel types of the square fuel assembly by Hofmeister et al. [75]

The square fuel assembly in Figure 2.1 consists of 60 sub-channels in total with 32 sub-channels of type1, 20 sub-channels of type 2, 4 sub-channels of type 3 and 4 sub-channels of type 4. As shown in Figure 2.4, SC-1 represents the sub-channels adjacent to the side of the moderator flow channels (moderator tube and assembly gap), SC-2 represents the central sub-channels formed by four fuel rods. The sub-channel SC-3 is adjacent to the corner of the moderator tube and SC-4 is at the corner of the assembly gap. Taking the different sub-channel types into consideration the total coolant mass flow rate in the core is expressed as:

$$\dot{m}_{TOT} = N_{as}.\left(32 \cdot \dot{m}_1 + 20 \cdot \dot{m}_2 + 4 \cdot \dot{m}_3 + 4 \cdot \dot{m}_4\right) \tag{2.6}$$

N_{as} is the total number of fuel assemblies in the core

The mass exchange between connecting sub-channels is modelled in STAFAS as described by Todreas and Kazimi [76].

25

2.2.2 Flow path modelled in STAFAS

The one-eighth square fuel assembly was modelled in STAFAS. The axial flow region modelled is between the lower steam plate and the upper boundary of the lower plenum. The flow in the upper plenum, hot box, lower plenum and down-comer was not considered. The coolant flows upwards through the sub-channels. The inlet boundary conditions of the coolant are obtained at the first cell describing the region between lower boundary of the active height and upper boundary of the lower plenum. The moderator water flows downwards from the top of the active height. The moderator water inlet boundaries are defined at the first cell describing the region between the lower steam plate and the top boundary of the active height. The flow path in the vertical cross-section of the one-eighth fuel assembly is shown in Figure 2.5. The axial meshing of one part of the fuel assembly is described in chapter 3.1.
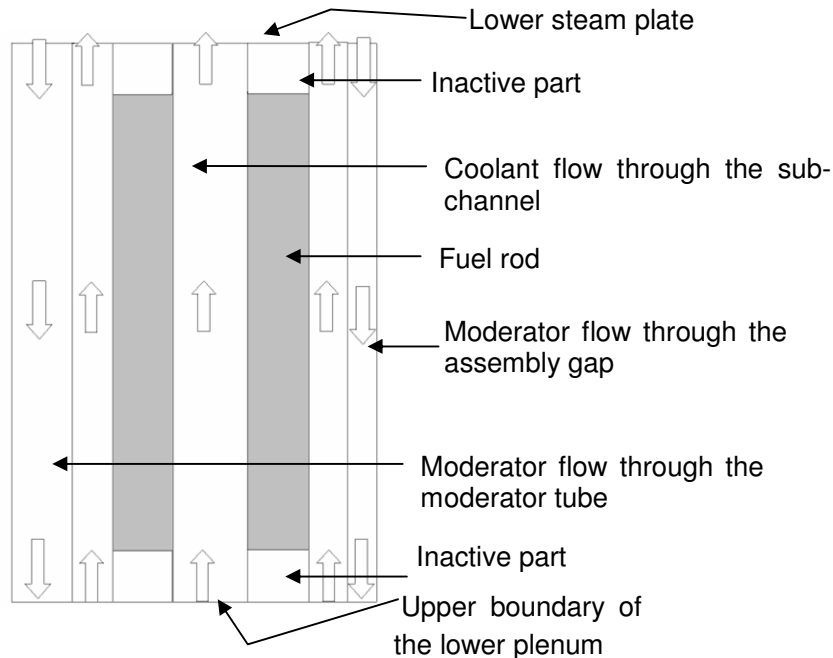
Figure 2.5: Vertical cross-section of the one-eighth fuel assembly

Assumptions in the STAFAS model

i) The moderator tube thickness and assembly box thickness is neglected.

ii) For the test analysis 25% of the total mass flow goes as moderator water $\dot{m}_{Mod}$, out of which 8.32% flows through the moderator tube $\dot{m}_{MT}$ and the remaining 16.65% through the assembly gap $\dot{m}_{AG}$. The mass flow is defined as follows:

$$\dot{m}_{Mod} = 0.25 \cdot \dot{m}_{TOT} \tag{2.7}$$

$$\dot{m}_{MT} = 0.0832 \cdot \dot{m}_{TOT} \tag{2.8}$$

$$\dot{m}_{AG} = 0.1665 \cdot \dot{m}_{TOT} \tag{2.9}$$

iii) Heat conduction in cladding, gap and fuel pellet is modelled as described in chapter 2.3.

iv) The pressure drop in the sub-channels at the same axial elevation is assumed to be the same.

The mathematical models i.e. the basic equations of continuity, momentum and energy are solved numerically in the STAFAS code to obtain the thermal-hydraulics conditions in each volume cell of a sub-channel. A typical volume cell of a sub-channel represented by k is shown in Figure 2.6.
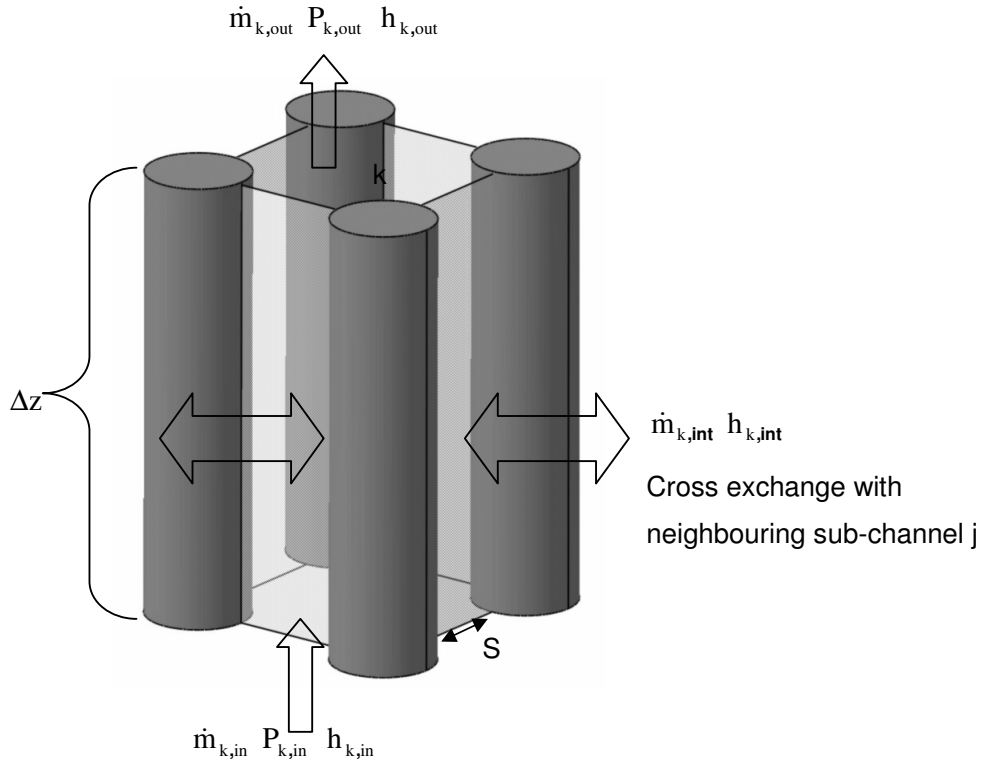
Figure 2.6: Axial representation of a single sub-channel

2.2.3 Continuity equation

The continuity equation implemented in the STAFAS code describes the mass balance in a volume cell taking into account axial flow and the transverse flow between the neighbouring sub-channels. For a steady state condition, the continuity equation of a sub-channel is expressed as:

$$\dot{m}_{k,out} = \dot{m}_{k,in} + \dot{m}_{k,\text{int}} \tag{2.10}$$

Equation 2.10 describes that, the axial mass flow rate leaving the volume cell of sub-channel k $\dot{m}_{k,out}$ is equal to the mass flow rate entering the volume cell $\dot{m}_{k,in}$ plus the transverse mass flow entering the volume cell through the interfaces to adjacent sub-channels $\dot{m}_{k,\textbf{int}}$. The transverse flow is created by two mechanisms: turbulent mixing that drives turbulent mass interchange and transverse pressure gradients that drive directed cross flow. Note that the axial mass flux through each volume cell is determined under the condition of equal pressure drop after the computation of the transverse pressure gradient. The mass flow rate at the interfaces of adjacent sub-channels can be expressed by the turbulent mixing mass flux G', directed cross flow mass flux G* and the interface geometry as:

$$\dot{m}_{k,\text{int}} = \sum_{j}^{J} S_{kj} \, \Delta z \left(G_{kj}' - G_{jk}' \right) + \sum_{j}^{J} S_{kj} \, \Delta z \, G_{kj}^{*} \tag{2.11}$$

where Δz is the height of the volume cell and S_{kj} is the width of the gap between both sub-channels k and j. The parameter S_{kj} is set to zero if there is no direct transversal connection between both sub-channels

2.2.4 Axial momentum equation

The axial momentum equation of the volume cell of sub-channel k is defined as:

$$\left(P_{k,in} - P_{k,out} \right) A_k - \left(f \frac{\Delta z}{D_h} + \zeta \right)_k \left(\frac{|G_k| G_k}{2\rho_k} \right) A_k - A_k \rho_k g \Delta z =$$
$$\frac{\dot{m}_{k,out} \, G_{k,out}}{\rho_{k,out}} - \frac{\dot{m}_{k,in} \, G_{k,in}}{\rho_{k,in}} + \sum_{j}^{J} S_{kj} \, \Delta z \left(G_{kj}' u_k - G_{jk}' u_j \right) + \sum_{j}^{J} S_{kj} \Delta z \, G_{kj}^{*} u_{kj}^{*} \tag{2.12}$$

The first term at the left hand side is the pressure force term , where $P_{k,in}$ and $P_{k,\,out}$ denote the pressure at inlet and outlet of sub-channel k. The second and third term at the left hand side represent the hydraulic resistance force and the body force due to gravity. In the terms, f is the friction factor, ζ is the hydraulic resistance coefficient, D_h is the hydraulic diameter, A_k is the cross-sectional area of sub-channel k, ρ_k is the fluid density, g is the gravitational acceleration and Δz is the axial height of the volume cell. The first two terms at the right hand side represent the momentum exiting from the volume cell and entering into the volume cell. The last two terms describe the inter-channel exchange of momentum caused by turbulent mixing flow and directed cross flow. u_k and u_j are the axial velocities in sub-channels k and j.

The average velocity in sub-channel k is defined as:

$$u_k = \frac{\dot{m}_k}{\rho_k} \tag{2.13}$$

$u_{kj}^* = u_k$ When the flow is exiting sub-channel k

$u_{kj}^* = u_j$ When the flow is exiting sub-channel j

2.2.5 Energy equation

For steady state condition, the energy balance in the volume cell is implemented in the STAFAS code as shown below:

$$Q_k = \dot{m}_{k,out} h_{k,out} - \dot{m}_{k,in} h_{k,in} + \sum_{j=1}^{J} S_{kj} (G'_{kj} h_k - G'_{jk} h_j) \Delta z + \sum_{j=1}^{J} S_{kj} G_{kj}^* h_{kj}^* \Delta z \tag{2.14}$$

Q_k is the heat added to sub-channel k from neighbouring fuel rods. The first two terms at the right hand equation are the axial transport of enthalpy and the last two terms are the enthalpy carried by turbulent mixing and directed cross-flow.

$h_{kj}^* = h_k$ When the flow is exiting sub-channel k

$h_{kj}^* = h_j$ When the flow is exiting sub-channel j

In the present study the heat source term Q_k has been modified in STAFAS. A fuel rod model has been implemented in the STAFAS code to obtain the heat generated in the fuel rod by fission process. The heat from the fuel rods transferred to sub-channel k is expressed in Equation (2.15), as the sum of the heat generated in the fuel rod Q_{rod} multiplied by the

fraction of the fuel rod perimeter that has contact to the sub-channel F_{rod}. The sum taken is over the total fuel rods that have contact to sub-channel k as shown Figure 2.7.

$$Q_k = \sum Q_{rod} \cdot F_{rod} \tag{2.15}$$
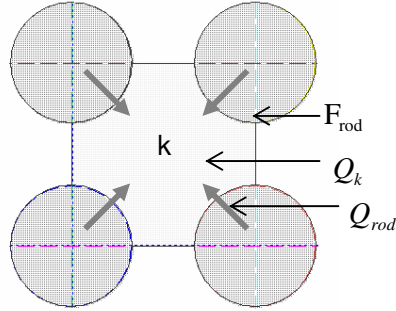
Figure 2.7: Heat from the fuel rod to sub-channel

To compute the outer cladding surface temperature it has been taken into account that the surface temperature around the circumference of a fuel rod is varied because of the temperatures variation in the different sub-channels. The outer cladding surface temperature T_{co} of a fuel rod facing to one sub-channel is defined as:

$$T_{co(rod,sc)} = T_{sc} + \frac{q''_{rod}}{\alpha_{sc}} \tag{2.16}$$

The average outer cladding surface temperature over the circumference of one fuel rod is given as:

$$T_{co(rod)} = \frac{1}{SC} \sum_{sc=1}^{SC} T_{co(rod,sc)} \tag{2.17}$$

where T_{sc} is the bulk temperature in a sub-channel, α_{sc} is the heat transfer coefficient of the fluid on the cladding and q''_{rod} is the heat flux density of the fuel rod and SC represents the total number of sub-channels that have contact to the same fuel rod. The subscript rod represents the fuel rod and sc the sub-channel.

To solve the equation system of continuity, momentum and energy, additional physical models for turbulent mixing and directed cross flow described in the report by Cheng et al.

[29] were used. A modification was made on heat transfer coefficient model used as described in chapter 2.2.6. In the present study the model used for turbulent mixing is based on the assumption that the effective turbulent fluctuations of the fluid velocity at both sides of the interface are the same. The inter-channel mass flux fluctuations are defined as:

$$G'_{kj} = \beta \left(\frac{u_k + u_j}{2} \right) \rho_k \tag{2.18}$$

and

$$G'_{jk} = \beta \left(\frac{u_k + u_j}{2} \right) \rho_j \tag{2.19}$$

with β representing the mixing coefficient, u the flow velocity in the sub-channel and ρ the fluid density. This model has been recommended by Cheng and Mueller [77], because of the large density variation of supercritical fluids. The study by Cheng and Mueller [77] discussed the mixing coefficient value depending on the flow conditions as well as on the sub-channel geometry. The mixing coefficient value used in this study was 0.004, same as in the study by Cheng and Schulenberg [31]. A sensitivity study of different mixing coefficient values was not done in the present work. There is still a need to validate mixing coefficient values for supercritical water conditions with experiments.

2.2.6 Heat transfer coefficient

For computing the heat transfer coefficient between the solid walls and the fluid, the Bishop correlation [78] for heat transfer in smooth tubes at supercritical water conditions was implemented in the STAFAS code. The original STAFAS code includes only the Dittus-Boelter correlation. Bishop's correlation defines the Nusselt-number in Equation (2.20) with Reynolds number Re, Prandlt number Pr and the geometric parameters i.e. the hydraulic diameter D_h and the axial height z. For a relatively small hydraulic diameter and large z the last term can be negligible

$$Nu_B = 0.0069 Re_B{}^{0.90} . Pr_B{}^{0.66} . \left(\frac{\rho_{wall}}{\rho_B} \right)^{0.43} . \left(1 + \frac{2.4 D_h}{z} \right) \tag{2.20}$$

The Prandlt number, Pr, is defined by the average specific heat $\overline{C}_P$ and the ratio of the bulk dynamic viscosity (μ_B) to the bulk thermal conductivity (λ_B).

$$\mathbf{Pr}_B = \left(\overline{C}_P \cdot \frac{\mu_B}{\lambda_B} \right) \qquad (2.21)$$

The average specific heat $\overline{C}_P$ is defined as:

$$\overline{C}_p = \frac{h_{wall} - h_B}{T_{wall} - T_B} \qquad (2.22)$$

where h_{wall} and h_B are the wall and bulk enthalpies T_{wall} and T_B are the wall and bulk temperatures.

The Reynolds number is defined by the mass flux of the fluid G, the hydraulic diameter D_h and the dynamic viscosity μ_B as:

$$Re_B = \frac{GD_h}{\mu_B} \qquad (2.23)$$

The application of the Bishop correlation for the HPLWR analysis was recommended in a literature review carried out by Cheng and Schulenberg [31]. A test calculation was performed with the square fuel assembly described in Figure 2.2 to compare the heat transfer coefficient with the Bishop's and Dittus-Boelter correlation. Figure 2.8 shows the heat transfer coefficient in sub-channel (SC-4) with the two correlations. The results show that the heat transfer coefficients calculated by the Dittus-Boelter and Bishop's correlation are similar if the temperature is far away from the pseudo-critical point. However, in the vicinity of the pseudo- critical point a deviation was observed especially where the maximum peak occurs. The Bishop's correlation calculates a maximum value that is twice as high as with Dittus-Boelter. The maximum heat flow in sub-channel SC(4) with the Bishop's correlation is about 1.04 MW/m^2 (see Figure 4.5). Due to unavailable experiment data for heat transfer of supercritical water in bundles available correlations still need to be validated.
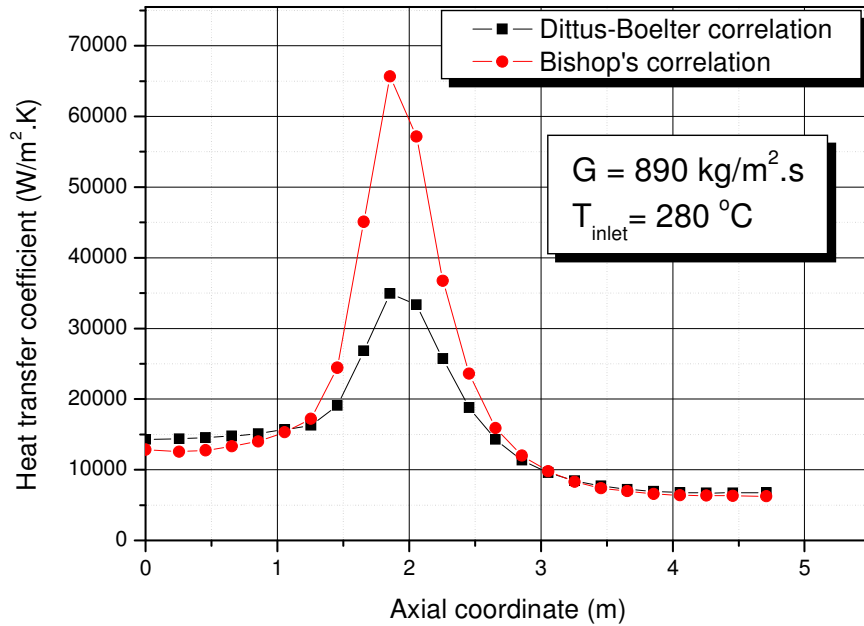
Figure 2.8: Heat transfer coefficient of sub-channel 4

2.2.7 Effect of the grid spacers on mixing

For the present analysis simple grid spacers are assumed without any additional mixing vanes. The pressure loss induced by grid spacers is taken into account by giving an additional loss coefficient for every sub-channel type, which is defined in the paper by Cheng et al. [29].

2.2.8 Inlet conditions of the coolant sub-channels

i) Mass flux

Two different options are available in the STAFAS code to determine the mass flux at the inlet of each sub-channel, Cheng et al. [29]. In the first option a uniform distribution of the mass flux at the entrance of the fuel bundle is assumed, i.e. the inlet mass flux is the same for all sub-channels. In the second option, which was considered in this study, it is assumed that the pressure drop across the first axial mesh is the same for all sub-channels, hence the mass flux is adjusted as described in chapter 2.1 to achieve this condition.

ii) Temperature

The inlet temperature of the coolant sub-channels is obtained from the energy balance in the lower plenum, i.e. taking into account the mixture of the moderator water at the exit and down-comer flow.

$$h_{inlet} = \frac{\left(h_{MT,exit} \cdot \dot{m}_{MT} + h_{AG,exit} \cdot \dot{m}_{AG} + h_{DC} \cdot \dot{m}_{DC} \right)}{\dot{m}_{TOT}}$$ (2.24)

where h is the enthalpy and $\dot{m}$ is the mass flow rate . The subscript MT represents the moderator tube, AG represents assembly gap and DC stands for down-comer. The mass flow rate is fixed in the moderator tube and assembly gap.

2.3 Fuel rod model

2.3.1 Temperature distribution in the fuel rod

In the original STAFAS version, a fuel rod model was not included. In the present study, the STAFAS code was modified to add the fuel rod model in order to compute the average fuel temperature. This was computed by considering heat conduction in the fuel rod (i.e. cladding, gap and pellet). An annulus fuel rod as shown in Figure 2.9, was modelled in the STAFAS code for a general application to derive the expression for the averaged fuel temperature.
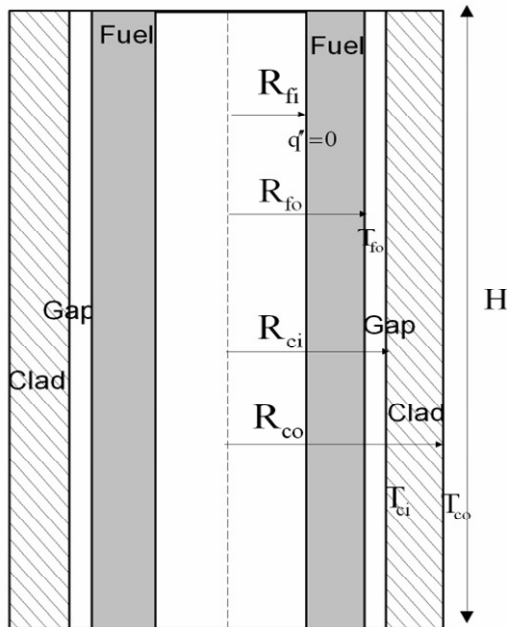
Figure 2.9: Sketch of annular fuel rod model (not to scale)

where, R_{fo} and R_{fi} are the outer and inner radius of the fuel pellet, R_{co} and R_{ci} are the outer and inner radius of the cladding, T_{co} and T_{ci} are the outer and inner surface cladding temperature of the fuel rod.

The derivation of the equations that were implemented in the STAFAS code to calculate the heat conduction in the cladding, gap and fuel pellet, and finally the average radial fuel temperature is presented in this section.

2.3.2 Temperature in the cladding – radial calculation

The heat conduction equation of a cylindrical body from [79] is applied to calculate inner cladding as derived below:

By assuming steady state and a one-dimensional temperature dependence (i.e. in the radial direction) the heat conduction equation in the cladding is written as:

$$-\lambda_c \frac{dT}{dr} = \frac{q'}{2\pi r}$$
(2.25)

where λ_c is the thermal conduction of the cladding, which is assumed constant, q' is the linear heat along the length and T is the temperature variable.
The heat generation in the fuel pellet from fission is a function of the height (z) and is constant in the radial direction. The heat conduction in the axial direction is neglected.

Re-arranging the Equation (2.25) and integrating across the cladding with respect to the temperature and radius, the expression for the inner cladding surface temperature T_{ci} is as follows:

$$T_{ci} = T_{co} + \frac{q'}{\lambda_c 2\pi} \ln\left(\frac{R_{co}}{R_{ci}}\right)$$
(2.26)

The relationship between the linear heating q' and volumetric heating q''' of the fuel rod is given as:

$$q' = \pi\left(R_{fo}^2 - R_{fi}^2\right) \cdot q'''$$
(2.27)

where q''' and q' are constant radially.

Substituting the term of volumetric heat into Equation (2.26) yields:

$$T_{ci} = T_{co} + \frac{q'''\left(R_{fo}^2 - R_{fi}^2\right)}{2\lambda_c}\ln\left(\frac{R_{co}}{R_{ci}}\right)$$

(2.28)

2.3.3 Heat conduction in the gap

Following similar procedure as above and integrating between the outer fuel rod radius R_{fo} and inner cladding radius R_{ci}, the fuel temperature at the outer surface of the fuel pellet T_{fo} was computed from the following equation:

$$T_{fo} = T_{ci} + \frac{q'''\left(R_{fo}^2 - R_{fi}^2\right)}{2\lambda_{gap}}\ln\left[\frac{R_{ci}}{R_{fo}}\right]$$

(2.29)

λ_{gap} is the thermal conductivity of the gap filled with helium, which was obtained from Ho and Taylor [80].

2.3.4 Temperature profile in the fuel pellet

The equation used to compute the average temperature distribution in the radial direction was derived from the following heat conduction equation from [79]:

$$\frac{1}{r}\frac{d}{dr}\left(\lambda_f\, r\frac{dT}{dr}\right) + q''' = 0$$

(2.30)

λ_f is the thermal conductivity of the fuel material and is assumed constant. Equation (2.31) is solved in [78] to obtain the expression for calculating the average fuel temperature distribution in the fuel pellet as:

$$\overline{T}_f = T_{fo} + \frac{q'''R_{fo}^2}{8\lambda_f}$$

(2.31)

where R_{fo} is the outer diameter of the fuel pellet.

2.4 Monte Carlo modelling

2.4.1 Monte Carlo technique

The Monte Carlo code MCNP is used to calculate the heating energy deposition in the fuel rods from fission process. This heating energy deposited corresponds to the power distribution in the fuel rods. The power distribution obtained as a function of the axial height is provided into the STAFAS code as a heat source for the sub-channel (see coupling procedure in chapter 3.4). The same geometry model in STAFAS is used for neutronics analysis. The physics of MCNP for power distribution calculation is well described the MCNP manual [58]. In this section, a brief extension to the introduction of Monte Carlo technique is given to obtain a good understanding of the modelling.

The basic idea of Monte Carlo is to create a series of life histories of particles (e.g. neutrons) by using sampling techniques to sample the probability laws that describe the real particle behaviour and to trace out step by step the particle random walk. The history of a particle is followed until it can no longer contribute to the information of interest to the problem at hand. It can therefore be said that Monte Carlo is essentially based on statistical concepts: the answer it gives is an estimate, which should lie within some confidence interval about the true answer. The magnitude of the statistical error (uncertainty) associated with the result, the confidence interval, is a function of the number of particle histories simulated (see chapter 3.5). The more histories run, the smaller the confidence interval about the true average behaviour of the particles. From the law of large numbers the estimated quantity will improve if averaged over larger samples (of independent observations) of the quantity. For example the Monte Carlo simulation yields successive independent scores, $x_1, x_2, x_3 \dots x_N$ of the random variable x. Then the sample mean ($\bar{x}$) is formed where N is the total number of histories.

$$\bar{x} = \frac{1}{N} \sum_{i=1}^{N} x_i \qquad (2.32)$$

The law of large numbers state that the sample mean with a probability that approaches 1 as $N \rightarrow \infty$ approaches the population mean or true mean. In this case x might represent the neutron flux, heating energy deposition, K_{eff} etc.

ii) Monte Carlo analogue

37

Neutrons are 'born'/started according to user-specified directives (where in the geometry, direction, energy). Energy and direction are sampled randomly from their cumulative distribution functions. Neutron path lengths between collisions depend on the total macroscopic cross section Σ. The geometry determines whether a neutron leaks out or experiences a collision at the end of its path. Collision types are selected randomly in accordance with the appropriate reaction cross-sections. Scattering events change the energy and direction of the neutron before it continues through the system. Leakage, capture or fission terminate the history and signal the start of the next neutron history.

2.4.2   Power distribution in MCNP

The Monte Carlo code MCNP code is used in this study to simulate neutron particles and their average behaviour in the material of the geometry cells are tracked with the evaluated cross section data from the ENDF/B and JEF-2.2 libraries. The collected tracks of the neutrons represent the neutron flux distribution and are folded track by track with the reaction cross sections and heating functions to obtain the estimated heating energy, which corresponds to power distribution. The heating energy tally (output) used is represented in MCNP by the F6 tally card, which takes into account the total cross section of the neutron reaction. The quantity F6 for heating energy is defined in MCNP as:

$$F6 = Wt \cdot Tl \cdot \sigma_{TOT}(E) \cdot H(E) \cdot \frac{\rho_a}{m} \tag{2.33}$$

Where:

Wt particle weight

Tl track length

$\sigma_{TOT}(E)$ microscopic total cross section (barn)

H(E)   heating number (MeV/collision)

ρ_a the atom density (atoms/barn-cm)

m   mass of the cell (g)

Note that the F6 tally is a volume tally, it provides the average heating energy deposited in a volume cell of a fuel rod.

The microscopic cross section is defined as the probability of a particular reaction occurring between a neutron and a nucleus (material). It is expressed in units of area or square centimetres. The heating number H(E) and the total cross section are stored in MCNP cross data library. Equation (2.33) can be expressed in terms of particle flux and heating function as derived below:

i) The integrated particle flux ϕ in a volume cell (V), as a function position, $\vec{r}$ energy, E and time t is defined in MCNP as:

$$\int_V \int_t \int_E \phi(\vec{r}, E, t) = \frac{Wt \cdot Tl}{V} \tag{2.34}$$

The particle flux is considered to be the total path length covered by all neutrons in one cubic centimetre during one second. Mathematically it is defined as:

$$\phi = nv \tag{2.35}$$

Where:

ϕ is the neutron flux (neutrons/cm^2-s)

n   is the neutron density (neutrons/cm^3)

v   is the neutron velocity (neutrons/sec)

ii) The microscopic total cross section multiplied by the heating number in Equation (2.33) gives the heating function H(E) summed over nuclides in a material. The heating energy is therefore defined by the particle flux as a function of time, energy and position in the volume and heating function as:

$$F6 = \frac{\rho_a}{\rho_g} \int_V \int_t \int_E H(E) \phi(\vec{r}, E, t) dE \, dt \frac{dV}{V} \tag{2.36}$$

The unit of the heating tally F6 is in MeV/g (Million electro-volts/gram).

For use in the STAFAS code, the heating energy from MCNP simulation is converted into power units by using the following expression:

$$Q_{rod,z} = \frac{Q_{TOT}}{\sum e_{rod,z}} \cdot e_{rod,z} \tag{2.37}$$

where $e_{rod,z}$ represents the heating energy deposited in the fuel rod from fission process as a function of the axial height z, and Q_{TOT} is the total power assumed for the fuel assembly modelled and $Q_{rod,z}$ in the power in the fuel rod as a function of the axial height.

39

2.4.3   Total microscopic cross section

The total microscopic cross section (σ_{TOT}) is defined by the neutron interaction by scattering σ_{sca} and absorption σ_a:

$$\sigma_{TOT} = \sigma_{sca} + \sigma_a \tag{2.38}$$

Both scattering and absorption cross section are sub-divided into two parts. The scattering microscopic cross section is sub-divided into elastic and inelastic cross section. The absorption cross section is sub-divided into fission and capture. In general, the heating energy deposited by the F6 tally card is from the event of a neutron from creation in the source, fission, (n, 2n) and reactions to its death by absorption or escape from the geometry.

2.4.4   Nuclear cross section data

The nuclear cross section data describes the frequency and outcome of interactions between particles (neutrons) and materials through which they are passing. The form of nuclear data used in MCNP is a point energy. In this form the nuclear data is stored at a significantly large number of energy points that little point data retains the particle energy as a continuous variable. The cross section data for neutron interaction are obtained from the evaluated MCNP libraries ENDF/B. Cross section data provided with the MCNP are for a limited number of temperatures. An additional library requested from NEA, JEF-2.2 data library containing more temperatures (300 K, 500 K, 600 K, 760 K, 800 K, 1000 K, 1500 K) was added the MCNP data directory.

2.4.5   Treatment of thermal neutrons

A collision between a neutron and an atom is affected by the thermal motion of the atom and in most cases the collision is also affected by the presence of other atoms nearby. MCNP uses a thermal treatment based on the free gas approximation to account for the thermal motion. It also has an explicit S(α,β) capability that takes into account the effects of chemical binding and crystal structure for incident neutron energies below about 4 eV, but is available for only a limited number of substances and temperatures. Due to the lack of cross section data for supercritical water the free gas model is used for the treatment of the thermal neutrons. With the free gas model MCNP assumes that the hydrogen is a free gas. The

range of atomic weight and neutron energy where thermal effects are significant the elastic scattering cross section at zero temperature is nearly independent of the energy of the neutron and that the reaction cross sections are nearly independent of temperature. The free gas model is included in MCNP calculation with the use of the temperature card 'TMP card' in the input. The application of the free gas model is described in more detail in the MCNP manual [58]. The effect of using the free gas model and the $S(\alpha,\beta)$ model has been reported by Bernnat et al. [81]

2.4.6   Doppler Effect

Doppler Effect is referred to as the degree of change in fuel temperature. At high fuel temperature the resonance of the neutron capture cross section is broadened and more thermal neutrons are captured. A large number of captured neutrons mean a smaller number of neutrons are available for inducing fission. In heterogeneous reactors, the Doppler Effect normally leads to a negative temperature coefficient of reactivity.

2.4.7   Fuel temperature (Doppler Effect) included in MCNP

The feedback of fuel temperature from the STAFAS code into MCNP is included in the coupling procedure. The fuel temperature in MCNP is defined on the "Material card" by giving the identifier number of the library, from which the cross section data at the required temperature are to be obtained. Additionally, the fuel temperature value is directly entered on the "TMP card" in MeV by multiplying the temperature in Kelvin with 8.617 x 10 $^{-11}$ to define the free gas temperature model for the thermal neutrons. The JEF-2.2 library is used to obtain the cross section data for the fuel isotopes as it contains data for more temperatures levels, compared to the ENDF/B libraries in MCNP. Although the JEF-2.2 library has cross section data for more temperatures, a large temperature range with cross section data is required. Due to the lack of cross section data with finer temperature range a mixture technique of the same isotope with existing cross section data in the JEF-2.2 library at two temperatures is used to account for the individual fuel temperatures with missing cross section data. The amount of atomic mixture of the material composition is determined by the mixture fraction X, which is calculated by linear interpolation of the available temperatures with cross section data and the calculated average temperature T_f from STAFAS. The mixture technique assumes that the calculated average fuel temperature lies between a high temperature value noted by T_H and low temperature T_L that are available in the library.

$$X = \frac{T_f - T_C}{T_H - T_C} \qquad\qquad (2.39)$$

i) Example of the mixing technique for missing cross section data in MCNP

An example of the mixture technique is shown in Figure 2.10. If for instance the average fuel temperature computed from STAFAS is 699 K (T_f) and cross section data are available for fuel temperatures at 600 K, (T_L) and 760 K, (T_H) from the JEF-2.2 library, then a mixture of the fuel material with cross section at the two temperatures with available cross section is performed to account for the missing cross section data at this temperature.
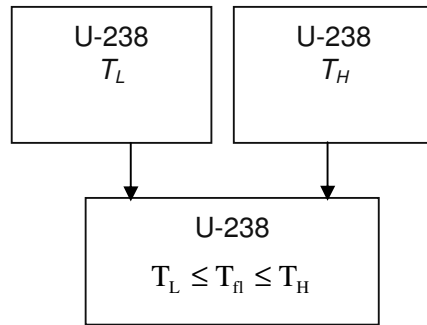
Figure 2.10: Demonstration of the mixture technique

The technique of mixing fuel material with cross section data from two temperatures was first used by Bernnat et al. [81]. For the present study the material mixing technique was tested with the JEF-2.2 library for a simplified geometry i.e. a single tube surrounded by moderator water. Two cases were studied. In the first case, the fuel temperature used was defined as available in the JEF-2.2 library. In the second case the same fuel temperature was mixed with two different temperatures from the JEF-2.2 library. The calculation conditions were used for each case. The multiplication factor k-effective (k_{eff}) was calculated as the testing parameter. The results given in Figure 2.11 show a good agreement of the mixed materials at different temperatures from the JEF-2.2 library with the temperature used directly from the JEF-2.2 library. A small variation is observed at temperatures 560 and 760 K. This could be due to the different evaluation methods that may have been used at these two temperatures.
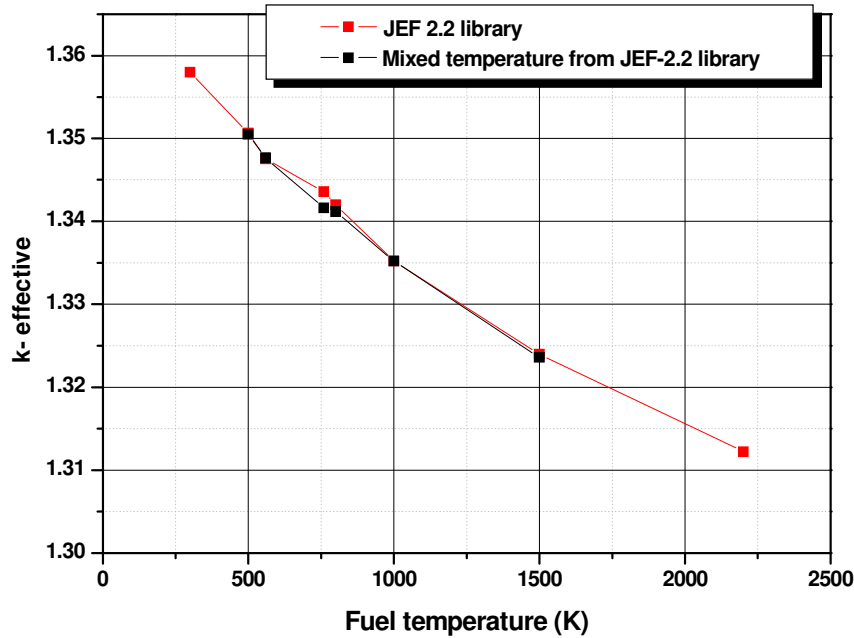
Figure 2.11: k-effective variation with fuel temperature

2.4.8   Multiplication factor

Nuclear criticality, the ability to sustain a chain reaction by fission neutrons is monitored by the eigenvalue (or multiplication factor).   In the MCNP calculation performed for power distribution, the multiplication factor is obtained by using the criticality source specification to run MCNP. The multiplication factor (k) is defined as the dominant eigenvalue of the neutron transport equation. In MCNP the multiplication factor k-effective is calculated. The definition of the k-effective is given in MCNP as the ratio of the number of neutrons in one generation to the number in the previous generations in a system containing fissionable material and in the absence of any external source. A generation is the life of a neutron from birth in fission to death by escape, parasitic capture, or absorption leading to fission. Neutron generations are referred to as batches or cycles.

$$k_{eff} = \frac{fission\, neutrons\, in\, generation\, i+1}{fission\, neutrons\, in\, generation\, i} \qquad (2.40)$$

For critical systems, k_{eff} = 1 and the chain reaction will just sustain itself. For subcritical systems, k_{eff} < 1 and the chain reaction will not sustain itself. For supercritical systems, k_{eff} > 1 and the number of fissions in the chain reaction will increase with time.

3   NUMERICAL MODEL

3.1   Cell nodalization in STAFAS and MCNP

The coupling is performed on a 1-D representation of a fuel assembly in the axial direction and symmetry planes are assumed in radial boundaries. A node in the thermal-hydraulics code represents the boundary of a volume cell. On the other hand, a node in the neutronics code represents the centre point of the volume cell of a fuel rod, sub-channel, moderator tube, or assembly gap. The axial nodalization for a single volume cell is shown in Figure 3.1. At the first node, $z=0$ in the thermal-hydraulic code the inlet boundary conditions of the coolant sub-channels are obtained.
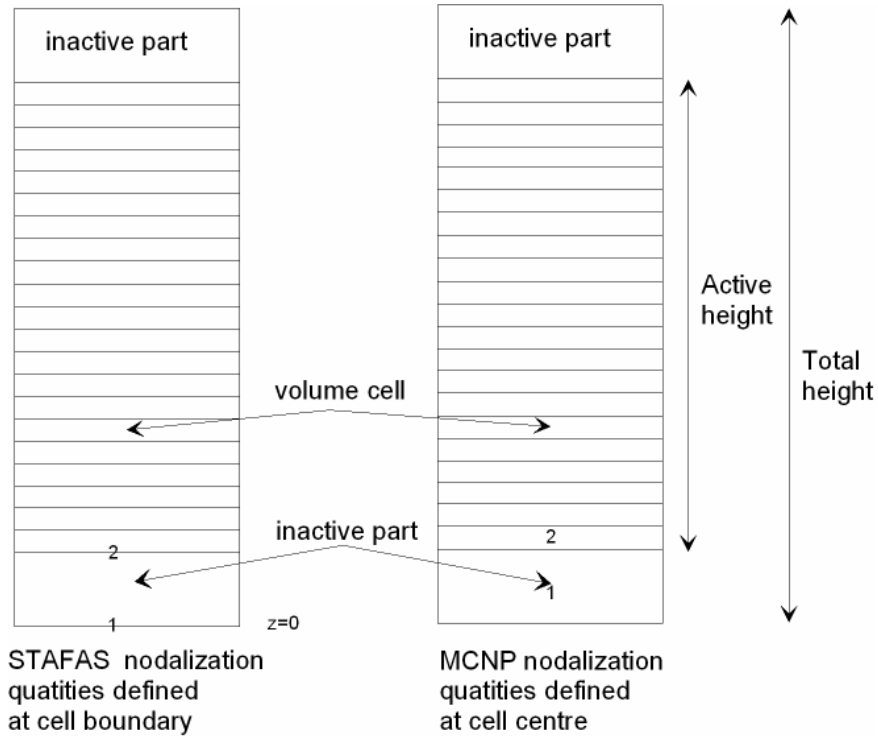
Figure 3.1: Axial nodalization in a volume cell

The geometry representation is the same in both STAFAS and MCNP code. The STAFAS code provides output parameters of temperature, density, pressure and mass flux for each volume cell at the boundary as a function of the axial height, while MCNP provides an output of power at the cell centre. In total, 23 volume cells and 24 cell boundaries are generated out of which 21 volume cells at the centre represent the active region. For data transfer between the two codes, the second node in STAFAS at the boundary represents the first node in MCNP at the cell centre and vice-versa.

3.2 MCNP flow chart for power distribution

The power distribution in MCNP is defined by the heating energy tally (F6 tally) as described in chapter 2.4.2. The procedure performed by MCNP for this analysis is described in the flow chart shown in Figure 3.2.
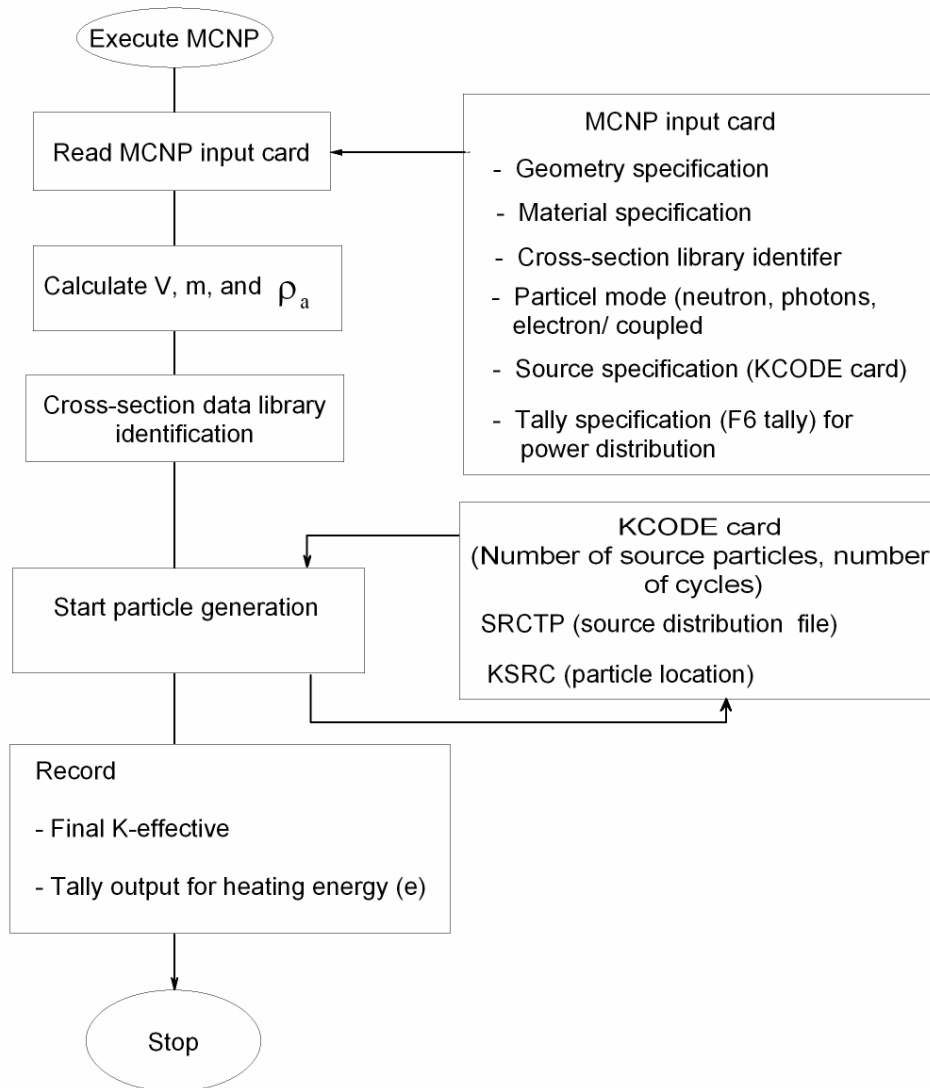
Figure 3.2: Flow chart of the MCNP code for power distribution calculation

The input card for MCNP simulation describes the physical model: the geometry specification, materials used to fill the geometry volume or the surface, cross section data library for the material isotopes, type of source specified and the type of output required (tally specification). The temperature card (TMP card) is included in the input card to switch on the

free-gas model for the treatment of the thermal neutrons. Detailed description of the MCNP input format for different types of geometries is given in the MCNP manual, edited by Briesmeister [58].

When the Monte Carlo calculation is started, the input card is read and data is interpreted to obtain information on what the type of MCNP calculation is to be performed i.e. a criticality calculation for k_{eff} output only, tally calculation for power distribution only or both. In this study MCNP calculation is performed using both criticality source specification card and tally card to obtain power distribution from fission process. For power distribution, MCNP calculates the parameters needed to describe the tally, for example for the F6 tally it calculates the volume of the different cells describing the geometry, the atomic density and mass of the material, as have been shown in Equation (2.36). The gram density is given in the input file. The cross section data libraries specified for each material isotope of the fuel, cladding, material structure and water are read from MCNP data directory. The type of particles (i.e. neutrons, electrons or photons) to be simulated in MCNP is defined in the input file. In this case neutron particles are simulated.

The particle generation in MCNP is started with the criticality source type specified by the KCODE card. The KCODE card contains information about the total number of particles to be initiated per generation (cycle) and the total number of cycles to be run before MCNP neutron simulation is terminated. For the initial cycle, fission sites for the neutrons can be defined by an external source distribution file of the type SRCTP from a similar geometry or from a KSRC card, which defines the positions and direction of the particles to be initiated [58]. After the initial cycle, fission sites for each cycle are those points generated by the previous cycle. In this study an external source is used, which is obtained from the same geometry analysed. If the analysis is done for a different geometry, then the location of the initial fission site will change, hence the KSRC card is required.

MCNP iteration for particle generation is done for the total number of cycles specified and when the total number of particles is reached, the particle generation is stopped. The finial k-effective value defined in [58] and heating energy deposited with the F6 tally in the fuel material are recorded and produced at the output. The quality (or precision) of MCNP results is discussed in the chapter 3.5. Note that the heating energy in volume cells as a function of the axial height gives information about the axial power distribution in the fuel rod.

3.3 STAFAS numerical model

Figure 3.3 shows schematically the numeric flow chart of the STAFAS code.
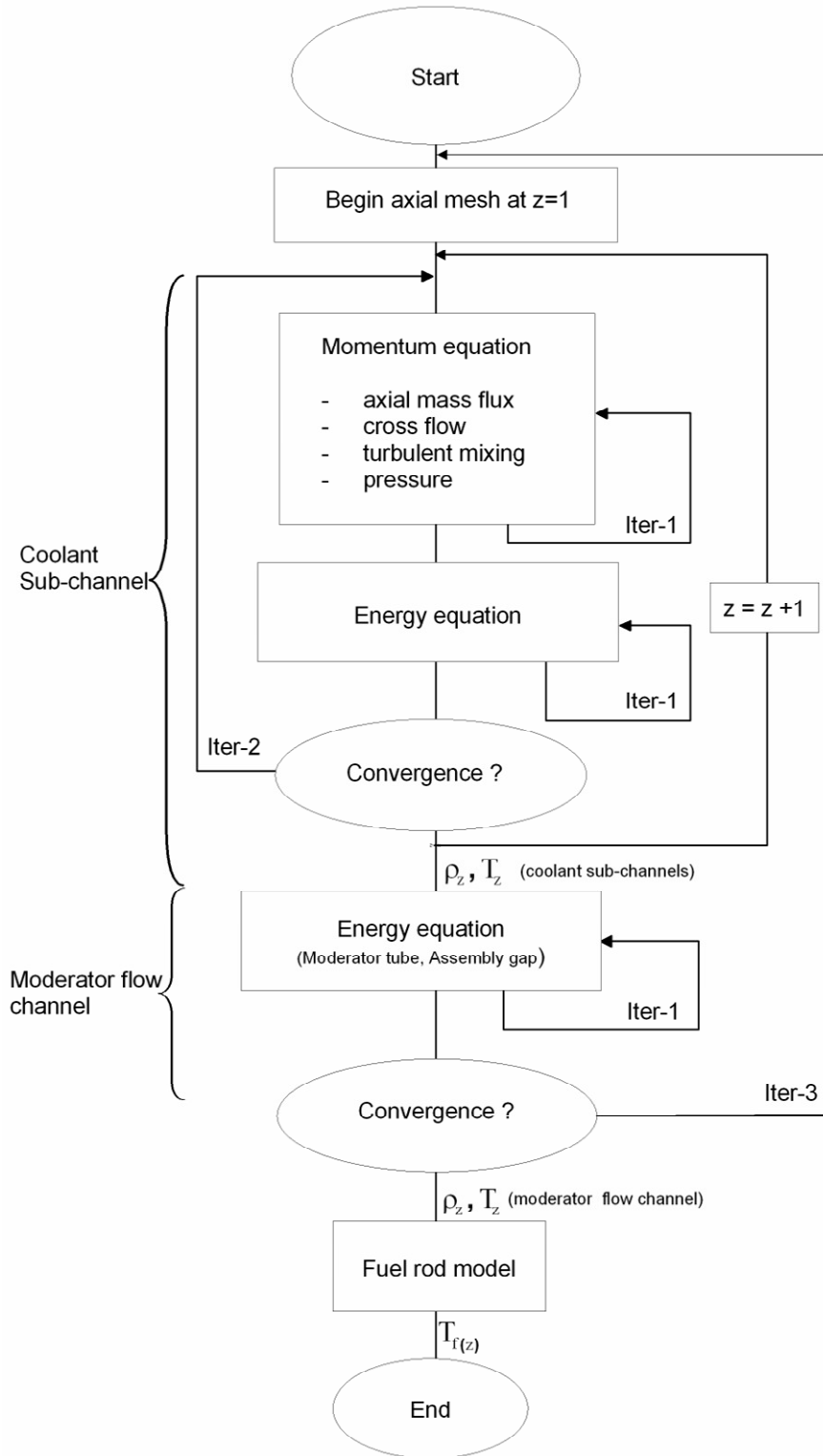
Figure 3.3: Numeric flow chart of the STAFAS code

47

The STAFAS output required for the coupling procedure include: water density and water temperature distribution of the coolant sub-channels and moderator channels and fuel temperature distribution in the fuel rods, as a function for the axial height (z). The axial meshing in STAFAS is shown in Figure 3.1. Note that, the STAFAS quantities, which are obtained at the cell boundary of a volume cell, are the same as the bulk values, i.e. $\rho_z = \rho_{B,z}$ where the subscript B represents the bulk condition.

The original STAFAS version, described by Cheng et al. [29], is modified in this study to include the heat source for the sub-channels from the MCNP code.
When the STAFAS code is started, a user sub-routine is first executed to read the power distribution in the fuel rods obtained from MCNP run. This power data of the fuel rods is then used to calculate the sub-channel heat source.

In the STAFAS analysis, the non-linear momentum and energy equation (Equation 2.12) and Equation (2.14) are first converted in to linear equation systems. The linear equation systems are then solved directly and separately without any iteration. The convergence of the momentum and energy equation is achieved by the inner iteration loop (iter-1) with under-relaxation factor, which is dynamically determined. This direct solution approach for the linear equation system coupled with the under-relaxation factor has shown a high numeric stability and satisfactory convergence.

The momentum and energy equation are coupled with the second iteration loop (Iter-2). The first and second iteration loops solve the axial momentum and energy equation in the coolant sub-channels. A third loop (Iter-3) is included to solve the equation in the other flow channels such as the moderator tube and assembly gap, which are in thermal-hydraulic connection with the sub-channels. The iteration for the flow in the moderator tube and assembly gap is only done for energy equation as the mass flux is fixed. The addition of the assembly gap is also a modification to the original STAFAS version.

Further modification of the original STAFAS code is the implementation of the fuel rod model. After the convergence of the momentum and energy equation, the equation for the fuel rod is then solved directly without any iteration to obtain the temperature distribution in the fuel rod.

The axial mesh location is started from the bottom to the top.

3.4   Description of the coupling procedure

3.4.1   Flow chart of the coupling procedure of MCNP/STAFAS

The Monte-Carlo code MCNP and sub-channel code STAFAS are coupled by the heating energy distribution (power distribution) in the fuel rod as a function of axial height (z), from the MCNP analysis denoted by e_z, water density and water temperature distribution in the flow channels (coolant and moderator) denoted by ρ_z and T_z, respectively and the fuel temperature distribution in the fuel rod $T_{f(z)}$ from STAFAS analysis. Figure 3.4 shows the flow chart of the coupled procedure of the Monte Carlo code MCNP with the sub-channel code STAFAS.
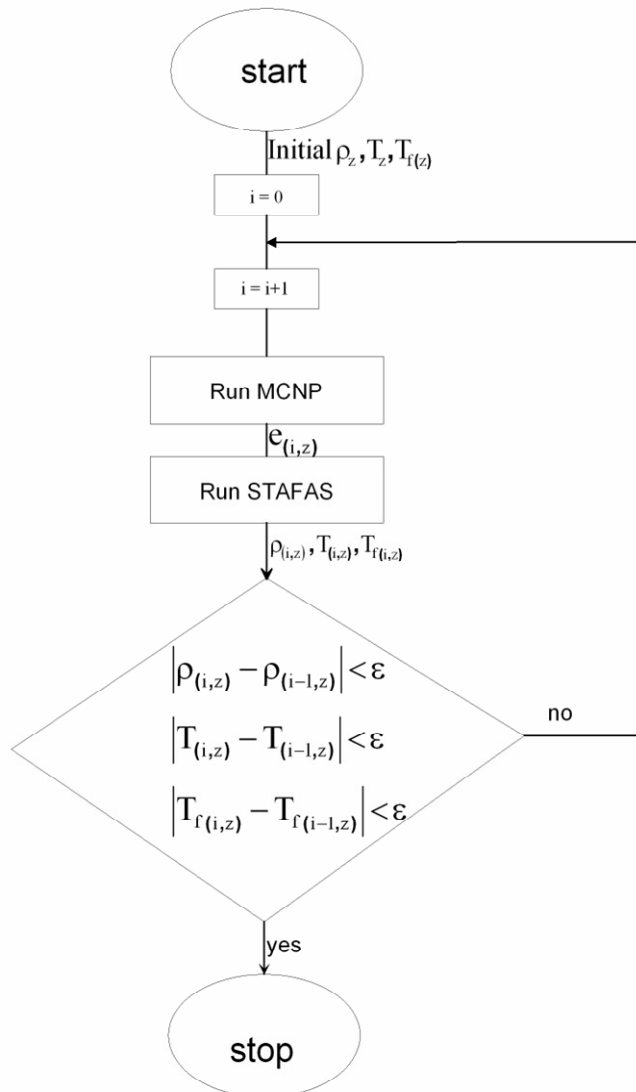

Figure 3.4: Flow chart of the coupled procedure of MCNP/STAFAS

The coupling procedure is realized automatically on a Windows system. The executables files for MCNP code and STAFAS code are run in the command prompt window (DOS). The two codes are run separately in the same command prompt window and exchange data after each run. The neutronics calculation is started in MCNP at iteration i=0 with defined initial distributions for water density, water temperature and fuel temperature[1]. MCNP run is performed, from which the heating energy distribution in units of million electron-volts (MeV) for each fuel rod as a function of the axial height z is obtained, for the corresponding iteration denoted as $e_{(i, z)}$. The heating energy distribution is then transferred automatically into the STAFAS code by a separate sub-routine, where it is converted into power units (see Equation (2.37) and used to calculate the heat source of the sub-channels. The STAFAS calculation is then performed using the power profile from MCNP to obtain the corresponding thermal-hydraulic properties of water density distribution ($\rho_{(i,z)}$), water temperature distribution ($T_{(i,z)}$) and the fuel temperature distribution ($T_{f\,(i,z)}$) as a function of the axial height.

The first coupling in MCNP is done at i=1 when the STAFAS output is transferred to generate a new MCNP input, where the previous values for water density, water temperature and fuel temperature are overwritten. The modified MCNP input for the next iteration is run and the corresponding heating energy distribution is obtained, which is again transferred into the STAFAS code to calculate the new thermal-hydraulic properties. The coupled iteration is repeated until a converged solution is achieved. A convergence check is performed on the STAFAS output before running a new MCNP calculation.

A converged state is defined to be reached when the difference (absolute value) of the coupled quantities at each z of the corresponding iteration and the previous distribution is much smaller than the defined convergence criterion ε. Different convergence criterions are defined for all the quantities.

To check the convergence of the coupled procedure shown in Figure 3.4 a coupled analysis was performed for six iterations with the one-eighth fuel assembly model described in Figure 2.2. The boundary conditions in the STAFAS and MCNP code defined in Table 2.4, Table 2.5 and 2.6 were applied. The calculations in MCNP were limited to 700 cycles and 10000 particles per cycles, because of large computation time required. The results of the six iterations are given for the linear power distribution averaged over the fuel rods along the active height and the water density distribution averaged over the sub-channels, moderator

---

[1] Coupling procedure can also be started in STAFAS with pre-defined conditions for power distribution.

tube, assembly gap and the entire fuel assembly (i.e. including coolant and moderator) along the total height i.e. including the inactive part is shown in Figure 3.1.

i) Iteration-1

The iteration started in MCNP with constant input values for water density and temperature at 475 kg/m^3 and 287 °C, respectively, and fuel temperature at 1227 °C produces a power profile following a cosine shape, which is similar to that assumed by Cheng et al. [29] without coupling.

When the cosine power profile is transferred into STAFAS code for the corresponding thermal-hydraulics analysis, the average coolant density profile obtained has a maximum at the inlet and decreases from about 749 kg/m^3 at the bottom to below 100 kg/m^3 at the top. The average water density in the fuel assembly volume is about 500 kg/m^3, which is 4% more than that calculated by Cheng et al. [29] because of the different input conditions for the power distribution.

ii) Iteration-2

With the STAFAS output from iteration 1, a new input was generated for MCNP iteration 2. A new power profile is produced with the maximum peak shifted from the center in iteration -1 to the lower part of the core. This is because of the high water density and hence higher moderation in the lower part.

The power profile of MCNP iteration 2 with a maximum peak in the lower part produces an average water density profile in the cross section of the fuel assembly with maximum at the inlet of about 510 kg/m^3. The density decreases to about 280 kg/m^3 at the axial height 1.5 m and starts to increase again, because of the high water density in the moderator channels at the top. The average water density in the entire fuel assembly volume is reduced by 100 kg/m^3. The average coolant density in the sub-channel drops rapidly from 700 kg/m^3 at the inlet to 200 kg/m^3 at 2 m because of the high power peak.

iii) Iteration-3

The average power profile obtained in iteration-3 shows the maximum peak shifted to the upper part, because of the high water density obtained in the moderator channels from STAFAS iteration-2. The average water density in the fuel assembly axial cross section has a maximum of about 700 kg/m^3 at the inlet and decreases slowly to about 450 kg/m^3 at 4 m and starts to increase again because of the cold moderator flow from the top. The average coolant density decreases steadily along the axial height from 750 kg/m^3 at the inlet and drops gradually to 100 kg/m^3 at the outlet. The average water density in the fuel assembly volume is increased by 200 kg/m^3, compared to iteration-2.

iv) Iteration- 4

The average power profile obtained in iteration- 4 shows the maximum power peak, shifted back to the lower part, because of the high coolant density obtained from iteration -3. The corresponding thermal-hydraulics properties show the average water density in the fuel assembly cross section decreasing from about 590 kg/m^3 at the inlet to 300 kg/m^3 and increasing again to 500 kg/m^3. The average water density in the fuel assembly volume is reduced by 200 kg/m^3 compared to iteration-3.

v) Iteration- 5

With iteration- 5, the average power profile starts to develop a small peak in the lower part, because of the slightly high coolant density below 1 m. The maximum power peak occurs in the upper part because of the higher water density in the moderator channels obtained from iteration- 4. The average water density in the fuel assembly volume is increased by 200 kg/m^3 compared to the iteration- 4.

vi) Iteration-6

The average power profile and water density profiles of iteration-6 are comparable to iteration-4 profiles. The maximum power peak of 25 kW/m occurs at about 1.5 m axial height, due to the high coolant density. The average water density in the fuel assembly volume is the same as in iteration- 4 at 400 kg/m^3.

vii) Summary

An oscillation of power peak is observed from lower part of the active height to the upper part, because of the high water density of the coolant in the lower part and high water density of the moderator in the upper part of the core. With this oscillation, the iteration does not converge with coupled procedure in Figure (3.4). However, it can be concluded that a converged solution is expected to produce a power profile with two peaks, in the lower and the other in the upper part, because of the counter flow of the coolant and moderator water. A numerical technique must be introduced to accelerate convergence of the coupling procedure. The modified coupled procedure is described in Figure 3.6.
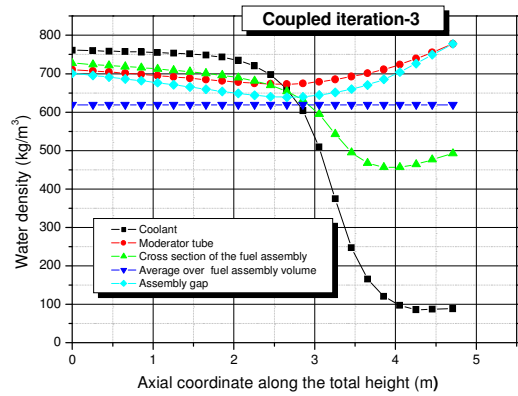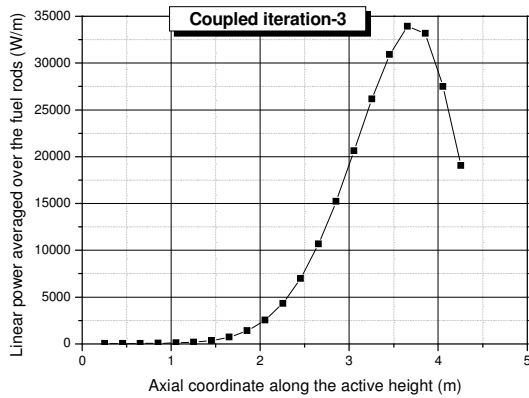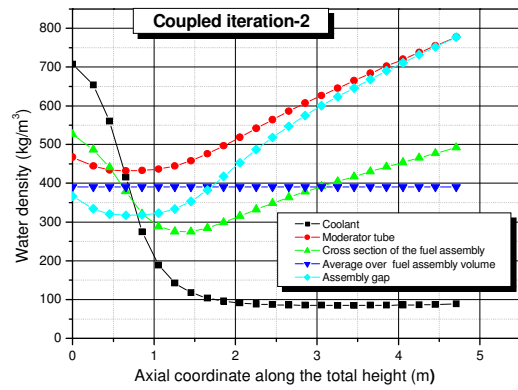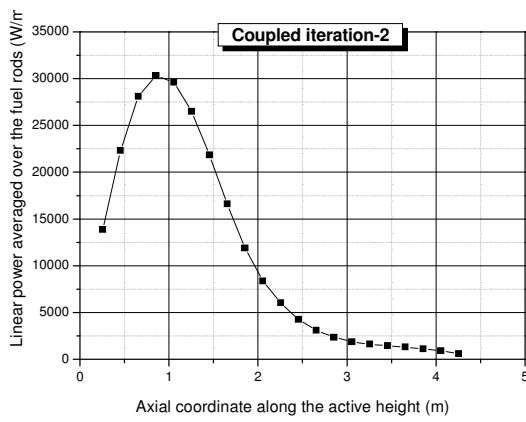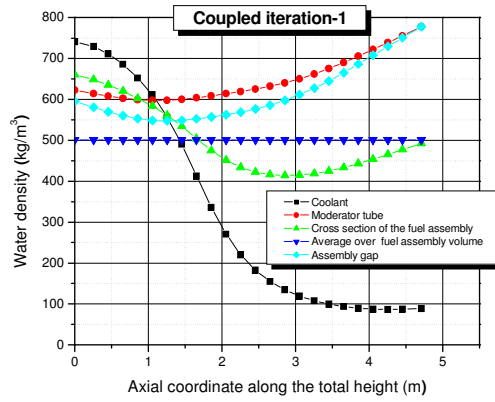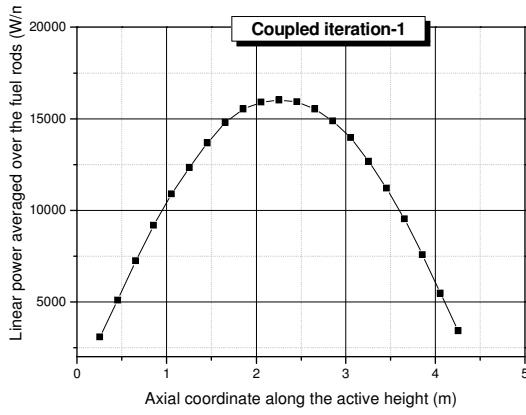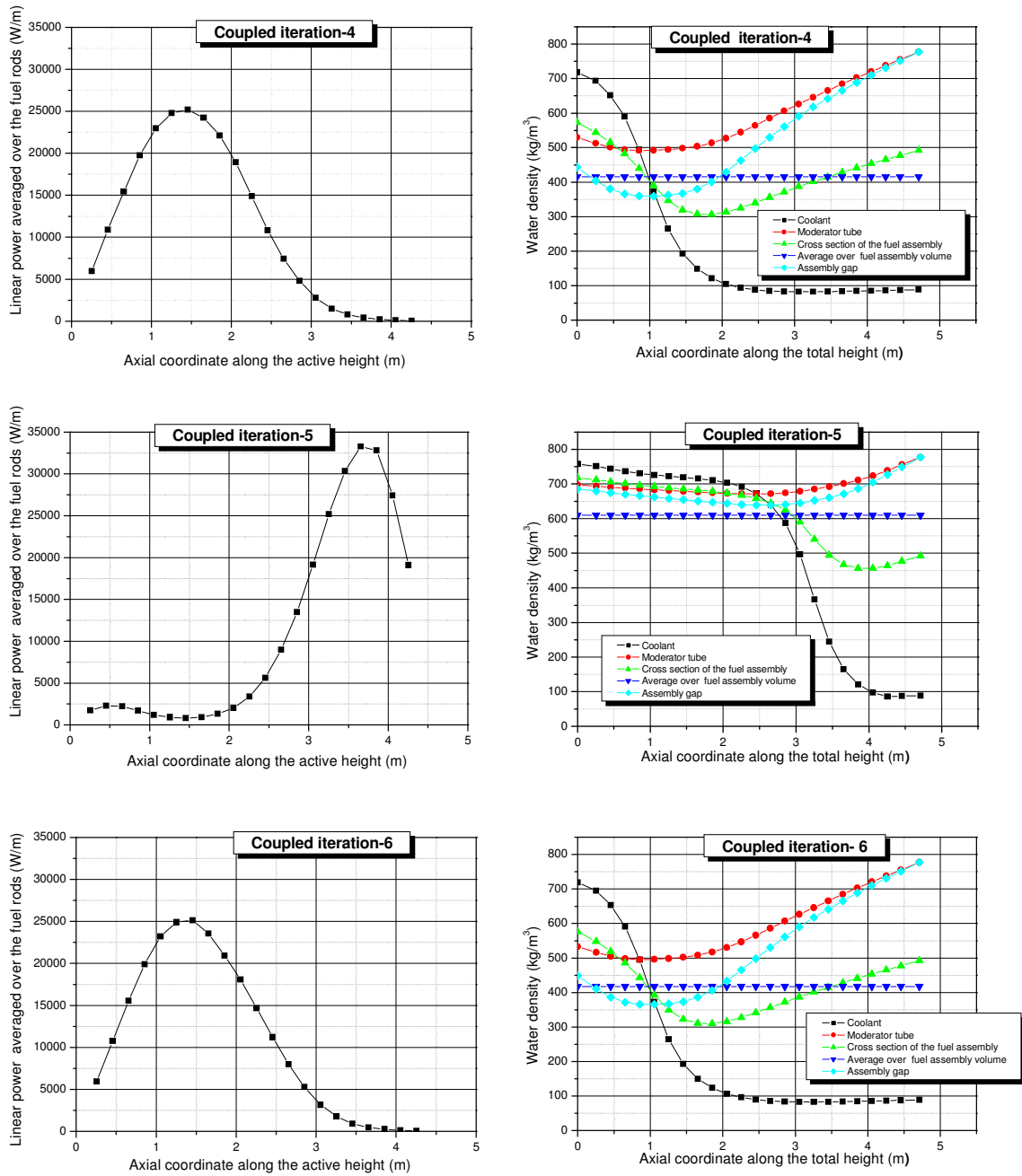
Figure 3.5: Convergence history of the coupling iteration without relaxation

3.4.2 Coupled procedure with relaxation

Figure 3.6 shows schematically the coupling procedure of MCNP/STAFAS code with relaxation.
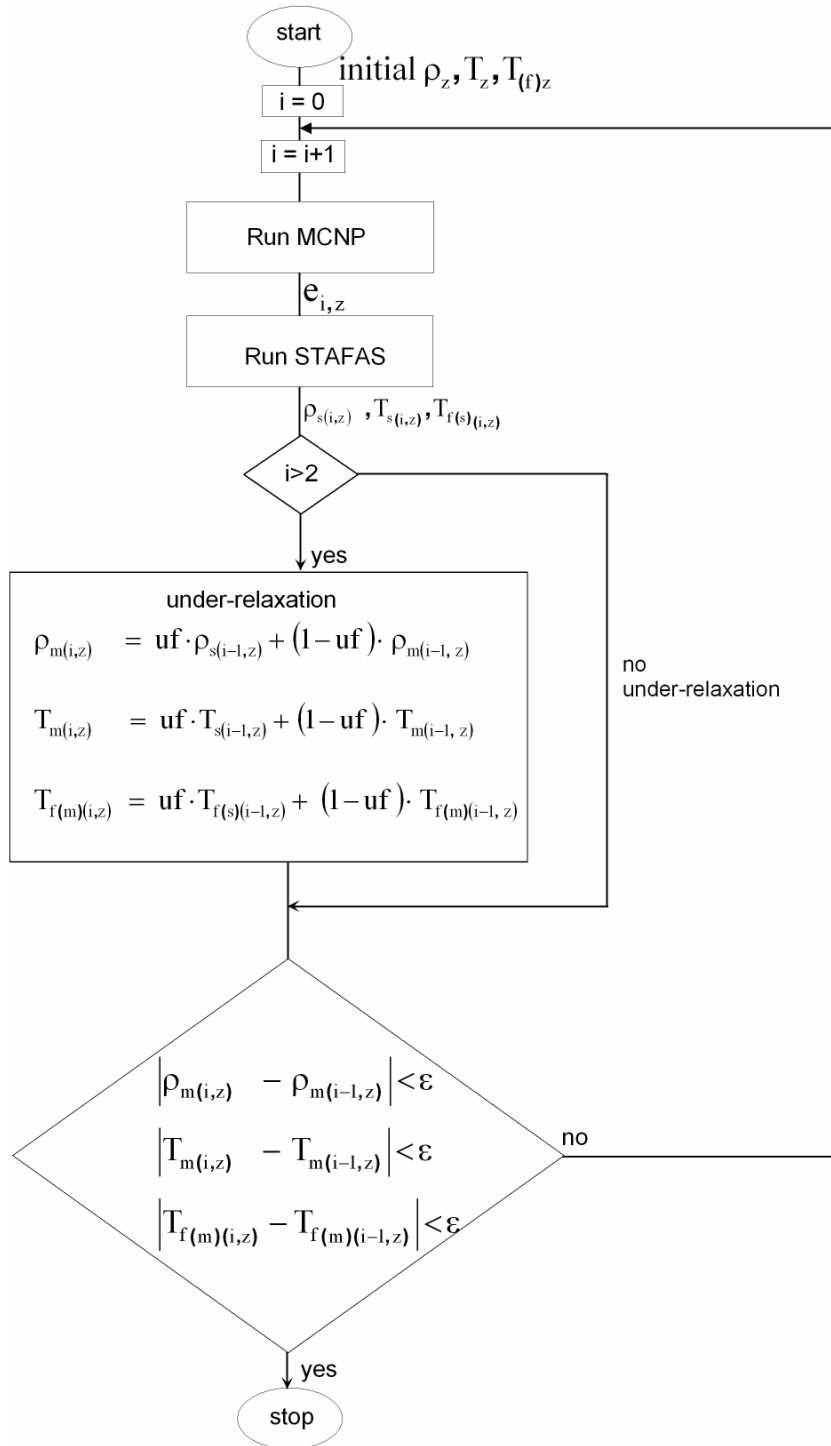
Figure 3.6: Flow chart of coupled algorithm with under-relaxation factor (uf)

In the modified flow chart of the coupling procedure, the subscripts s and m are introduced to indicate STAFAS output without relaxation and MCNP input with relaxation, respectively.

For the application of the relaxation at least two iterations are required in order to solve the equations shown in Figure 3.6. Therefore, the relaxation is applied at i >2. The first two iterations at i=0 and i=1 in MCNP are as described in Figure 3.4. The relaxation is applied on the STAFAS output of water density, water temperature distribution and fuel temperature distribution before they are used to generate a new MCNP input to start the next iteration. With the relaxation, the new MCNP input of water density, water temperature and fuel temperature distribution is denoted by $\rho_{m(i, z)}$, $T_{m(i, z)}$ and $T_{f(m)(i, z)}$, respectively. These are defined by the MCNP input data for the previous iteration, represented by $\rho_{m(i-1, z)}$, $T_{m (i-1, m)}$ and $T_{f(m) (i-1, z)}$, respectively and the subsequent STAFAS output without relaxation denoted by $\rho_{s (i-1, z)}$, $T_{s (i-1, z)}$ and $T_{f(s) (i-1, z)}$. The under-relaxation factor represented by uf is the same as in the preceding iteration.

To check the convergence of the coupled procedure with relaxation, two different under-relaxation factors, 0.5 and 0.2 have been tested for 10 iterations. The same calculation conditions in STAFAS and MCNP used to test the coupling procedure in Figure 3.4 were applied. For comparison of the different relaxation factors, the heating energy in fuel rod (6) at axial elevation 2.21 m is shown in Figure 3.7 for the different iterations. For the first two iterations without relaxation the heating energy is the same for the both cases. With an under-relaxation factor of 0.5, an oscillation is still observed, before it converges to the same magnitude at iteration-7. It is observed that with an under-relaxation of 0.2, a faster convergence is reached. The heating energy converges to the same magnitude from iteration-5 and the oscillation of the peaks from lower part to the upper part for different iterations is eliminated.

The computer time for one coupled iteration is about 280 minutes, most of which is from MCNP calculation with 10000 particles per cycle and 700 cycles. STAFAS calculation is in seconds.
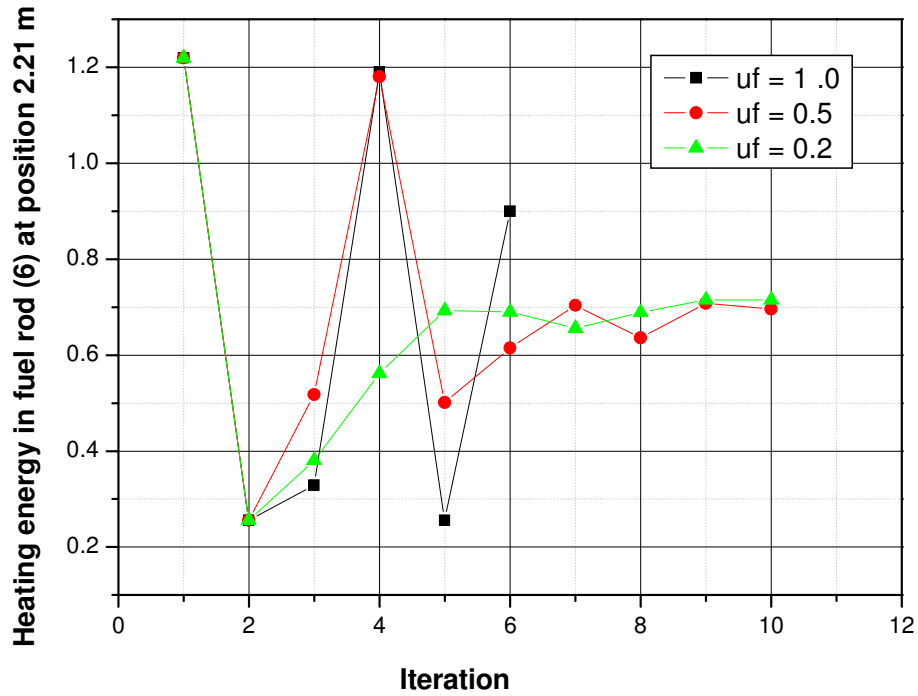
Figure 3.7: Convergence of the heating energy in fuel rod 6 at axial position 2.21 m

Figure 3.8 shows the convergence history of the average linear power distribution in the fuel rods and average water density distribution in the fuel assembly with under-relaxation uf= 0.2. The profiles for iterations-1 and 2 are the same as in Figure 3.5 without relaxation. A two-peak power profile is immediately developed in iteration-4. The peak in the upper part is due to the high density of the moderator flow. The power peak in the lower part results from the coolant density effect. The average water density distribution over the cross section of the fuel bundle in iterations 6, 7 and 8 are almost similar, which reflects on the linear power profiles obtained. For iteration-9 and iteration 10, two power peaks in the lower part at axial position 0.8 m and in the upper part at 3.5 m are developed. The average power profile and water density distribution from iteration 6 are assumed to be iterating between the converged solutions if the uncertainties in the MCNP code is taken into account.

Coupled iteration -6 / Coupled iteration-6

Coupled iteration -7 / Coupled iteration-7

Coupled Iteration -8 / Coupled iteration-8
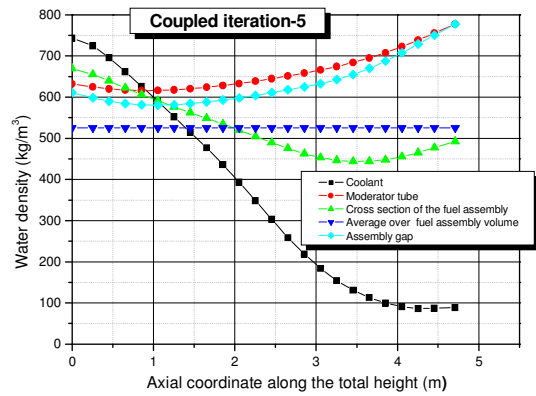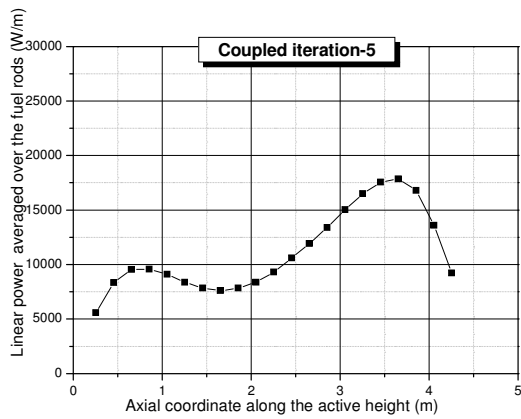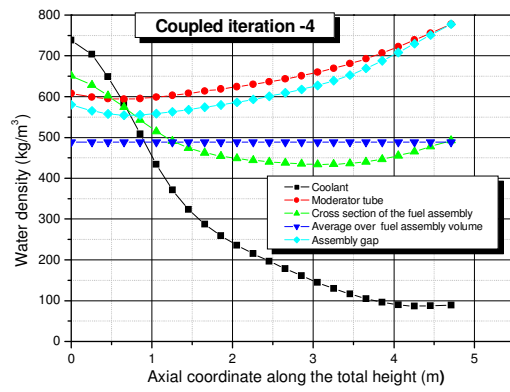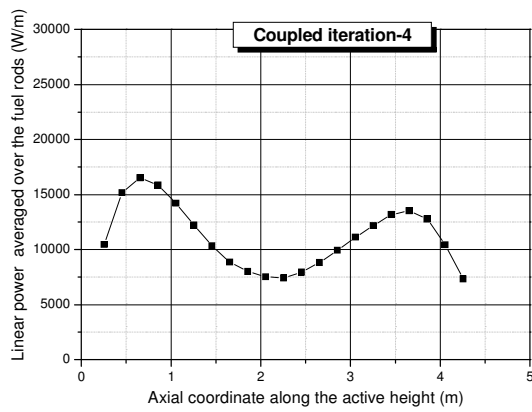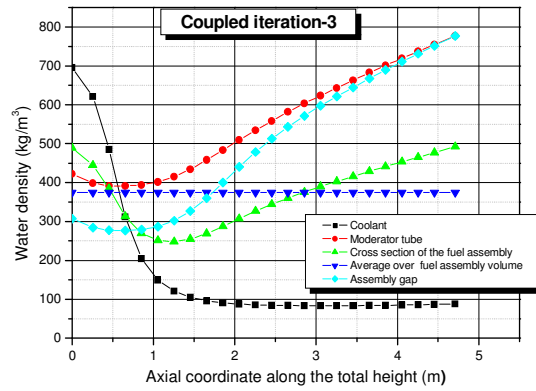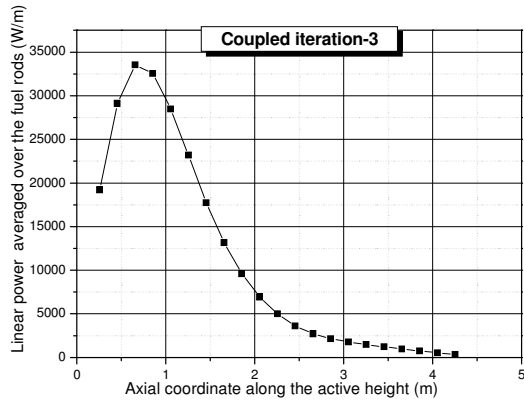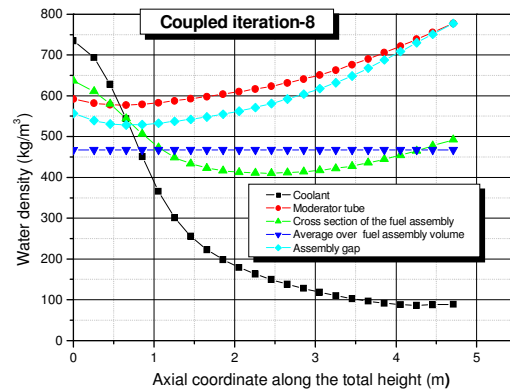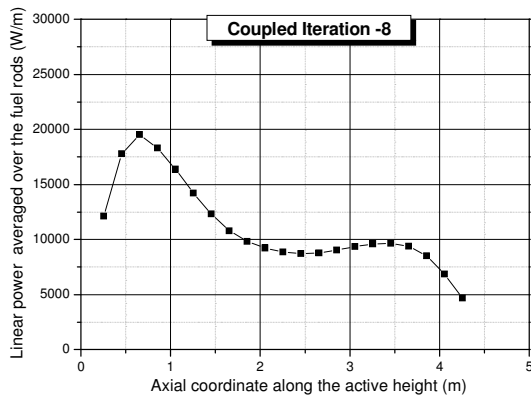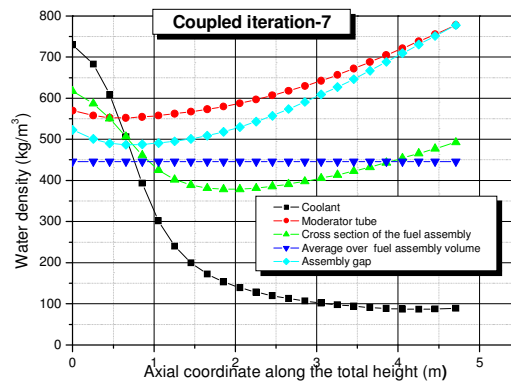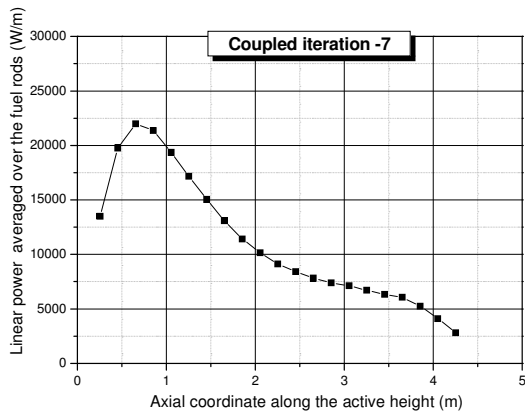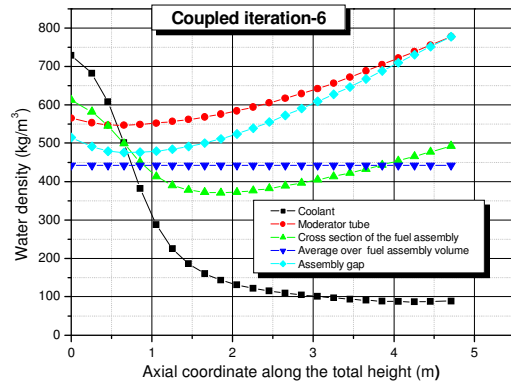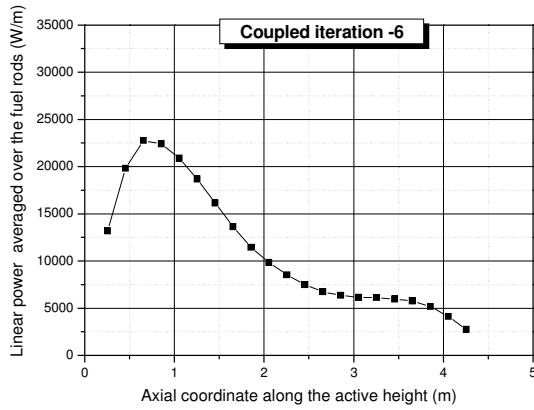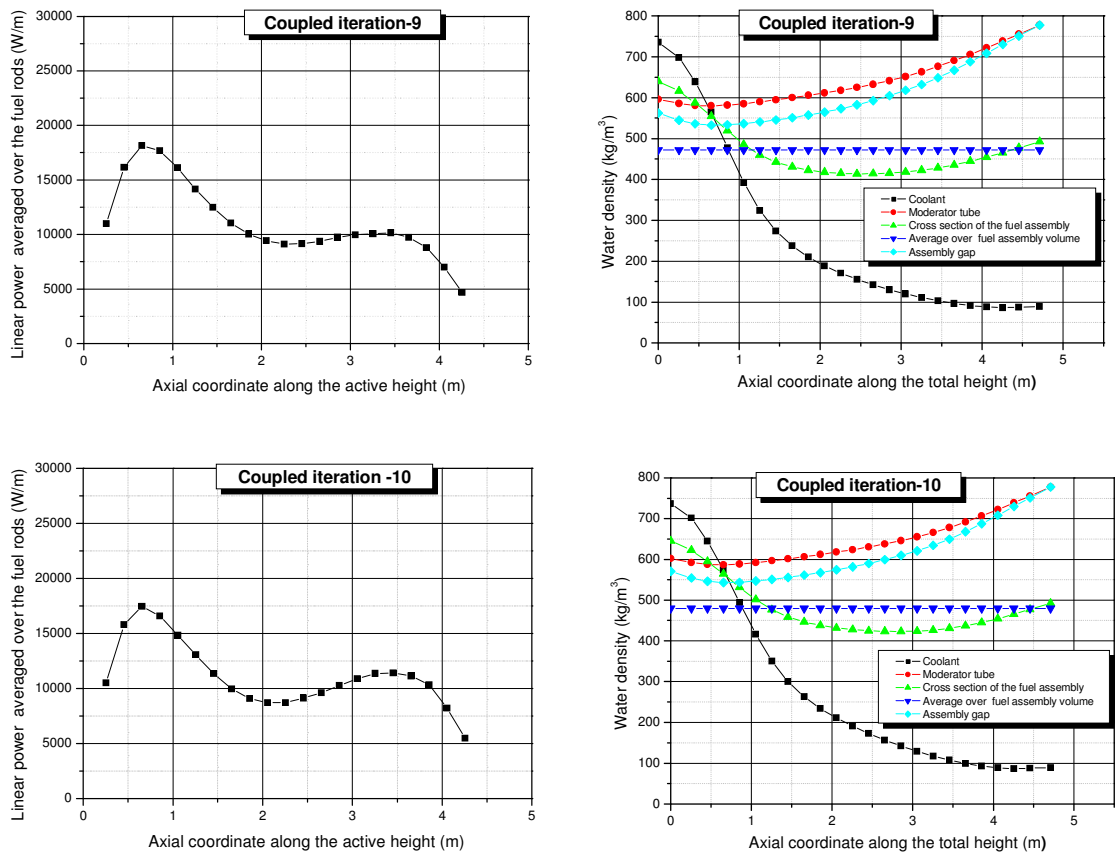
Figure 3.8: Average linear power and water density distribution using uf=0.2

3.5 Estimation of Monte-Carlo precision

3.5.1 Accuracy and precision

MCNP results represent an average of the contributions from many histories sampled during the course of the problem. An important quantity equal in stature to the MCNP answer (or tally) itself is the statistical error or uncertainty associated with the results. If a tally is not well behaved, the estimated error associated with the result generally will not reflect the true confidence interval of the result and, thus, the answer could be erroneous [58]. To understand the error associated with MCNP results, the difference between precision and accuracy of Monte-Carlo calculation is discussed [58]. Precision is defined in MCNP as the uncertainty in $\bar{x}$, the estimated mean of the tally, caused by the statistical fluctuations of $x_i's$ for the portion of the physical phase space sampled by Monte-Carlo process. Accuracy on the other hand is a measure of how close the expected value of $\bar{x}$ is to the true physical quantity being estimated. It is important to note that errors or uncertainty estimate for the results of Monte-Carlo calculations refer only to the precision of the results, not to the accuracy. It is quite possible to calculate a highly precise result that is far from the physical truth because nature has not been modeled faithfully.

3.5.2 Factors affecting MCNP accuracy

In the MCNP manual [58], the three factors that affect the accuracy of a Monte-Carlo result are presented as follows:

i) The code – this encompasses: the physics features included in a calculation, as well as the mathematical models used; uncertainties in the data such as the transport and reaction cross sections in energy; and coding errors. MCNP is a mature and heavily used production code. With steadily increasing use over the years, the likelihood of a serious coding error continues to diminish. The error by cross section can only be caused when different cross sections data are used. In this study, the same cross section data were used throughout. Mori et al. [60] studied the effect of the different cross sections which shown to have effect.

ii) The second area, problem-modelling factors, can contribute to a decrease in the accuracy of a MCNP calculation. Many calculations produce seemingly poor results because the model of the energy and angular distribution of the source is not adequate. In this study, a continuous energy model is used, which is reported to produce a more accurate result compared to multi-group or few group energy models [58].

A test MCNP run was performed on a parallel computer by Bernnat [82] using the same input file with relaxation factor of 0.2 for iteration 10 and iteration 11 and for 100000 particles with up to 4000 generations. The two iterations were run with different starting source distribution. In the first case for iteration -10, the starting source particles were generated from a very poor distribution, but stored after 100 cycles. Convergence in MCNP was achieved after 300 cycles. In the other case for iteration-11, the starting source was generated from a converged source from iteration-10 and the results converged after about 100 cycles. The results reported for relative power distribution in rod (5) is shown in Figure 3.9. The relative error calculated for the two cases is about 12%, which indicates a significant effect of the source distribution on MCNP results.
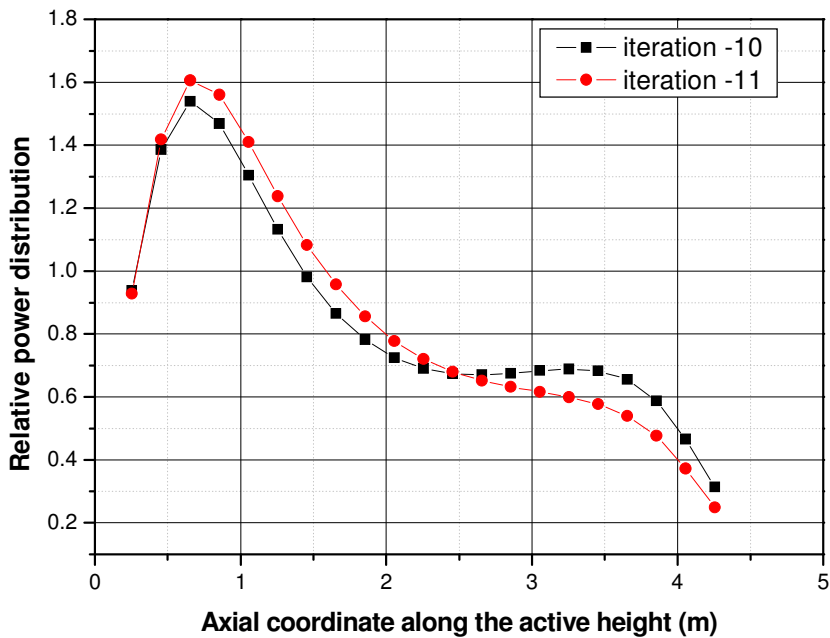
Figure 3.9: Relative power distribution in rod 5 from Bernnat [82]

Bernnat [82] showed that the final tally distribution does not differ significantly from 2000 – 4000 cycles. Results of the calculations for 100000 particles per cycles and varied number of cycles from 300 – 4200, are compared with the results for 10000 particles per cycles and 700 cycles as shown in Figure 3.10.
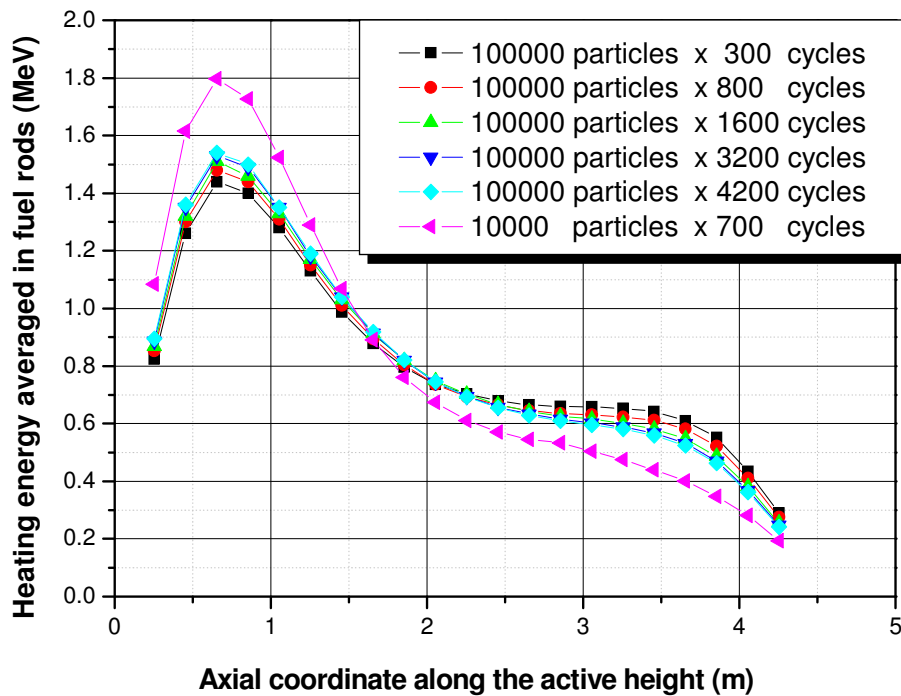
Figure 3.10: Heating energy distribution with varied number of cycles

The accuracy of the results with 100000 particles by 4200 cycles with respect to 10000 particles by 700 cycles is about 7%, which is much higher than the MCNP precision of 0.04% with 10000 particles by 700 cycles. The precision given in MCNP on the other hand is a convenient number, which represents the statistical error as a fractional result with respect to the estimated mean. It does not reflect the source distribution error calculated, which indicates MCNP accuracy problem.

The following conclusions were drawn from MCNP calculation:
   a) For a well converged tally, a well distributed starting source from a previous converged solution is required.
   b) Large number of cycles must be performed (> 800) and large number of generations must be skipped (up to 300) if the starting distributions differ remarkably from the final distribution.
   c) A larger number of particles/cycle should be used (e.g. 100000)

iii) Other factor that affected MCNP accuracy problem is the user, through input problems and abuse of variance reduction technique. Error on the geometry can be detected earlier, when neutron particels leak out of the geometry. The MCNP input was created automatically

from the coupling procedure, which eliminates input problem error during the coupling iteration. Variance reduction techniques were not used in MCNP because all the parts of the geometry were important for neutron transport.

3.5.3 Factors affecting MCNP precision

MCNP provides information about the precision of the results in the output. The factors that affect the MCNP precision problem are summarized from [58] as follows:

i) Forward Vs adjoint calculation

The choice of a forward vs. adjoint calculation depends mostly on the relative size of the source and detector regions. Forward calculations transports particles from source to detector (tally) regions and are preferable, when the detector region is large and the source is small. Adjoint calculations transports particles backwards from detector region to the source and are preferable, when the source region is large and detector is small.

ii) Tally type

An efficient tally region will average over a region in phase space as practical. In this connection, tally dimensionality is extremely important. A one-dimensional tally is typically 10 to 100 times easier to estimate than a two-dimensional tally.

iii) Variance reduction technique

Variance reduction techniques can be used to improve the precision of a given tally by increasing the non-zero tallying efficiency and by decreasing the spread of non-zero history score.

iv) Number of histories

More histories can be run to improve precision, because the precision is proportional to $1/\sqrt{N}$, where N is the total number of histories. However, running more histories is costly in computation time and therefore is viewed as the method of last resort for difficult problems.

3.6 Accuracy of coupling procedure

The MCNP accuracy problems have been discussed in the previous section. It was shown that, with the calculation conditions (10000 particles by 700 cycles) used in MCNP to test the coupled procedure, a 7% error was computed from MCNP accuracy problem. This is subsequently expected to have an effect on the convergence of the coupling procedure.

To check the accuracy of the coupling procedure a large number of iterations were performed with the under-relaxation factor of 0.2. The local results for heating energy in fuel rod(6) at axial elevation of 2.21 m for each iteration is shown in Figure 3.11. It is observed, that from iteration-5, the heating energy oscillates in the energy range of 0.6 – 0.8 MeV. It can be concluded that the converged solution is oscillating within the 7% error bar due to the MCNP accuracy problem.
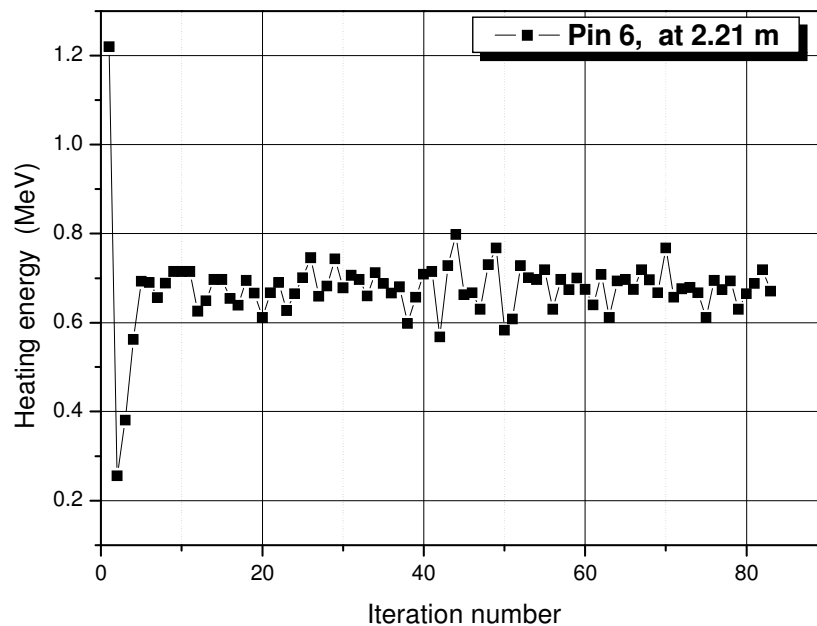
Figure 3.11: Heating energy versus number of iteration

A small standard deviation of 0.041 MeV from iteration 5 to 83 was computed, which is less than the accuracy of 0.086 MeV described in chapter 3.5.2. This already indicates a good accuracy of the coupled solution.

The accuracy error in MCNP can be reduced with large number of particles, which will subsequently improve the accuracy of the coupling procedure.

4   RESULTS

4.1   Effect of the coupling on the linear power distribution

In the previous chapter the coupled procedure of MCNP and STAFAS was presented. The coupled procedure was tested for convergence and an under-relaxation was introduced to achieve convergence. For the test analyses, the one-eighth square fuel assembly in Figure 2.2 was modeled. It was shown that a converged solution could be defined after 5 iterations with an under-relaxation factor of 0.2, taking into account the error due MCNP accuracy problem.

In this chapter, analyses of the design parameters for the square fuel assembly design are presented for a converged solution. Note that all the results presented in this chapter are preliminary, they include the 7% error computed from MCNP accuracy problem.

Before discussing the design parameters of the fuel assembly, the effect of the coupling i.e. density variation on the power distribution is described to indicate the necessity of the coupling procedure. Figure 4.1 shows the linear power distribution, averaged over all the fuel rods of the fuel assembly along the active height for three cases: i) an uncoupled case, ii) coupled case with water density and water temperature effect only and iii) a coupled case with water density, water temperature and fuel temperature feedback (Doppler Effect).
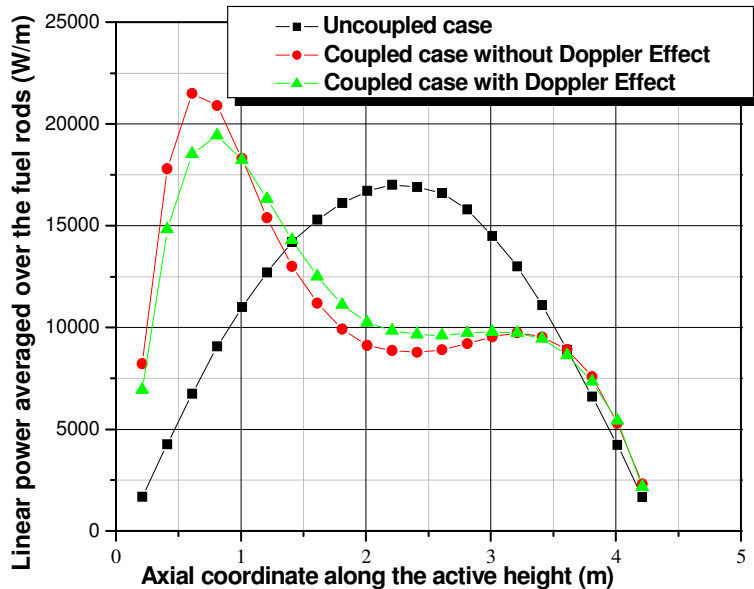

Figure 4.1: Linear power distribution averaged over the fuel rods

The uncoupled case with constant values of water density at 476 kg/m^3, water temperature at 287 °C and fuel temperature at 1227 °C produced a power profile similar to a cosine shape with a maximum at the centre. This is similar to the power profile in a PWR. The converged solution for the coupled case with water density and water temperature feedback only produced a power profile with two power peaks, one strong peak with a maximum of 22 kW/m at the lower part and a weaker peak of about 19 kW/m in the upper part. The two power peaks produced are due to the high moderation from the coolant in the lower part and high moderation in the upper part from the moderator water.

The coupled case with the fuel temperature feedback produced a flatter peak in the lower part at 19 kW/m. The power peak is flattened because at high power, which corresponds to high fuel temperature. At high fuel temperature, more fission neutrons are captured, as the resonance region is widened and hence less power is produced.

The difference of the power profile between the uncoupled case and coupled case is large due to the counter flow of the coolant and moderator flow. To correctly predict the power profile of such fuel assembly design a coupled analysis of neutronics for power distribution and thermal-hydraulics is necessary, which emphasizes the significance of the coupling method.

4.2 k-effective values

Table 4.1 shows the k-effective values for the three cases that were studied with or without the coupled procedure. The uncoupled case and the coupled case without Doppler Effect were performed with constant fuel temperature of 1227 °C. Comparisons made with the coupled case with Doppler Effect show that the k_{eff} value obtained with the Doppler Effect is about 0.6 % higher than that without Doppler Effect, which is due to the temperature reduction. This means that the negative temperature coefficient as expected by the Doppler Effect is obtained. A reduction in fuel temperature increases the k-effective value and the fission power generation increases.

	Uncoupled case	Coupled case without Doppler Effect	Coupled case with Doppler Effect
k-effective (k_{eff})	1.16619	1.16365	1.17112
Standard deviation	0.00022	0.00022	0.00023

Table 4.1: k-effective values computed

4.3 Analyses of results for the HPLWR fuel assembly design

4.3.1 Linear power distribution in the fuel rods

Figure 4.2 shows the linear power distribution along the active height in each individual fuel rod of the one-eighth fuel assembly. The labeling of the fuel rods of the fuel assembly modeled is depicted in Figure 2.2. The corner fuel rod(7) was modeled with a 4% fuel enrichment and the other fuel rods with 5% enrichment. The power distributions in the half rods: rod(1), rod(3), rod(4) and rod(7) are multiplied by a factor of two to obtain a good comparison.
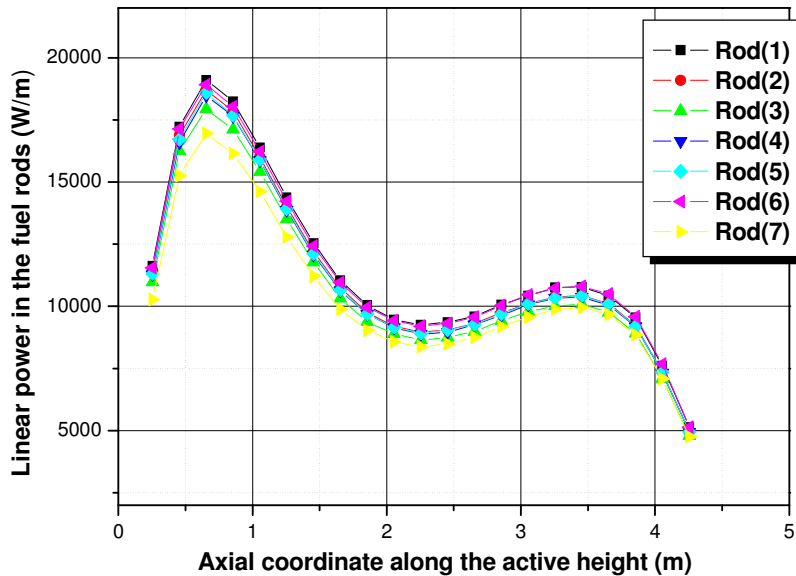
Figure 4.2: Linear power distribution in each fuel rod along the active height

A well uniform power distribution is obtained in the fuel rods with exception in rod(7) and rod(3). A slightly lower power profile is obtained in rod(7) because of the 20% lower enrichment. The enrichment reduction in the corner rod was introduced after analysis by Waata et al. [83] with uniform enrichment in the fuel rods showed a higher power profile in the corner rod as it is higher moderated at the corner. This subsequently led to a hot spot at the corner. The fuel rod(3) is slightly positioned far away from the moderator tube and therefore receives less moderation and produces subsequently less power.

4.3.2 Fuel temperature distribution in the fuel rods

Figure 4.3 shows the fuel temperature distribution in the fuel rods varying along the active height. The converged solution shows a temperature profile with two peaks, one in the lower part at 1400 K (1127 °C) and the other in the upper at 1200 K (927 °C). The temperature profile is closely related to the power profile. At a high power peak the maximum fuel temperature occurs.
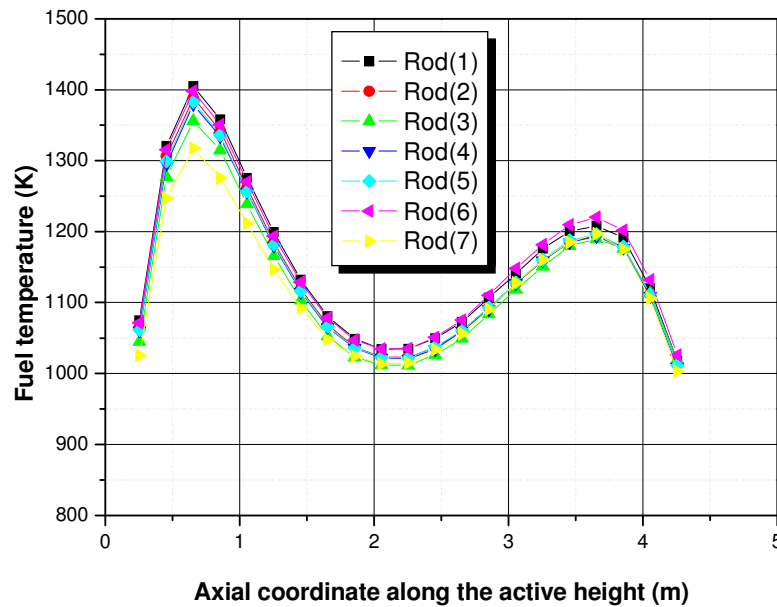
Figure 4.3: Fuel temperature distribution in each fuel rod along the active height

4.3.3 Power distribution in the sub-channels

Figure 4.4 shows the power distribution in the sub-channels as defined in Equation (2.15) from conduction within the fuel rods. The labeling of the sub-channels is given in Figure (2.2). The power profile in SC(9) is lower because it is being heated-up by an equivalent of one-eighth of the power in the rod(7), which also has the lowest power. The power profile in SC(3) is contributed by one-eighth of power distribution in rod(3), which was shown to be slightly lower power and one-fourth power from rod(2). The heat-up in SC(1), SC(5), SC(6), SC(7) and SC(8) are similar as they are heated-up by an equivalent of half a fuel rod. The power profile in the center sub-channels SC(2) and SC(4) is highest as they are being heated by an equivalent of one whole fuel rod.
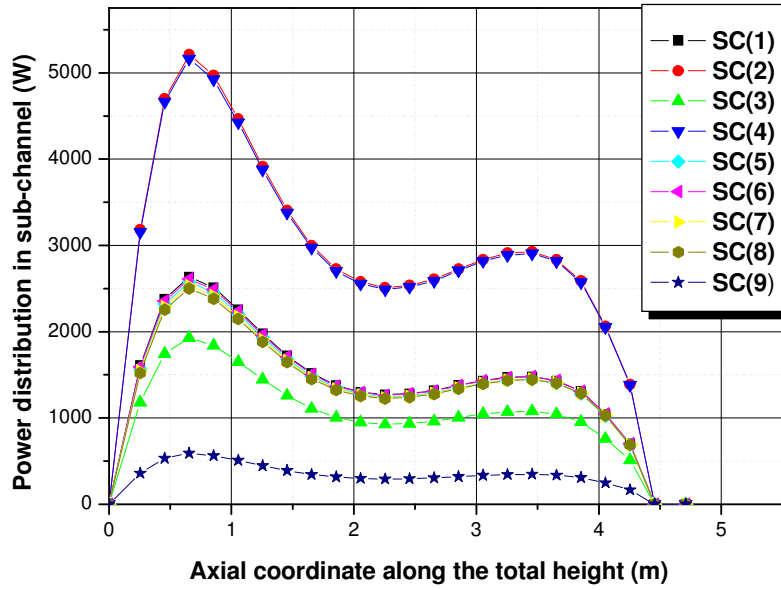
Figure 4.4: Power distribution in the sub-channels long the total height

4.3.4 Heat flux distribution in the sub-channels

Figure 4.5 shows the heat flux distribution on the sub-channel walls along the total height. At an axial elevation of about 0.7 m, a maximum heat flux of about 1.04 MW/m^2 is obtained in the centre sub-channels.
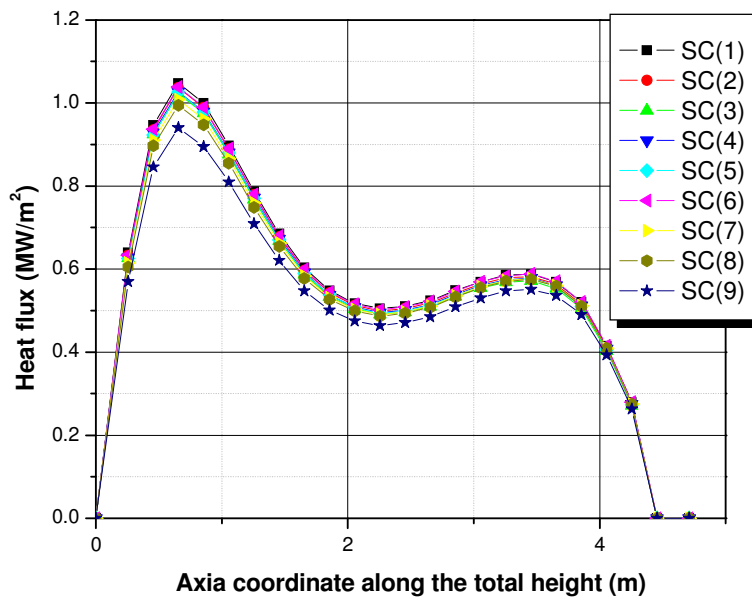

Figure 4.5: Heat flux distribution in the coolant sub-channels along the total height

4.3.5 Mass flux in the sub-channels

Figure 4.6 shows the coolant mass flux distribution in the different coolant sub-channels along the total height. The sub-channels are thermal-hydraulically connected; hence the effect of the mixing between neighboring sub-channels is included. The analysis in STAFAS was carried out with 14 grid spacers with no additional vanes. The first grid spacer is positioned at the bottom of the active height and the distance between each grid spacer is 0.3 m. A mass flux redistribution is observed due to the presence of the grid spacers.

A strong non-uniformity of the mass flux distribution in the different sub-channels is obtained due the different hydraulic diameters of the sub-channels (see Table 2.3). The mass flux distribution in SC(9) is lowest with a small hydraulic diameter of 2 mm. A high profile of the coolant mass flux in the center sub-channels SC(2), SC(4) and SC(7) is obtained with hydraulic diameter of 5.5 mm. A good mixing in center sub-channels SC(2), SC(4) and SC(7) is observed as they have no contact to any wall boundaries of the moderator tube and assembly gap. After each spacer, the mass flux is shown to be decreasing in the center-channels due to the mixing. The other sub-channels are connected to the moderator flow channels (moderator tube and assembly gap) and exchange heat by conduction. The mass flux is shown to be decreasing after each grid spacer due to the poor mixing.
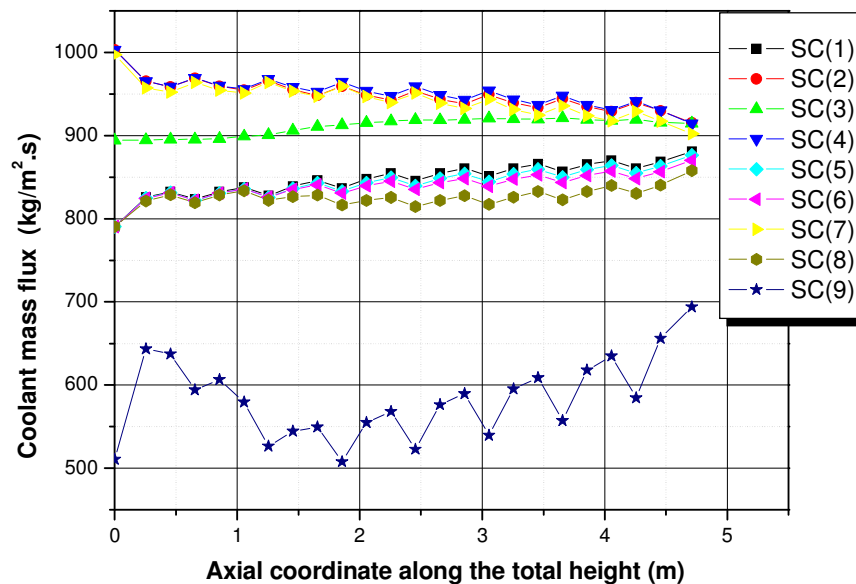
Figure 4.6: Mass flux distribution in the sub-channels along the total height

4.3.6 Coolant temperature distribution in the sub-channels

Figure 4.7 shows the coolant temperature in the different sub-channels along the total axial height. A well uniform temperature distribution is obtained in sub-channels SC(1), SC(3), SC(5), SC(6) and SC(8). The pseudo-critical temperature of 384 °C is reached close to the inlet region at 1.0 m. A temperature spread of about 50 ^{o}C is obtained in the upper part. The maximum temperature occurs in the center sub-channels SC(2), SC(4) and SC(7).

The coolant temperature profile in SC(9) is slightly higher compared to the other sub-channel due to the low mass flux (See Figure 4.6). The coolant temperature in SC(9) drops rapidly above 3.5 m because of the heat exchange with the cold moderator entering from the top of the active height. At the exit the average outlet temperature of 507 ^{o}C was evaluated.
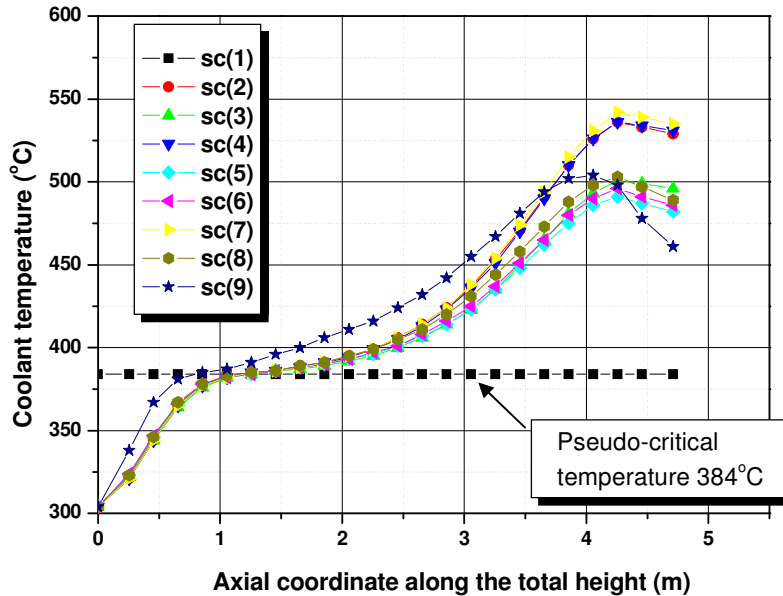
Figure 4.7: Coolant temperature distribution in the sub-channels along the total height

4.3.7 Coolant density distribution in the sub-channels

Figure 4.8 shows the coolant density distribution in the sub-channels along the total height. As the coolant temperature increases, the coolant density decreases. A uniform density distribution along the active height is obtained in the SC(1) – SC(8). The coolant density drops from 750 kg/m^3 at the inlet to about 100 kg/m^3 at the outlet. The density distribution in SC(9) is lower because of the high temperature obtained due to the low mass flux.
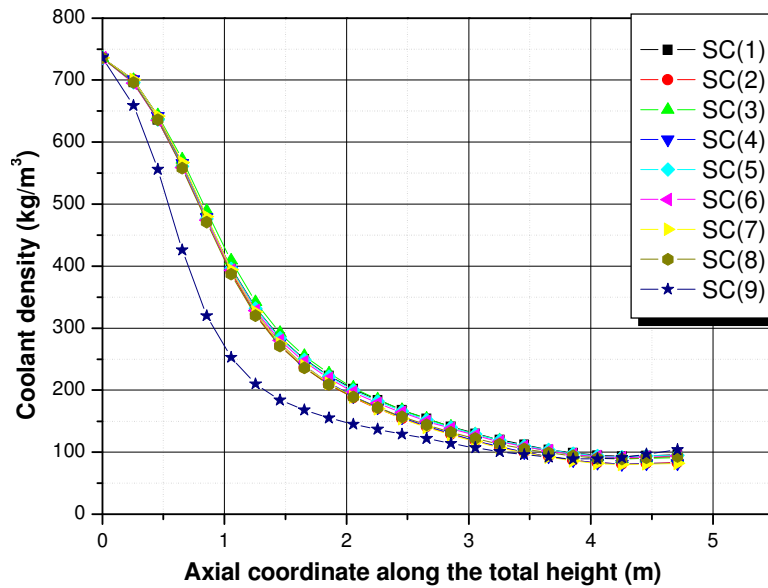
Figure 4.8: Coolant density distribution in the sub-channels along the total height

4.3.8 Heat transfer coefficient of the coolant sub-channels

Figure 4.9 shows the heat transfer coefficient on the cladding surface in the sub-channels. The heat transfer coefficient was computed with Bishop's correlation defined in Equation (2.20). From the inlet the heat transfer coefficient increases and when it reaches the pseudo-critical line, a maximum is obtained. Beyond the pseudo-critical line the heat transfer coefficient decreases. A maximum heat transfer coefficient of 65 kW/m^2.K is obtained in the center sub-channels SC(2), SC(4) and SC(7). The maximum values vary between the different sub-channels because of the different mass flux. The maximum peak is reached first in SC(9) because of the low mass flux.

73
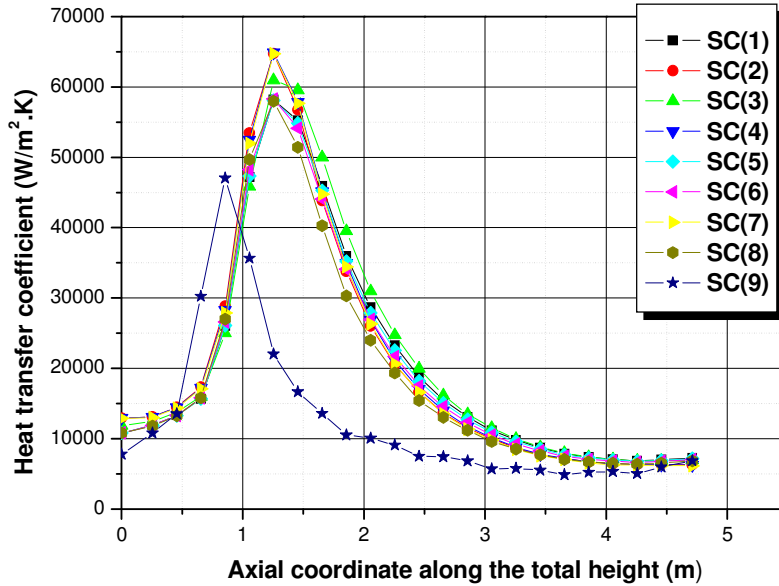
Figure 4.9: Heat transfer coefficient in the sub-channels along the total height

4.3.9 Cladding temperature distribution in the sub-channels

Figure 4.10 shows the cladding surface temperature distribution of each individual sub-channel. The cladding temperature increases from the inlet as the heat transfer coefficient increases. At the point where the heat transfer coefficient has a maximum, the cladding temperature decreases. Beyond the pseudo-critical line, where the heat transfer coefficient decreases, the cladding temperature increases. The maximum cladding temperature in the different sub-channels does not exceed the allowable limit of 620°C for the HPLWR. A well uniform distribution is obtained in the different sub-channels with exception of SC(9). The cladding temperature distribution in SC(9) shows fluctuations along the total height due to the poor mixing in the corner sub-channel with the low mass flow rate. A temperature spread of about 50 °C between the different sub-channels is obtained at the upper part of the active height. In an analysis with uniform enrichment Waata et al [83], a temperature spread of 100 °C between the sub-channels was obtained because of the hot corner fuel rod, which was similar to that obtained in the analysis by Cheng et al. [26].
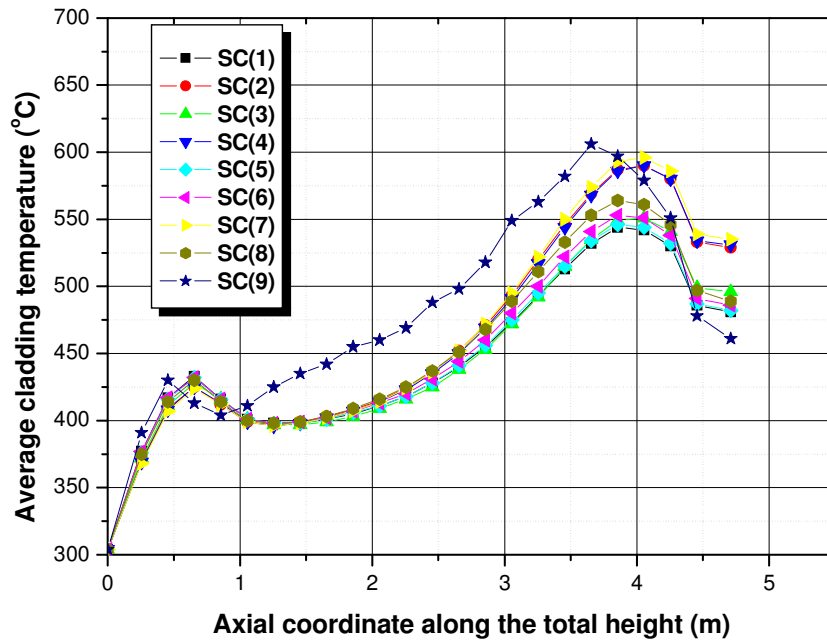
Figure 4.10: Cladding surface temperature distribution in the sub-channels

4.3.10 Average water density distribution

Figure 4.11 shows the average water density distribution in the sub-channels, the moderator tube, in the assembly gap, over the cross section of the fuel assembly and the total average over the entire fuel assembly volume.

The overall water density obtained over the entire fuel assembly volume is 476 kg/m^3 as shown in Figure 4.10. The average coolant density decreases significantly from above 700 kg/m^3 to below 100 kg/m^3 as the pseudo-critical temperature is crossed. The water density is highest at the inlet of moderator channels. The moderator density in both the moderator tube and assembly gap decreases in the flow direction downwards from about 780 kg/m^3 to 550 – 600 kg/m^3 as it flows downwards and is warmed up. The density in the moderator tube is slightly higher than in the assembly because of the low heat-up. The average water density in the cross section of the fuel assembly is highest at the inlet at 650 kg/m^3, decreases to below 410 kg/m^3 at axial height of 2 m and increases again to about 500 kg/m^3 because of the high moderator density in the upper part.
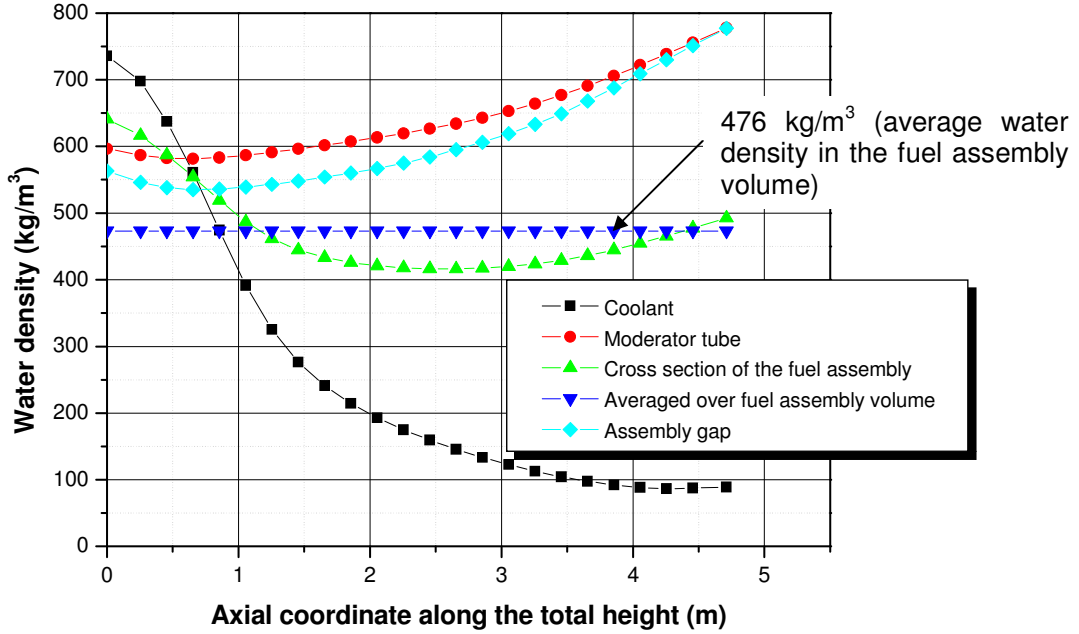
Figure 4.11: Water density distribution in the fuel assembly

4.3.11 Pressure drop in the sub-channels and moderator channels

Figure 4.12 shows the pressure distribution in the sub-channels. It was assumed that the pressure drop in all sub-channels at same axial elevation is the same.
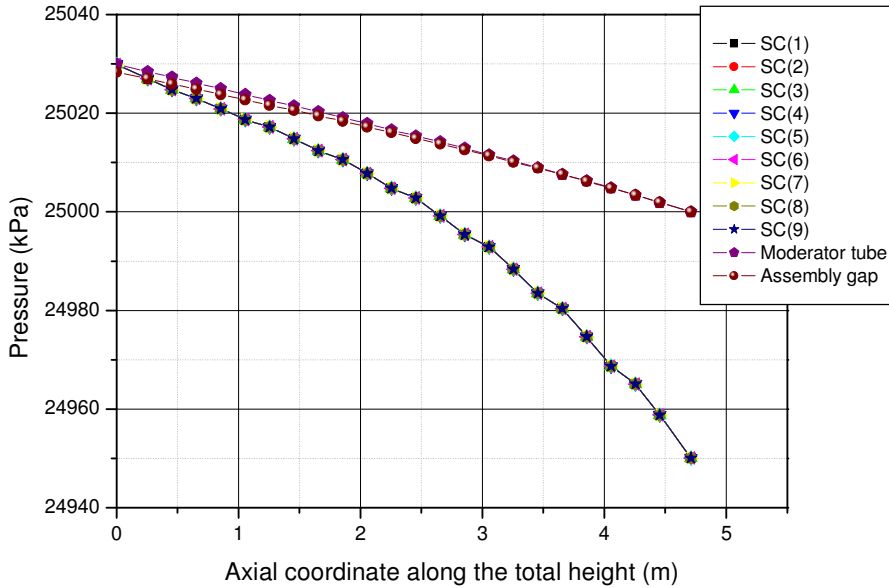
Figure 4.12: Pressure distribution in the sub-channels, and moderator channels

The total pressure loss in the coolant sub-channels is about 60 kPa. The pressure at the first node z=0 (i.e. inlet condition of the coolant) is calculated by taking into account the pressure drop in the moderator tube and assembly gap. The reference pressure is at 25 MPa, which is the inlet pressure of the moderator tube and assembly gap. The pressure in the moderator tube and assembly gap increases in the flow direction (downwards) due to the gravitation.

4.3.12   Temperature distribution in the moderator channels

Figure 4.13 shows the temperature distribution in the moderator tube and assembly gap. Due to the heat transfer between the coolant and the moderator, the water temperature in the moderator tube and assembly gap increases from the inlet at 280°C to 360 °C - 365 °C. The temperature increase is higher in the assembly gap because the slightly low heat transfer coefficient. The moderator temperature does not reach the pseudo-critical temperature of 384 °C.
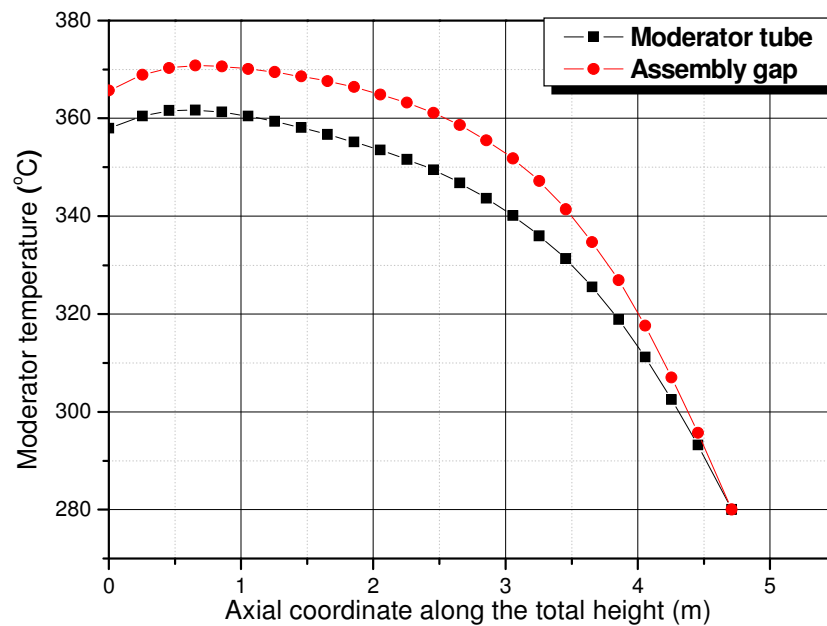
Figure 4.13: Temperature distribution in moderator channels along the total height

4.3.13 Heat from coolant sub-channels to moderator channels

Figure 4.14 and Figure 4.15 shows the heat that is transferred from the coolant to the moderator tube and assembly gap at each axial elevation.

The fuel assembly design (see Figure 2.2) shows that only sub-channel SC (1) and SC (3) have contact to the moderator tube and SC (5), SC(6), SC(7) and SC(9) have contact to the assembly gap. It is observed that below 0.8 m a negative heat is obtained which indicates that the moderator water close to the inlet of the sub-channels is heating the coolant water. The heat transferred from SC(3) in Figure 4.14 and SC(9) in Figure 4.15 is lower because of the small heat transfer surface area that cover the moderator channels.
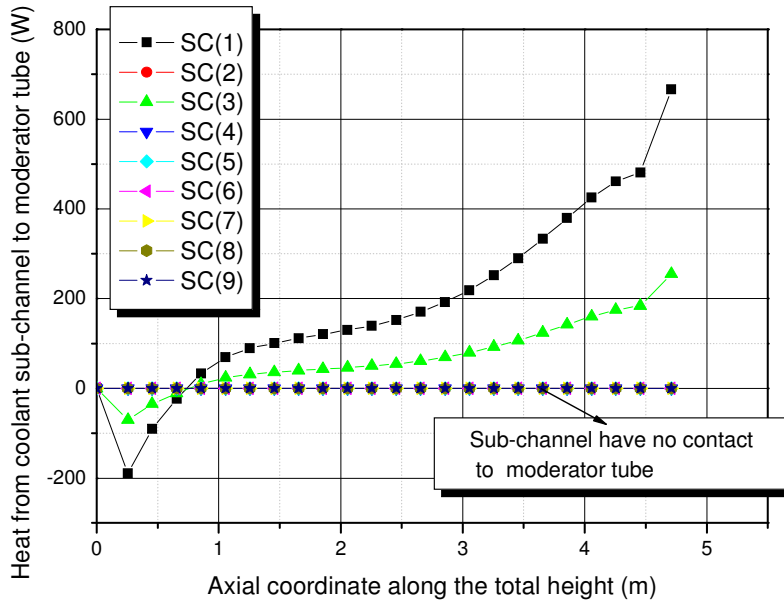
Figure 4.14: Heat from sub-channel to moderator tube
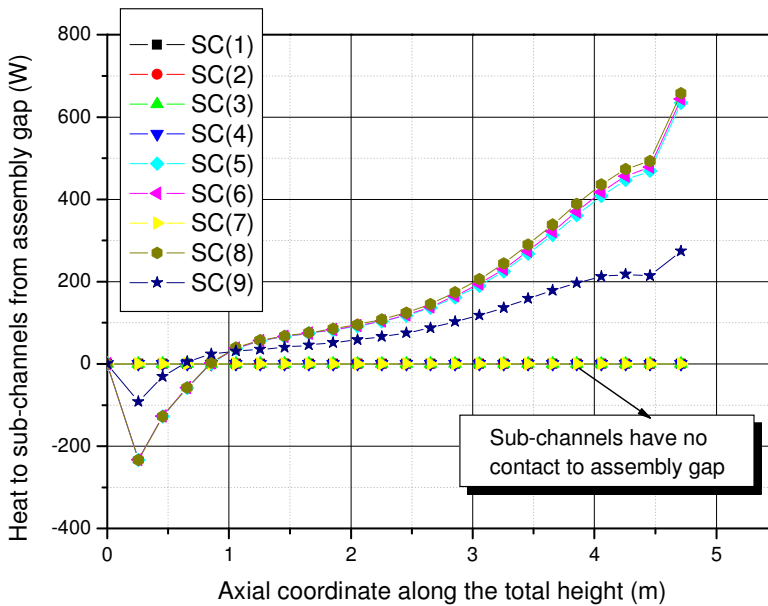
Figure 4.15: Heat from sub-channel to assembly gap

5   CONCLUSION

A new coupled code system with the Monte-Carlo code MCNP and the sub-channel code STAFAS has been developed for neutronics/thermal-hydraulics analysis of a fuel assembly design.

The coupling procedure of MCNP/STAFAS has been realized automatically. MCNP calculates the power distribution in each fuel rod, which is then transferred into STAFAS to obtain the corresponding thermal-hydraulics conditions in each sub-channel. The new thermal-hydraulic conditions are used to generate a new input deck for the next MCNP calculation. This procedure is repeated until a converged state is achieved.

The coupled code system was successfully tested on a proposed fuel assembly design of a HPLWR. An under-relaxation was introduced in the coupling procedure to achieve convergence. The test results showed a satisfactory convergence with a small under-relaxation factor of 0.2. Due to the accuracy problem in MCNP with the small number of particles, the coupled procedure was shown to converge within a 7% error bar after 5 iterations. To improve the error a large number of source particles are required in MCNP calculation.

Comparison of the results with and without coupling showed a significant difference. A power profile close to a cosine shape was obtained in the case without coupling. The results with the coupling produced a power distribution with two peaks, one strong peak in the lower part and a weaker one in the upper part. The power profile corresponds to the average water density distribution in the axial cross section of the fuel assembly that has a high density at the inlet, decreases along the fuel assembly height and increases again due to moderator flow coming in from the top.

With the coupled system, a detailed local behaviour of various parameters of the fuel assembly was analysed. The power and fuel temperature distribution in a fuel assembly for individual fuel rods, water density and temperature distribution in each sub-channel was obtained. The results have shown a well uniform power profile with 4% enrichment in the corner fuel rod and 5% fuel enrichment in the other rods. The enrichment reduction in the corner rod removed the hot spot at the corner of the fuel assembly that was obtained in the study with uniform enrichment Waata et al. [83].

A local maximum cladding temperature of 600 °C was obtained, which is less than the design limit of 620°C set for the HPLWR. A temperature difference of 50°C between the hottest sub-channel and coldest sub-channel was obtained.

Apart from performing a neutronics/thermal-hydraulics for a fuel assembly design analysis, the coupled system can be used to identify areas for design modifications such as reduction of enrichment in corner rods, or enhancing mixing by grid spacers for the HPLWR.

The results presented for the fuel assembly have demonstrated the effectiveness of the coupling procedure developed. For more quantitative analyses of the fuel assembly design, reliable models for heat transfer correlations and mixing coefficients for supercritical water are required.

6 REFERENCES

[1]   U.S. DOE: Nuclear Energy Research Advisory Committee and the Generation IV International Forum, A Technology Roadmap for Generation IV Nuclear Energy Systems, Dec. 2002

[2]   Oka, Y., Koshizuka, S.: Design concept of Once-through Cycle Supercritical Pressure Light water cooled reactor, Proc. of SCR-2000, Tokyo University, pp. 1-22, Nov 6 – 8, 2000

[3]   Oka, Y., Koshizuka, S.: Supercritical – Pressure, Once-Through Cycle Light Water Cooled Reactor Concept, Journal of Nuclear Science and Technology, Vol. 38, No 12, pp.1081 – 1089, 2001

[4]   Oka, Y., Koshizuka, S Ishiwatari, Y., Yamaji, A.: Elements of Design consideration of Once-Through Cycle, Supercritical-Pressure Light Water Reactor, ICAPP, Hollywood, 2002

[5]   Oka, Y., Koshizuka, S.: Core Design of a Direct-Cycle, Supercritical Water Cooled Fast Breeder Reactor, Nuclear Technology 108, 24 – 23, 1994

[6]   Oka, Y., Koshizuka, S., Ishiwatari, Y., Yamaji, A and Yi, T.: High Temperature LWR Operating at Supercritical-Pressure, Global 2003, New Orleans, United States, Nov. 16 – 20, 2003, pp. 1128 – 1135.

[7]   Yamaji, A., Oka, Y., Koshizuka, S.: Fuel Design of High Temperature Reactors Cooled and Moderated by Supercritical Light Water. GENES4/ANP2003, Kyoto, Japan, 2003, paper 1040

[8]   Yamaji, A., Oka, Y., Koshizuka, S.: Core design of a High Temperature Reactor Cooled and Moderated by Supercritical Light water. GENES4/ANP2003, Kyoto, Japan, Sept. 15 -19, 2003, paper 1041

[9]   Ishiwatari, Y, Oka, Y., Koshizuka, S.: Control of a High Temperature Supercritical Pressure Light Water Cooled and Moderated Reactor with Water Rods, Journal of Nuclear Science and Technology, Vol. 40, No. 5, pp. 298 – 306 May 2003

[10]   Mukohara, T., Koshizuka, S., Oka, Y.: Sub-channel Analysis of Supercritical Water Cooled Reactors, Proc. of SCR-2000, Tokyo, Nov 6 – 8, 2000, paper no 301

[11]   Tanabe, T., Koshizuka, S Oka, Y.: A Sub-channel Analysis code for supercritical –Pressure LWR with Downward flowing water rods, ICAPP, Pittsburgh, June 13 – 17, 2004, pp. 502 – 508.

[12]   Yamaji, A., Oka, Y., Koshizuka, S.: Three-dimensional Core Design with Neutronics and Thermal-hydraulics Coupling Global 2003, New Orleans, LA, Nov. 16 – 20, 2003, pp. 1763 - 1771.

[13]   Yamaji, A., Kamei, K., Oka, Y., Koshizuka, S.: Improved Core Design of High Temperature Supercritical-Pressure Light Water Reactor, ICAPP, Pittsburg, USA, paper 4331, 2004

[14]   Oka, Y., Koshizuka , S., Jervremovic, T.: Supercritical–Pressure, Light-Water Cooled Reactors for Improving Economic, Safety, Plutonium Utilization and Environment, Progress in Nuclear Energy 29, 431 – 438, 1993

[15]   Dobashi, K., Oka, Y., Koshizuka, S.: Core and Plant Design of the Power Reactor Cooled and Moderated by Supercritical Light Water with Single Tube Water Rods, Ann. Nucl. Energy, Vol. 24, pp 1281 – 1300, 1997

[16]   Dobashi, K., Oka, Y., Koshizuka, S.: Conceptual design of High Temperature Power Reactor Cooled and Moderated by Supercritical Light Water, ICONE-6, San Diego, California, May 10 – 15, 1998, New York: ASME, CD-ROM.

REFERENCES

[17]   Okano, Y., Koshizuka, S., Oka, Y.: Design of Water Rod Cores of a Direct Cycle Supercritical-Pressure Light Water Reactor, Ann. Nucl. Energy, Vol. 21, pp 601 - 611, 1994

[18]   Buongiorno, J., MacDonald, P.E.: Study of Solid Moderators for the Thermal-Spectrum Supercritical Water Cooled Reactor (Neutronics), ICAPP, Cordoba, Spain, May 4. - 7, 2003, paper 3328.

[19]   Buongiorno, J., MacDonald, P.E.: Study of Solid Moderators for the Thermal-Spectrum Supercritical Water Cooled Reactor (Thermal-Mechanics and Cost), ICAPP, Cordoba, Spain, May 4. - 7, 2003, paper 3329.

[20]   Joo, H.K., Yoo, J.W., Noh, J.M.: Conceptual Design for Rectangular Fuel Assembly for Thermal SCWR system, Global, New Orleans, United States, Nov. 16 – 20, 2003, pp. 1149 - 1154

[21]   Bae, Y.Y., Joo, H.K., Jang, J., Song, J., Yoon, H.Y.: Research of a Supercritical Pressure Water Coolant Reactor in Korea, Proc. of ICAPP, Pittsburg, USA, paper 4247, 2004

[22]   Bae Y.Y and Kang, H.O.: Thermo-Hydraulic Study of Supercritical Pressure Water-Cooled Reactor Option, Proc. of ICAAP, Pittsburg, USA, paper 3223, 2004

[23]   Kuznetsov, Yu.N., Babaraev, B.A.: Channel Type Reactors with Supercritical Water Coolant, Proc. of ICAPP, Pittsburgh, pp 4232, 2004

[24]   Heusener, G., Mueller, U., Schulenberg, T., Squarer, D.: A European Development Program for a High-Performace Light-Water Reactor (HPLWR), Proc. of SCR-2000, Tokyo, pp 23 -28, 2000

[25]   Squarer, D., Bittermann, D., Schulenberg, T., Oka, Y., Aksan, N., Maraczy, C., Kyrki-Rajmaki, R., Souyri, A., Dumaz, P. and Struwe D.: High Performance Light Water Reactor, Nuclear Engineering and Design, 221, 167 – 180, 2003

[26]   Bittermann, D., Squarer, D., Schulenberg, T., Oka, Y., Dumaz, P., Kyrki-Rajmaki, R., Aksan , N., Maraczy, C. and Souyri.: A Potential Plant Characteristics of a High Performance Light Water Reactor, ICAPP, Cordoba, paper 3046, 2003

[27]   Rimpault, G., Maraczy, C., Kyrki-Rajmaki, R., Oka, Y., Schulenberg, T.: Core design Features Studies and Research Needs for High-Performance Light-Water Reactors, ICAPP, Cordoba, paper 3194, 2003

[28]   Broeders, C.M., Sanchez, V., Stein, E., Travleev, A.: Validation of Coupled Neutron Physics and Thermal-Hydraulics Analysis for HPLWR. ICAPP, Cordoba, Spain, 2003

[29]   Cheng, X., Schulenberg, T., Bittermann, D., Rau, P.: Design Analysis of Core Assemblies for Supercritical Pressure Condition, Nuclear Engineering and Design, 223, 279-294, 2003

[30]   Cheng, X., Schulenberg, T., Koshizuka, S., Oka, Y., Souyri, A.: Thermal-Hydraulics Analysis of Supercritical Pressure Light Water Reactors, ICAPP, paper 1051, Hollywood Florida, USA, June 9 – 13, 2002

[31]   Cheng, X., Schulenberg, T.: Heat Transfer at Supercritical Pressure – Literature Review and Application to an HPLWR, Wissenschaftliche Berichte, FZKA- 6609, May 2001

[32]   Ehrlich, K., Heikinheimo, L., Arnoux, P., Bittermann, D., Oka, Y and Schulenberg, T.: Material requirement of High performance Light Water Reactors, 4th Workshop on LWR Coolant Water Radiolysis and Electrochemistry, Avignon, France, April 2002

[33]   Aksan, N., Schulenberg, T., Squarer, D., Cheng, X., Struwe, .D., Sanchez, V., Dumaz, P., Kyrki-Rajmaki, R., Souyri, A., Oka, Y., Koshizuka, S.: Potential Safety Features and Safaty Aspects for High Performance Light Water Reactor, GENES4/ANP2003, Kyoto, Japan, paper-1223, 2003

[34] Bittermann, D., Squarer, D., Schulenberg, T., and Oka, Y.: Economic Prospects of the HPLWR, GENES4/ANP2003, paper 1003, Kyoto, Japan, 2003

[35] Wagner, W., Kruse, K.: Properties of Steam Table, ISBN 3-540-64339 Springer-Verlag Berlin Heidelberg, 1998

[36] CRISSUE-S Partners, CRISSUE-S WP-1-Report: Neutronics/Thermal-hydraulics Coupling in LWR Technology, Data Requirements and Databases Needed for Transient Simulations and Qualifications (DATABASE), ISBN 92-64-02083-7, OECD (2004).

[37] CRISSUE-S Partners, CRISSUE-S WP-2-Report: Neutronics/Thermal-hydraulics Coupling in LWR Technology: State-of-art Report (REAC-SOAR), ISBN 92-64-02084-5, OECD)

[38] CRISSUE-S Partners, CRISSUE-S WP3-Report: Neutronics/Thermal-hydraulics Coupling in LWR Technology, Achievements and Recommendations Report (FINARES), ISBN 92-64-02085-3, OECD (2004)

[39] Miller, M.R., Downar, T.J.: Completion Report for the Coupled TRACS-M/PARCS Code, University of Purdue, Report PU/NE-99-20

[40] Lee, D et al.: Analysis of the OECD/NRC BWR Turbine Trip Transient Benchmark with the coupled Thermal-hydraulics and Neutronics Code TRAC-M/PARCS, Nuclear Science and Engineering, Vol. 148, Page 291 – 305, 2004

[41] Bousbia-Salah, A. et al.: Analysis of the Peach Bottom Turbine Trip 2 Experiment by Coupled RELAP-PARCS Three-Dimensional Codes, Nuclear Science and Engineering, Vol. 148, pp 337– 353, 2004

[42] Grundmann, U., Lucas, D., Rohde, U.: Coupling of the Thermo-hydraulic Code ATHLET with the Neutron Kinetic Core Model DYN3D, Proc. International Conf. on Mathematics and Computation, Reactor Physics and Environmental Analyses

[43] Grundmann, U., Kliem, S., and Rohde, U.: Analysis of the Boiling Water Reactor Turbine Trip Benchmark with the Codes DYN3D and ATHLET/DYN3D. Nuclear Science and Engineering, Vol. 148, Page 226 – 234, 2004

[44] Asaka, H., Zimin, V.G., Iguchi, T., Anoda, Y.: Coupling of the Thermal-hydraulic codes with 3D Neutron Kinetic Code SKETCH-N, Preliminary Proceedings of the OCED/CSNI Workshop on Advanced Thermal-hydraulics and Neutronics Codes: Current and Future Applications, Vol.2, pp. 1 – 15, Barcelona, Spain, 2000

[45] Lee, D., Downar, T.J., and Kim, Y.: A Nodal and Finite Difference Hybrid Method for Pin-by Pin Heterogeneous Three-Dimensional Light Water reactor Diffusion Calculations, Nuclear Science and Engineering, Vol. 146, pp. 319 – 339, 2004

[46] Ivanov, K.N., Beam, T.M., Baratta, A.J.: Multidimensional TMI-1 Main Steam Line Break Analysis Methodology Using TRAC-PF/NEM, Nuclear Technology, Vol. 133 Page 169 – 185, February 2001

[47] Ivanov K.N., Juan, R.M., Irani, A., Baratta, A.J.: Features and Performance of a Coupled Three Dimensional Thermal-hydraulic/kinetics TRAC-PF1/NEM PWR analysis code, annals of Nuclear Energy 26, 1407 – 1417, 1999

[48] Ziabletsev, D.N., Ivanov, K.N.: Improved verification methodology for TRAC-PF1/NEM Using NEA/OECD Core Transient Benchmarks, Annals of Nuclear Energy, 27, 1319 – 1331, 2000

[49] Fu, H., Rodarte, J.S., Ivanov, K.N.: TRAC-PF1/NEM Modelling and Results of OECD/NEA BWR core Transient Benchmarks, Annals of Nuclear Energy, 27, 1051 – 1058, 2000

REFERENCES

[50]   Turinsky, P.J.: NESTLE Few-group neutron diffusion equation solver utilizing the nodal expansion method for eigenvalue, adjoint, fixed source steady-state, EGG-NRE-11406, DE95 001903, Idoho Falls, USA, 1994

[51]   Langenbuch, S., Schmidt, K.-D., Velkov, K.: Analysis of OCED/NRC BWR Turbine Trip Benchmark by the Coupled-Code system ATHLET-QUABOX/CUBBOX, Nuclear Science and Engineering, Vol. 148, Page 270 – 280, 2004

[52]   Sanchez-Espinoza, V.H., Hering, W., Knoll, A., Boer, R.: Analysis of the OCED.NEA PWR Main Steam Line Break (MSLB) Benchmark Exercise 3 with coupled code system RELAP5/PANBOX, Wissenschaftliche Berichte, FZKA- 6518, 2002

[53]   Jackson, C.J., Finnemann, H.: Verification of the Coupled RELAP/PANBOX System with the NEACRP LWR Core Transient Benchmark, Proc. International Conference on Mathematic and Computations, Reactor Physics and Environmental Analyses

[54]   Pautz, A., Hesse, U., Zwermann, W., Langenbuch, S.: Fuel Assembly Calculation Using the Method of Discrete Ordinates, Nuclear Science and Engineering, Vol. 149, pp. 197 – 210, 2005

[55]   Rhoades W. A., Childs R. L.: TORT-DORT, Two- and Three-Dimensional Discrete Ordinates Transport, Version 2.7.3, RSIC-CCC-543, ORNL RSICC, Oak Ridge, TN (1993)

[56]   Pautz, A., and Birkhofer, A.: DORT-TD: A Transient Neutron Transport Code with Fully Implicit Time Integration, Nuclear Science and Engineering, Vol. 145, pp. 299 – 319, 2003

[57]   Broeders, C.H.M., Dagan, R., Sanchez-Espinoza, V, Travleev, A.: KAPROS-E: Modular Program System for Nuclear Reactor Analysis, Status and Results of Selected Applications, Jahrrestagung Kerntechnik, Düsseldorf, 2004

[58]   Briesmeister J.F, Editor, MCNP – A General Monte Carlo N-Transport code, Version 4C, Los Alamos National Laboratory report LA-12625, 1993

[59]   Misu, St., Kiehlmann, H.D., Spierling, H., Wehle, F.: The Comprehensive Methodology for Challenging BWR Fuel Assembly and core Design used in Framatome ANP, Physor, Seoul, Korea, 2002

[60]   Mori, M., Rineiski, A., Kretzschmar, F., Maschek, W., Morita, K.: Coupled MCNP/MXN Calculations for the SCFR, CAPRA-CADRA, International Seminar, Aix-en-Provence, France, 2004

[61]   Mori, M., Maschek, W., Laurien, E., Morita, M.: Monte-Carlo/Simmer-III Reactivity Coefficient Calculation for the Super-Critical Water Fast Reactor, Proc. of the ANS/ENS Topical Meeting GLOBAL, New Orleans, 2003

[62]   Burwell, M.J.,Lerchl, G., Miro, J., Teschendorff, V., Wolfert, K.: The Thermal-hydraulic Code ATHLET for Analysis of PWR and BWR Systems, Proceedings Fourth International Topical Meeting on Nuclear Reactor Thermal-hydraulics, Vol. 2, pp 1234 – 1239, Oct. 10 – 13th,1989

[63]   Glaeser, H.: Validation and Uncertainty Analysis of the ATHLET code Thermal-hydraulics computer code, Nuclear Society of Slovenia, 2nd Regional Meeting: Nuclear Energy in Central Europe Portoroz, Slovenia, 1995

[64]   Langenbuch, S., Austregesilo, P., Fomitchenko, P., Rohde, U., Velkov, K.: Interface Requirements to Couple Thermal-Hydraulics Codes to 3D Neutronic Code, OCED/CSNI Workshop on Transient Thermal-Hydraulic and Neutronic Codes Requirements, Annapolis, United State, 1996

[65]   Sanchez-Espinoza, V., Hering, W., Knoll, A.: Analysis of the OECD/NEA PWR MSLB Benchmark Exercise 1 using the RELAP5 Code with Point Kinetics Option, FZKA 6427, 2002

[66]   Sanchez-Espinoza, V., Hering, W.: Investigations of the Appropriateness of RELAP5/MOD3 for the Safety Evaluation of an Innovative Reactor Operated at Thermodynamically Supercritical Conditions, FZKA 6749, 2002

[67]   Nigro, A.L., Spadoni, A., D'Auria, F., Saiu, G.: MSLB Coupled 3D Neutronics-Thermal-Hydraulics Analysis of a Large PWR using RELAP5-3D, International Conference Nuclear Energy in Central Europe, Portoroz, Slovenia, 2001

[68]   Bovalini, R., D'Auria, F., Galassi, G.M., Spadoni, A., Hassan, Y.: TMI-MSLB Coupled 3-D Neutronics/Thermal-hydraulics Analysis: Application of RELAP5-3D and Comparison with Different Codes, RELAP5 International Users Seminar, Sun Vally, Idaho, 2001

[69]   Mignot, G., Royer, E., Rameau, B., Todorova, N.: Computation of a BWR Turbine Trip with CATHARE-CRONOS2-FLICA4 Coupled Codes, Nuclear Science and Engineering, Volume 148, Page 235 – 246, 2004

[70]   Wheeler, C.L., Stewart, C.W., Cena, R.J., Rowe, D.S., Sutey, A.M.: COBRA-IV -I An Interim Version of COBRA for Bundle Nuclear Fuel Element and Cores, BNWL-1962, UC-32, March 1976

[71]   Yoo, Y.J., and Hwang, D.H.: MATRA, Multichannel Analyzer for Steady States and Transients in Rod Arrays, Korea Atomic Energy Research Institute, October 2003

[72]   Allaire, G.: Solving Linear System Equation in FLICA, A Thermo-Hydraulic Code for 3-D Transient Computations, Proc. International Conference on Mathematic and Computations, Reactor Physics and Environmental Analyses

[73]   Fluent 5 Users Guide, Fluent Inc., Lebanon, NH (1998); http://www.fluent.com

[74]   CFX-4 User Manual ,1997 AEA Technology. http://www.software.aeat.com/cfx.default.asp

[75]   Hofmeister, J., Schulenberg, T., Starflinger, J.: Optimisation of a Fuel Assembly for a HPLWR, ICAPP 2005, Seoul, Korea, paper 5077, 2005

[76]   Todreas, N.E. and Kazimi, M.S.: Elements of Thermal-hydraulics Design Nuclear Systems II

[77]   Cheng, X., Müller, W.: Turbulent mixing and critical heat flux in tight 7-rod bundles, Int. J. Multiphase Flow, Vol.24, pp. 1245-1263, 1998

[78]   Bishop, A.A., Sandberg, R.O., Tong, L.S.: Forced convection heat transfer to water at near critical temperatures and supercritical pressures, WCAP-2056-P, Part-III-B, February, 1964

[79]   Todreas, N.E. and Kazimi, M.S.: Elements of Thermal-hydraulics Design Nuclear Systems I: Thermal Hydraulic Fundamentals, Massachusetts Institute of Technology, 1990.

[80]   Ho, C.Y, and Taylor, R.E.: Thermal Conductivity, Proc. from the Eighth Conference Thermal Conductivity, Purdue University, West Lafayette, Indiana, October 7-10, 1968, Plenum Press, New York, 1969.

[81]   Bernnat, W., Mattes, M., Keinert, J., Conti, A.: Application of the Monte Carlo Method for the Calculation of Safety Related Reactor Physics Parameter for Power Reactor with Consideration of Detailed Burn-up Distributions, Report Number IKE-6-2000, University of Stuttgart

[82]   Bernnat, W.: Private communication, IKE, University of Stuttgart, 2005

[83]   Waata, C., Schulenberg, T, Cheng, X., Starflinger, J., Laurien, E.: Coupling of MCNP with a Sub- channel code for analysis of a HPLWR Fuel, accepted for NURETH-11, Paper: 021, Avignon, France, 2005

NOMENCLATURE

Symbols	Units	Concept
A	mm^2	area
C_p	J/kg.K	specific heat
D	m	diameter
D_h	mm	hydraulic diameter
e	MeV	heating energy
f	-	friction factor
G	kg/m^2.s	mass flux
G^*	kg/m^2.s	mass flux due directed cross flow
$G^'$	kg/m^2.s	tranverse mass flux due to turbulent mixing
g	m/s^2	gravitational acceleration
h	J/kg	enthalpy
H	m	total height of the fuel rod
H(E)	MeV/collision	heating number
i	-	iteration
k_{eff}	-	effective multiplication factor
l	m	sub-channel length
m	kg	mass
$\dot{m}$	kg/s	mass flow rate
N	-	total number of histories
N_{as}	-	number of fuel assemblies
Nu	-	Nusselt-number
P	Pa	pressure
P_{ht}	mm	heated perimeter
Pr	-	Prandtl-number
P_{wt}	mm	wetted perimeter
Q	W	heating power
q'	W/m	linear heating per unit length
q''	W/m^2	heat flux
q'''	W/m^3	volumetric heating
R	m	radius
Re	-	Reynolds-number
S	m	Sub-channel gap size

T	°C	temperature
Tl	-	track length
u	m/s	velocity
uf	-	under-relaxation factor
V	m^3	volume
Wt	-	particle weight
X	-	mixing fraction
$\overline{x}$	-	sampled mean
z	m	axial elevation

Subscripts

a	absorption
B	bulk
C	coolant
ci	inner cladding surface
co	outer cladding surface
DC	down-comer
f	fuel
fi	inner fuel pellet surface
fo	outer fuel pellet surface
j, k	index of sub-channels
Mod	moderator
MT	moderator tube
AG	assembly gap
sca	scattering
TOT	total
w	water
m	MCNP
s	STAFAS
f	fuel
g	gram
i	iteration
rod	fuel rod

Greek Symbols

α	$W/m^2.K$	heat transfer coefficient
Σ	cm^{-1}	macroscopic cross section
ε	-	convergence criterion
β	-	turbulent mixing coefficient
ζ	-	hydraulic resistance coefficient
λ	W/m K	thermal-conductivity
μ	kg/m.s	dynamic viscosity
ρ	kg/m^3	density
σ	barn	microscopic cross section
Φ	$neutrons/cm^2$-s	particle flux

Acronyms

ATHLET	Analysis of Thermal-Hydraulics of LEaks Transient
BWR	Boiling Water Reactor
BOP	Balance of Plant
CEA	Commissariat à l'Énergie Atomique
CFD	Computational Fluid Dynamics
COBRA	Coolant Boiling in Rod Arrays
CSNI	Committee on Safety of Nuclear Installation
DNBR	Departure from Nucleate Boiling Ratio
DOE	Department of Energy
DORT	Discrete Ordinate code (Two-dimensional)
EPRI	Electric Power Research Institute
FA	Fuel Assembly
FFP	Fossil Fuel wer plant
FZKA	Forschungszentrum Karlsruhe Annual report
GEV-IV	Generation-IV reactors
GRS	Gesellschaft für Anlagen- und Reaktorsicherheit mbH
HPLWR	High Performance Light Water Reactor
ICAPP	International Congress on Advanced Nuclear Power Plants
ICONE	International Conference On Nuclear Engineering

KAERI	Korea Atomic Energy Research Institute
KAPROS	KArlsruhe PROgram System
LWR	Light Water Reactor
MATRA	Multi-channel Analyser for steady state and Transients in Rod Arrays
MCNP	Monte Carlo N-Particle code
MSLB	Main Steam Line Break
NEA	Nuclear Energy Agency
NEM	Nodal Expansion Methods
NPP	Nuclear Power Plants
NRC	Nuclear Regulatory Commission
NURETH	Nuclear Reactor Thermal-Hydraulics
OCED	Organisation for Economic Co-operation and Development
ORNL	Oak Ridge National Laboratory
PARCS	Purdue Advanced Reactor Core Simulator
PWR	Pressurised Water Reactor
RELAP	Reactor Excursion and Leak Analysis Program
RIA	Reactivity Initiated Accidents
RPV	Reactor Pressure vessel
SCFR	Supercritical Fast Reactor
SCWR	Supercritical Water Reactor
STAFAS	Sub-channel Thermal-hydraulic Analysis of a Fuel Assembly design under Supercritical conditions
TMI-1	Three Mile Island – Unit 1
TRAC	Transient Analysis code
TRAC-M	Modernized Transient Reactor Analysis Code
TT	Turbine Trip
UP/UZ	University of Piza/University of Zagreb